personal buildup for

Force Motors Ltd.

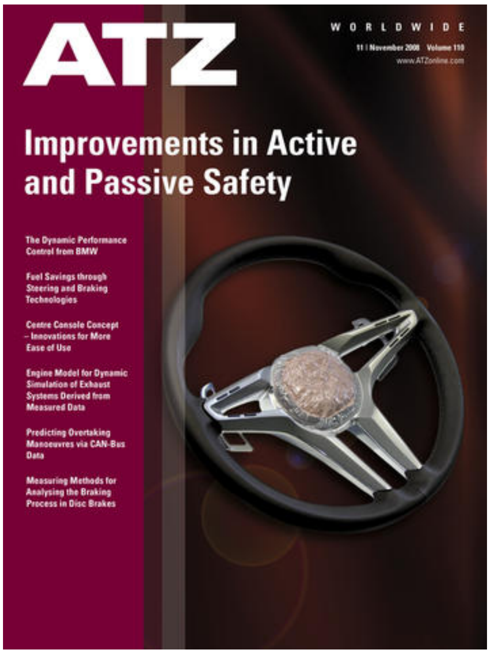

ATZ .worldwide 11/2008

ATZ
WORLDWIDE
11 | November 2008 Volume 110
www.ATZonline.com

Improvements in Active and Passive Safety

For more information visit:
www.ATZonline.com

COVER STORY

Improvements in Active and Passive Safety

4
Active and Passive Safety Systems become integrated and networked more and more. As two examples the ATZ cover story presents a system by Continental from the project Aprosys for side impact protection and a space saving airbag in the steering wheel by Takata-Petri.

COVER STORY

DEVELOPMENT

RESEARCH

RUBRICS

Surviving the Crisis

Dear Reader,

How are you dealing with the daily reports on the global financial crisis and its consequences? Are you concerned about how "weather-proof" your company is and how secure your personal finances are?

Typical human reaction patterns in times of crisis are impulsive action, denial or resignation. I believe that, as far as the automotive industry is concerned, there is little reason for any of these. Let's take denial to begin with. As financing becomes more expensive, the lack of available funds will have an impact on the investment behaviour of car makers and suppliers. And uncertainty among consumers will result in less willingness to buy, especially when it comes to expensive articles like cars. Denying that such problems exist would be irresponsible.

So what should we do? Putting investment entirely on hold and pursuing a radical austerity policy would certainly bring short-term financial benefits – but we would have to pay dearly in the long term. Even if environmental protection is not currently in the focus of public attention due to the sharp fall in the price of oil, sustainable economic management and producing eco-friendly vehicles will, in the medium and long term, be the preconditions for staying in business as an automotive company.

Let us therefore see this crisis as an opportunity to put our house in order. Companies will survive this crisis too – provided that they develop today what the customer wants tomorrow. Environmentally friendly drive systems and maximum safety are at the top of the list of priorities. As far as financing innovations in difficult times is concerned, it is more worthwhile than ever to enter into strategic partnerships in individual areas.

In other words, alertness yes, resignation no!

I wish you all the best for the last few weeks of 2008.

Johannes Winterhagen
Wiesbaden, 20 October 2008

Johannes Winterhagen
Editor-in-Chief

ATZ WORLDWIDE
11|2008

Organ of the VDI-Gesellschaft Fahrzeug- und Verkehrstechnik (FVT)

Organ of the Forschungsvereinigung Automobiltechnik e. V. (FAT) and of the Normenausschuss Kraftfahrzeuge (FAKRA) in the DIN Deutsches Institut für Normung e. V.

Organ of the Wissenschaftliche Gesellschaft für Kraftfahrzeug- und Motorentechnik e. V. (WKM)

Crash Safety through Side Impact Protection

Aprosys Project for Environmental Sensorics

In the moments before a collision, only fractions of a second remain, in which to activate additional side impact protection and provide the passengers with better protection. As part of the European Aprosys project, a system has been developed, which can detect accidents at an early stage by using radar and video sensors and which uses a new type of very rapid actuator to activate the side impact protection. The project has been headed by engineers at Continental, the international automotive supplier.

1 Introduction

Side collisions pose a particularly high risk of injury to drivers and passengers. Although frontal and side crashes occur with almost equal frequency, the number of injuries and fatalities from side crashes is greater. The reason for this is that, at the moment of initial impact, there is only a narrow gap between the occupants and any object, which penetrates the vehicle. The existing impact detection technology can only detect a crash on initial impact, allowing insufficient time for collision-mitigating measures to be triggered.

To overcome this, an integrated side impact protection system was built up in the sub-project No. 6 of the European Aprosys (Advanced Protection Systems) research project, made of two sub-systems. For the first time, this system combines the following innovative sub-systems in a car: a sensor sub-system and an actuator sub-system. The sensor sub-system consists of radar and stereo camera. It monitors the road area to the front and side of the vehicle, determines that a collision is imminent and activates the actuator sub-system before the impact occurs so as to reduce the effect on the passenger compartment. This gives other conventional devices such as airbags more time and space to protect the occupants.

The actuator sub-system is based on shape memory alloys made of wires. To reduce the severity of a side impact the structural deformation of the body should be decreased. This could be possible when directing the impact forces to those rigid vehicle structures not affected by the impact.

The system concept is based on a thorough analysis of accident statistics. Various side impact protection approaches were examined using multibody [1] and finite element [2] simulations. Human behavior in side impact situations was also investigated [3]. Following these studies, the sensor and actuator sub-systems were defined, developed, installed in various vehicles and finally tested.

2 Sensor Sub-System

Requirements for the sensor sub-system were derived from the detailed study of actual impact angles and related fatality numbers [4]. In order to detect the great majority of side impacts and to be able to deliver useable data to the actuator sub-system, the sensor sub-system had to:
- detect and track objects impacting the side of the vehicle
- determine the size and shape of the impacting objects (classification)

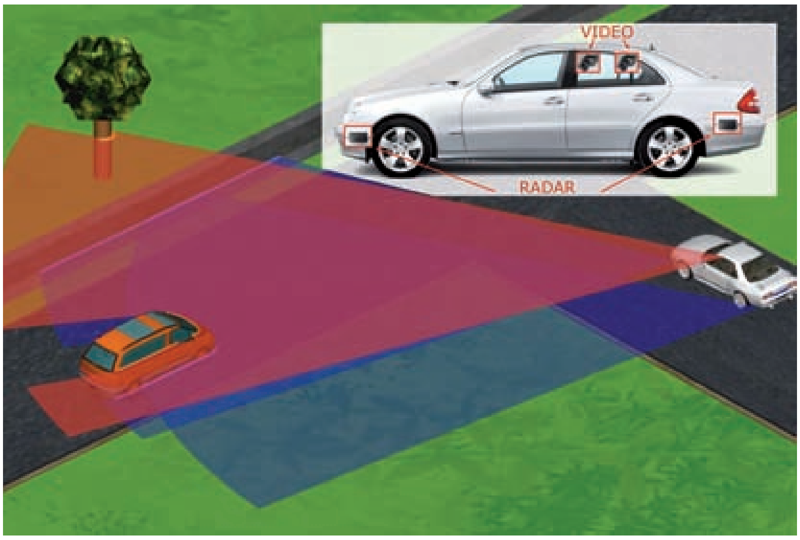

Figure 1: Installation position and surveillance field – the surveillance area lies to the side, both in front of and alongside the vehicle (blue: radar sensors, red: stereo camera); the two radar sensors are fitted below the front and rear bumpers; and the stereo camera in the region of the rear side window

The Author

Dr.
Joachim Tandler
is expert for radar and fusion systems in Continental's Chassis & Safety Division in Lindau (Germany).

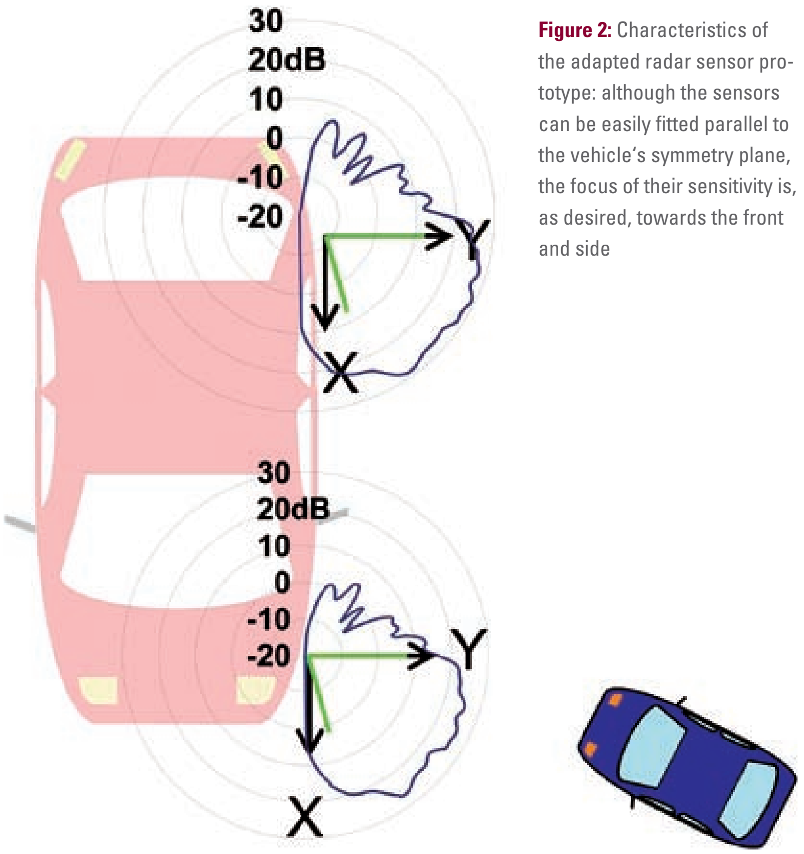

Figure 2: Characteristics of the adapted radar sensor prototype: although the sensors can be easily fitted parallel to the vehicle's symmetry plane, the focus of their sensitivity is, as desired, towards the front and side

- establish the risk of an impact and decide whether a collision was about to occur at least 200 ms before impact
- monitor an area over a range of 20 m both to the side and front of the vehicle; impacts occur most frequently at an angle of 90°, that means a classic accident due to a failure to give way, and at 60°, typical of a collision when turning off.

The task could be solved by a multi-sensor system, consisting of a radar sensor network (two sensors) and a stereo video camera on each side of the vehicle, **Figure 1**. Primarily was to process the data from each type of sensor separately. Then a fusion module collated the data before a decision module calculated the risk of an impact and finally triggered the actuator sub-system.

The short-range radar was adapted to meet the specific requirements for monitoring the side of the vehicle. It operated at a frequency of 24 GHz with a signal bandwidth of 1000 MHz. The sensors simultaneously measured the distance (accuracy: 0.1 m), angle (accuracy: 2°) and relative velocity (accuracy: 1 m/s) of an approaching object. The radar sensors were invisibly installed below the front and rear bumpers. So that it could be simply fitted parallel with the vehicle symmetry plane, the radar antenna was adapted to look forwards and sideways, **Figure 2**.

A stereo video camera was chosen to operate together with the radar network. When developing a sideways-looking video pre-crash system, a number of differences to a forward-looking perspective had to be dealt with. When the camera is oriented to the side of the vehicle, then other vehicles are mainly seen from the side, and they are so close that they are only partly seen in the video images. Consequently, a number of image properties that are successfully exploited in a forward-looking system (such as symmetry) are no longer available. In addition, lane markings are occluded most of the time, and hence unavailable to limit the area under surveillance and to identify those objects that are important more easily.

For these reasons, a more general approach had to be taken: Object hypotheses were obtained from so-called depth maps resulting from stereo analysis. Depth maps consist of three-dimensional point clouds. They are built up by finding corresponding pixels in the two video images. The distance from the camera can be calculated from the pair of pixels.

As soon as a depth map has been produced, the object's position on the road is estimated. The object points are then separated from the road points and grouped into clusters. Tracking these

Figure 3: A demanding task – raw images from a sideways-looking stereo camera; epipolar curves (magenta) for the correspondence search in the original image geometry have been drawn in

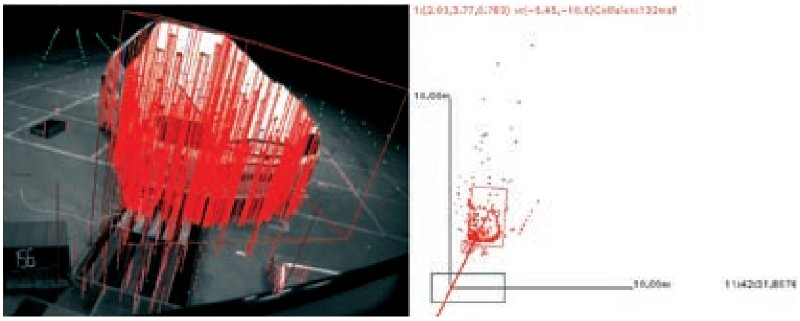

Figure 4: Results from side pre-crash detection, based on stereo analysis: on the left, an original image with the 3D points detected and their horizontal plane projection; on the right, a top view of the 3D points

clusters makes it possible to estimate how the objects being observed will move and to calculate their behavior in advance. Combining this with the estimate of one‘s own movement allows a collision prediction to be made.

In order to cover the surveillance area, the two cameras have wide opening angles and are arranged offset. As a consequence, the images cannot be transformed into epipolar geometry with reasonable computational effort, while this is standard in other stereo systems, **Figure 3** and **Figure 4**. The search for corresponding pixels takes place directly in the original images. During analogous features in epipolar geometry are localized on straight lines, now they have to be searched for on complex epipolar curves.

A box in Figure 4 represents the object hypothesis. The object‘s estimated position, relative speed and time to collision are printed in red.

Further challenges presented by a sideways-oriented pre-crash system are the short observation time and the object‘s generally complex trajectory. Additionally, the long period has to be mentioned, for which a prediction needs to be made.

The fusion system, **Figure 5**, joins matching video and radar objects together and transfers them to the decision module. The combination of the two types of sensor makes it possible to avoid false alarms but, at the same time, to remain highly effective as regards the early detection of imminent side collisions.

The decision module produces a risk estimate, **Figure 6**: it extrapolates from all the objects it identifies and calculates the time to collision (TTC). It decides whether it is physically possible to avoid a collision by braking or steering and calculates a collision probability. If the TTC and the collision probability exceed certain limits, the actuator system is alerted (compare also with [5]).

The lines in Figure 6 indicate, by means of linear extrapolation, where an object will be one second later. Small red squares on the test vehicle show possible impact points. In a case like this, a signal needs to be sent to trigger the actuator system.

In order to test whether the sensor and fusion system worked, trials were conducted in the crash laboratory of the company TNO, in which a test sled approached the vehicle under test at different angles at a speed of 50 km/h. Using an independent method, position and velocity of the sled were measured. The result: the system was capable of activating the additional impact protection approximately 200 ms before the expected crash – a major advantage over airbag systems, which can only be initiated 5 ms after impact.

The data diagrams a) to d) of **Figure 7** clearly show that the values calculated by the sensor system correspond to the actual positions during the crash test. A test sled approached at an angle of 37° at 50 km/h up to approximately 2 m distance to the host vehicle. Diagram e) shows the time to collision (TTC) calculated by the system‘s algorithms. The side impact system is only triggered if the TTC values fall below 400 ms. Diagram f) shows that the radar system achieved the additional threshold value of 80 % crash probability at the test time 160.251 s, while the video signal for the left front section detected this threshold at 160.492 s. The actuator system is only triggered, when both thresholds of both sensors are exceeded. Hence, there was still sufficient time for the side impact protection to be reliably activated. Diagram g) demonstrates that the data calculated by the sensors for the time of crash (TOC) varied only negligibly from the actual values. Lastly, the diagram h) gives a bird‘s eye view of the movement of the test sled with the points calculated by the video and radar sensors.

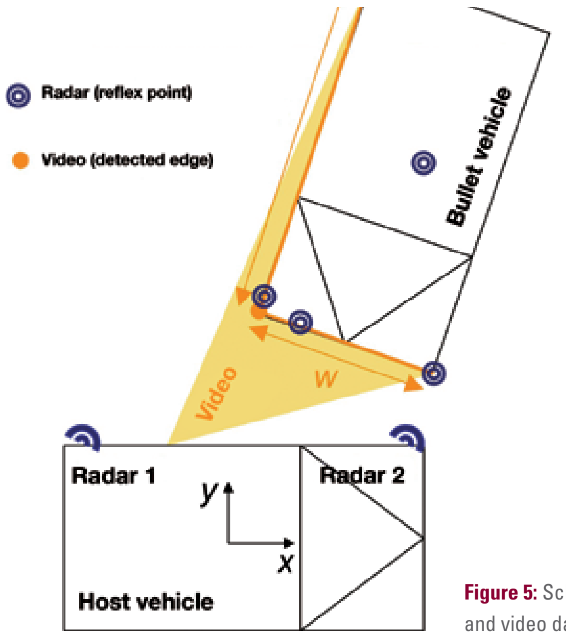

Figure 5: Scheme of the separate radar and video data before fusion

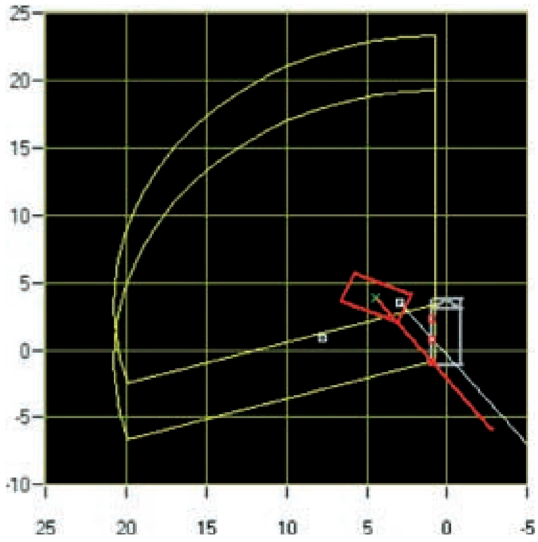

Figure 6: The decision module's view of the traffic situation: the test vehicle fitted with the sensors is shown as a gray rectangle; the red rectangle is an object, which the video system has detected; the small white square is a radar reflection object (all distances in the diagram are given in m)

forcing the B-pillar and directing the impact forces to those rigid vehicle structures not affected by the impact [7]. The latter concept turned out to be most effective. Diverting the impact forces actively opens up a new energy path during the initial contact phase and, as a consequence, relieves the load on the B-pillar and in areas where occupant is seated.

The active device (actuator) realised in this concept is located on the impact side and consists of two parts. The first part is a self-rotating door post, normally in a vertical position. Before the vehicle becomes involved in an accident, the door post moves in a horizontal position, filling the whole door frame. The second part is a tube containing a spring-loaded bolt, fitted crosswise in the seat, directly underneath the seat surface. When the sensors report an imminent crash, the spring-loaded bolt makes a rigid connection between the door and the transverse tube fitted in the seat.

3 Actuator Sub-System

Fatal injuries from a side impact normally occur within the first time segment (70 to 80 ms). These injuries are mainly caused by hard contact between the passenger and the interior fittings. There are narrow limits to what conventional protection systems such as side airbags can achieve because the side structure has only a small energy-absorbing zone.

Reducing the severity of a side impact required a two-pronged strategy. First, there had to be less structural deformation of the bodywork in the area where the occupant's life is at risk. Secondly, contact between the passenger and the interior fittings had to be gentler. In the context of Aprosys the developers concentrated on the first objective, that means on devices, which restrict penetration and thus reduce the deformation of the vehicle structure.

The aim was to evaluate the actuator sub-system through side impact tests with a deformable barrier. For this reason, a test of this nature was carried out at the very start of actuator development both for reference purposes and to optimize the simulation models (Chrysler Neon vehicles, model years 1994 to 1999, were used due to the availability of simulation models). As a result of this study, important structures, which encourage deformation (B-pillar, rocker panels, roof, floor pan, doors), were identified and analyzed.

Various concepts for reducing penetration depth were examined: These included among other things using strong bolts to join the doors to the bodywork, rein-

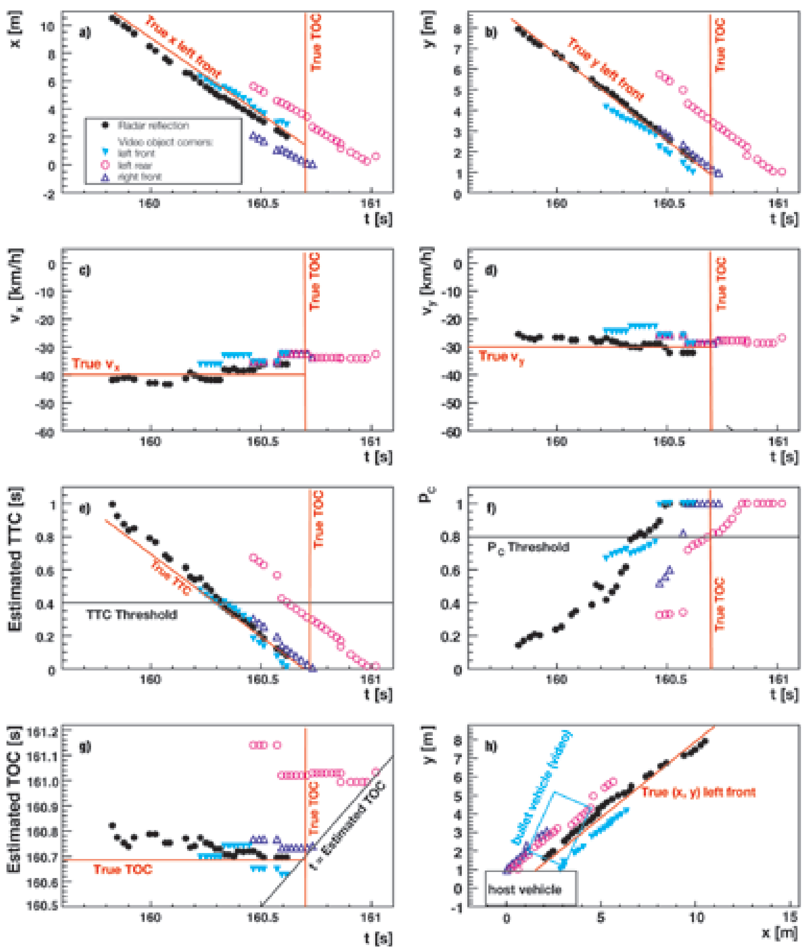

Figure 7: Data diagrams (explanations see text)

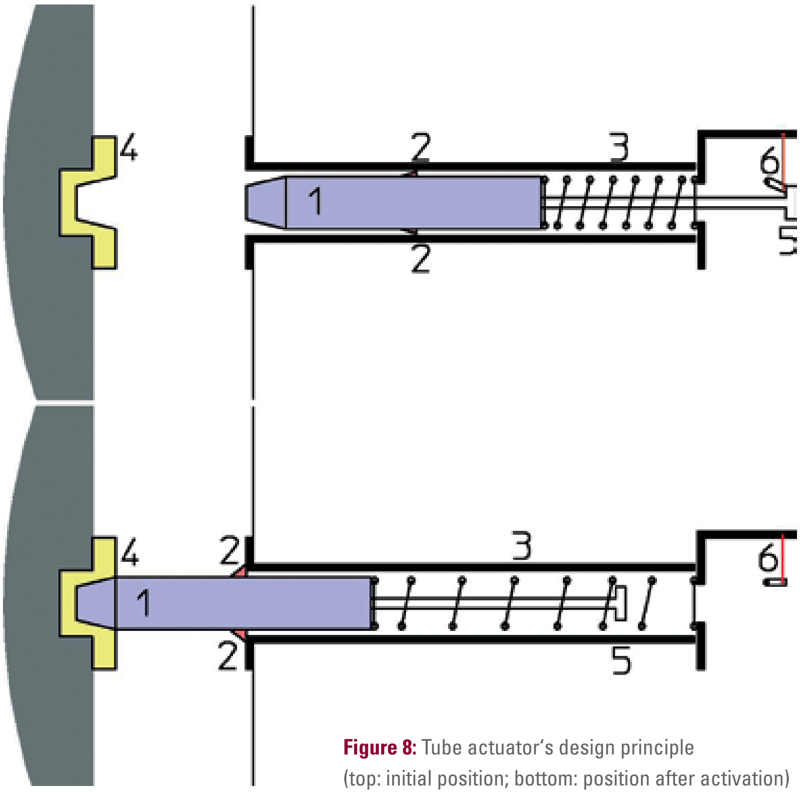

Figure 8: Tube actuator's design principle (top: initial position; bottom: position after activation)

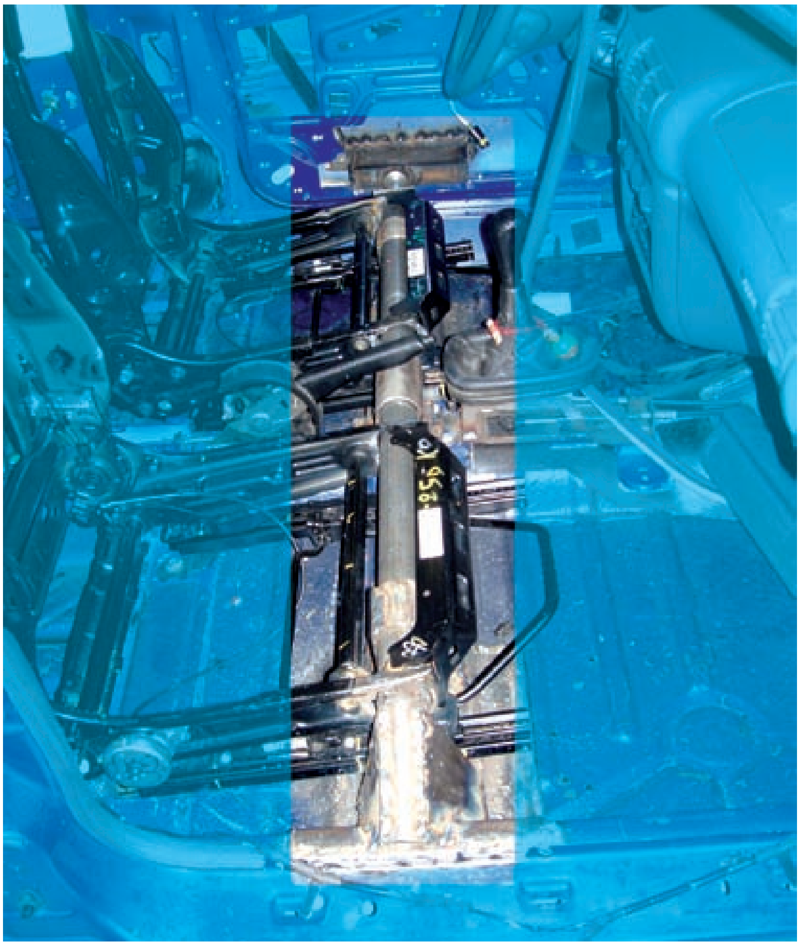

Figure 9: The actuator system, installed in a test vehicle

This seals all the gaps between the outer metal skin and the seat.

Figure 8 shows the tube actuator's design principle. A bolt (1), normally seated in a housing, can be propelled by a preloaded steel spring (3) from its original position (in the seat frame) to its activated position. In this activated position, the point of the bolt is guided by a mating piece in the door paneling (4). Small radially-mounted, expandable components (2) lock the bolt into position and prevent it from being pushed backwards. The trigger mechanism, which initiates the movement of the bolt, consists of two main parts: a small lever arm, which interacts with the rear end of the bolt (5), and a shape memory alloy wire (6), which, when activated, pulls the lever arm so as to release the bolt.

The transverse tubes of the actuator sub-system in the seats and the reinforcement in the center tunnel area can be clearly seen in **Figure 9**. The gap between the driver's seat and the reinforcement in the driver's door is sealed by the actuator; on the front-passenger side, the impact energy is diverted to the rocker panel.

3.1 Shape Memory Alloy Principle

Once both the concept and design for the actuator system had been established, the final actuator prototype was produced. It is fitted with a release mechanism, consisting of a shape memory alloy (SMA) wire [6]. It is well suited to the Aprosys project's time-critical safety application. Smart materials like sheet-like shape memory alloys or piezo-ceramics are not yet used as standard in crash applications.

The design principle of SMA is based on regrouping the molecular lattice. When heated, the material distorts; when cooled, it returns to its original shape. Several ways of heating an SMA module were examined. Using the vehicle's coolant, engine oil or chemicals was rejected due to safety risks. It was therefore decided to heat the module using electricity from a capacitor, which is charged by the vehicle's battery. A microcontroller realises the communication with the sensor system via the CAN bus and controls the activation of the SMA wire.

3.2 Actuator's Performance

The actuators and all the system components were installed in test vehicles and

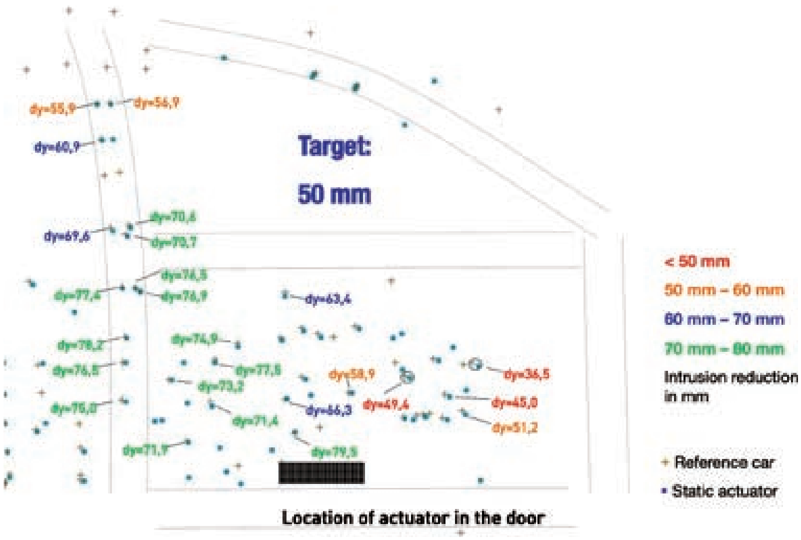

Figure 10: Crash analysis in detail: over a wide area, the penetration depth is reduced by more than the target of 50 mm

the development process was greatly assisted by simulation. The component tests evaluated the SMA actuator‘s mechanical performance and response time. The tests demonstrated the desired response time and clear repeatability; the actuator moved the bolt (approximately 400 g) 115 mm in 60 ms.

Four side crash tests with deformable barrier based on EuroNCAP, produced reference and improvement values for penetration depth at the B-pillar. The values for a production vehicle without actuator were 488 mm; and 418 mm for a vehicle with optimized actuator. With an actuator, the penetration depth, **Figure 10**, was significantly less, especially in the passenger seat area. During simulation runs in a variety of collision scenarios (collisions with vehicles or poles, at different impact angles and speeds), the actuator system showed itself to be robust, reducing the penetration depth in every case.

The essential gain produced by the actuator system is a reduction in the depth and velocity of penetration over a large area of the door. Interior protection systems (airbags) are given more time and space to deploy more effectively; the impact against the occupant is delayed, thus enabling the impact forces and other biomechanical values to be reduced. The depth of penetration is reduced precisely at the spot where the occupant is seated; survival space and time are won.

4 Evaluation of the Side Pre-Crash System

The final project phase saw an intensive series of tests for the side pre-crash system carried out using an evaluation methodology developed by Aprosys [8]:

- Evaluation of system behavior under normal driving conditions (false alarm rate and comfort aspects) using set maneuvers and a field trial: This test cluster concentrated on the sensor and decision system. The field trial was conducted over a distance of 2000 km through France, Italy, Austria and Germany and produced a total of 60 system false alarms. Although the system under consideration is reversible, this number of false alarms is too high for a series production product. However, the number can be reduced to an acceptable level by further optimization.
- Evaluation of the impact detection rate: the test conditions were based on the most important accident scenarios, taking system and test laboratory restrictions into account. Here, too, the focus was on the sensor and decision system.
- Evaluation of crash performance: a test protocol, based on the EuroNCAP side impact test, was chosen for this. Penetration depth and velocity were measured.

The whole integrated system was subjected to a performance test as the final crash trial. It should be borne in mind that the radar system‘s impact detection rate might possibly have been smaller due to the test environment in an enclosed hall. In addition, the floodlights installed for the high-speed cameras reduced the effective range of the stereo camera by more than half. Instead of a surveillance range of 20 m, a range of only 8 m was in effect available. The sensors needed to be adjust-

Project Participants and Co-authors

Several companies and institutes have collaborated on the Aprosys Sub-Project No. 6:

Dr. Dieter Willersinn, Michael Grinberg; Fraunhofer-IITB (Germany): development of the stereo camera system

Eric Zimmerman, Vlad Muntean; Faurecia (France): actuator subsystem integration, coordination of actuator development

Björn Seipel, Thorsten Koch, Dr. Tobias Melz; Fraunhofer-LBF (Germany): shape memory alloy technology, actuator development

Monica Diez; CIDAUT (Spanien), Jorge Ambrosio; Instituto Superior Técnico (Portugal): simulation and crash test analyses

Tomasz Dziewonski; Warsaw Technical University (Poland): study into driver behavior in side collisions

Richard Schram, Ronald de Lange; TNO (Netherlands): accident statistics analysis, pre-crash tests

Christian Mayer; Daimler (Germany): test coordination, test execution

Author and co-authors like to thank the European Commission for co-funding this Aprosys Sub-Project (TIP3-CT-2004-506503).

ed to compensate for these disadvantages. Despite the unfavorable conditions, the sensors identified the imminent accident approximately 321 ms before the collision and triggered the side impact protection system in good time.

5 Conclusion

Over the next few years, more and more cars on our roads will be equipped with environmental sensors, making pre-crash data available in good time. SMA actuators will also have a place in automotive engineering.

The conventional passive safety systems in vehicles can be significantly improved by using environmental sensors. Knowing that an accident is about to happen and where the impact will occur opens up many possibilities for providing vehicle occupants with better protection. Once there is a growing market for systems, which give early warning of rear-end collisions or of the vehicle leaving the road, systems for detecting side collisions will be available shortly afterwards.

References

[1] Ambrósio, J.: Improved Protection of Vehicle Occupants in Side Impacts by Using Active Structural Devices. Proceedings of the II International Conference on Computational Biomechanics, 2005, pp 989–1002

[2] Zimmerman, E.; Muntean, V.: Generic FE Simulation Model for the Layout of Pre-Crash Actuators in Side Impact. Proceedings of the Transfac Conference San Sebastian, Spain, 2006

[3] Matusiak, K.; Dziewoński, T.; Lozia, Z.; Guzek, M.: Assessment of Driver's and Passenger's Behaviour when Facing an Imminent Side Crash. Proceedings of the Ircobi Conference, 2005

[4] Tandler, J.; Preis, C.; Willersinn, D.; Grinberg, M.: Side Pre-Crash System Specification. Proceedings of the IEEE Intelligent Vehicles Symposium, Tokyo, Japan, June 13–15, 2006

[5] Tandler, J.; Willersinn, D.; Grinberg, M.: Data Analysis of the Aprosys Side Pre-Crash Sensing System. Proceedings of the IEEE Intelligent Vehicles Symposium, Istanbul, Turkey, June 13–15, 2007

[6] Seipel, B.: Smart Material Based Actuator for an Intelligent Safety System. In: ATZautotechnology 7 (2007), No 6, December 2007

[7] Zimmerman, E.; Muntean, V.: Pre-Crash Actuator to Improve Car Structural Performance in Side Impact. Proceedings of the EAEVC Conference, Budapest, Hungary, 2007

[8] Lange, R. de: Proposal of Generic Procedures for an Assessment of Pre-Crash Systems. Public Aprosys Deliverable D6.5.1, 2007

IMPRINT

ATZ WORLDWIDE

www.ATZonline.com

11|2008 · November 2008 · Volume 110
Springer Automotive Media | GWV Fachverlage GmbH
P. O. Box 15 46 · 65173 Wiesbaden · Germany
Abraham-Lincoln-Straße 46 · 65189 Wiesbaden · Germany

Managing Directors Dr. Ralf Birkelbach, Albrecht Schirmacher
Senior Advertising Thomas Werner
Senior Production Ingo Eichel
Senior Sales Gabriel Göttlinger

EDITORS-IN-CHARGE

Dr.-Ing. E. h. Richard van Basshuysen
Wolfgang Siebenpfeiffer

EDITORIAL STAFF

Editor-in-Chief
Johannes Winterhagen (win)
Phone +49 611 7878-342 · Fax +49 611 7878-462
E-Mail: johannes.winterhagen@springer.com

Vice-Editor-in-Chief
Dipl.-Ing. Michael Reichenbach (rei)
Phone +49 611 7878-341 · Fax +49 611 7878-462
E-Mail: michael.reichenbach@springer.com

Chief-on-Duty
Kirsten Beckmann M. A. (kb)
Phone +49 611 7878-343 · Fax +49 611 7878-462
E-Mail: kirsten.beckmann@springer.com

Sections
Body, Safety
Dipl.-Ing. Ulrich Knorra (kno)
Phone +49 611 7878-314 · Fax +49 611 7878-462
E-Mail: ulrich.knorra@springer.com

Chassis
Roland Schedel (rs)
Phone +49 6128 85 37 58 · Fax +49 6128 85 37 59
E-Mail: ATZautotechnology@text-com.de

Electrics, Electronics
Markus Schöttle (schoe)
Phone +49 611 7878-257 · Fax +49 611 7878-462
E-Mail: markus.schoettle@springer.com

Engine
Dipl.-Ing. (FH) Richard Backhaus (rb)
Phone +49 611 5045-982 · Fax +49 611 5045-983
E-Mail: richard.backhaus@rb-communications.de

Heavy Duty Techniques
Ruben Danisch (rd)
Phone +49 611 7878-393 · Fax +49 611 7878-462
E-Mail: ruben.danisch@springer.com

Online
Dipl.-Ing. (FH) Caterina Schröder (cs)
Phone +49 611 7878-190 · Fax +49 611 7878-462
E-Mail: caterina.schroeder@springer.com

Production, Materials
Stefan Schlott (hlo)
Phone +49 8191 70845 · Fax +49 8191 66002
E-Mail: Redaktion_Schlott@gmx.net

Service, Event Calendar
Martina Schraad
Phone +49 212 64 232 64
E-Mail: martina.schraad@springer.com

Transmission, Research
Dipl.-Ing. Michael Reichenbach (rei)
Phone +49 611 7878-341 · Fax +49 611 7878-462
E-Mail: michael.reichenbach@springer.com

English Language Consultant
Paul Willin (pw)

Permanent Contributors
Christian Bartsch (cb), Prof. Dr.-Ing. Peter Boy (bo), Prof. Dr.-Ing. Stefan Breuer (sb), Jens Büchling (jb), Jörg Christoffel (jc), Prof. Dr.-Ing. Manfred Feiler (fe), Jürgen Grandel (gl), Erich Hoepke (ho), Prof. Dr.-Ing. Fred Schäfer (fs), Bettina Seehawer (bs)

Address
P.O. Box 1546, 65173 Wiesbaden, Germany
E-Mail: redaktion@ATZonline.de

MARKETING | OFFPRINTS

Product Management Automedia
Sabrina Brokopp
Phone +49 611 7878-192 · Fax +49 611 7878-407
E-Mail: sabrina.brokopp@springer.com

Offprints
Martin Leopold
Phone +49 2642 9075-96 · Fax +49 2642 9075-97
E-Mail: leopold@medien-kontor.de

ADVERTISING | GWV MEDIA

Key Account Manager
Elisabeth Maßfeller
Phone +49 611 7878-399 · Fax +49 611 7878-140
E-Mail: elisabeth.massfeller@gwv-media.de

Ad Sales
Sabine Röck
Phone +49 611 7878-269 · Fax +49 611 7878-140
E-Mail: sabine.roeck@gwv-media.de

Heinrich X. Prinz Reuß
Phone +49 611 7878-229 · Fax +49 611 7878-140
E-Mail: heinrich.reuss@gwv-media.de

Display Ad Manager
Sandra Reisinger
Phone +49 611 7878-147 · Fax +49 611 7878-443
E-Mail: sandra.reisinger@gwv-media.de

Ad Prices
Price List No. 51

SUBSCRIPTIONS

VVA-Zeitschriftenservice, Abt. D6 F6, ATZ
P. O. Box 77 77, 33310 Gütersloh, Germany
Renate Vies
Phone +49 5241 80-1692 · Fax +49 5241 80-9620
E-Mail: SpringerAutomotive@abo-service.info

SUBSCRIPTION CONDITIONS

The emagazine appears 11 times a year at an annual subscription rate of 269 €. Special rate for students on proof of status in the form of current registration certificate 124 €. Special rate for VDI/ÖVK/VKS members on proof of status in the form of current member certificate 208 €. Special rate for studying VDI members on proof of status in the form of current registration and member certificate 89 €. The subscribtion can be cancelled in written form at any time with effect from the next available issue.

PRODUCTION | LAYOUT

Kerstin Gollarz
Phone +49 611 7878-173 · Fax +49 611 7878-464
E-Mail: kerstin.gollarz@gwv-fachverlage.de

HINTS FOR AUTHORS

All manuscripts should be sent directly to the editors. By submitting photographs and drawings the sender releases the publishers from claims by third parties. Only works not yet published in Germany or abroad can generally be accepted for publication. The manuscripts must not be offered for publication to other journals simultaneously. In accepting the manuscript the publisher acquires the right to produce royalty-free offprints. The journal and all articles and figures are protected by copyright. Any utilisation beyond the strict limits of the copyright law without permission of the publisher is illegal. This applies particularly to duplications, translations, microfilming and storage and processing in electronic systems.

Crash Safety through Side Impact Protection

Aprosys Project for Environmental Sensorics

In the moments before a collision, only fractions of a second remain, in which to activate additional side impact protection and provide the passengers with better protection. As part of the European Aprosys project, a system has been developed, which can detect accidents at an early stage by using radar and video sensors and which uses a new type of very rapid actuator to activate the side impact protection. The project has been headed by engineers at Continental, the international automotive supplier.

1 Introduction

Side collisions pose a particularly high risk of injury to drivers and passengers. Although frontal and side crashes occur with almost equal frequency, the number of injuries and fatalities from side crashes is greater. The reason for this is that, at the moment of initial impact, there is only a narrow gap between the occupants and any object, which penetrates the vehicle. The existing impact detection technology can only detect a crash on initial impact, allowing insufficient time for collision-mitigating measures to be triggered.

To overcome this, an integrated side impact protection system was built up in the sub-project No. 6 of the European Aprosys (Advanced Protection Systems) research project, made of two sub-systems. For the first time, this system combines the following innovative sub-systems in a car: a sensor sub-system and an actuator sub-system. The sensor sub-system consists of radar and stereo camera. It monitors the road area to the front and side of the vehicle, determines that a collision is imminent and activates the actuator sub-system before the impact occurs so as to reduce the effect on the passenger compartment. This gives other conventional devices such as airbags more time and space to protect the occupants.

The actuator sub-system is based on shape memory alloys made of wires. To reduce the severity of a side impact the structural deformation of the body should be decreased. This could be possible when directing the impact forces to those rigid vehicle structures not affected by the impact.

The system concept is based on a thorough analysis of accident statistics. Various side impact protection approaches were examined using multibody [1] and finite element [2] simulations. Human behavior in side impact situations was also investigated [3]. Following these studies, the sensor and actuator sub-systems were defined, developed, installed in various vehicles and finally tested.

2 Sensor Sub-System

Requirements for the sensor sub-system were derived from the detailed study of actual impact angles and related fatality numbers [4]. In order to detect the great majority of side impacts and to be able to deliver useable data to the actuator sub-system, the sensor sub-system had to:
- detect and track objects impacting the side of the vehicle
- determine the size and shape of the impacting objects (classification)

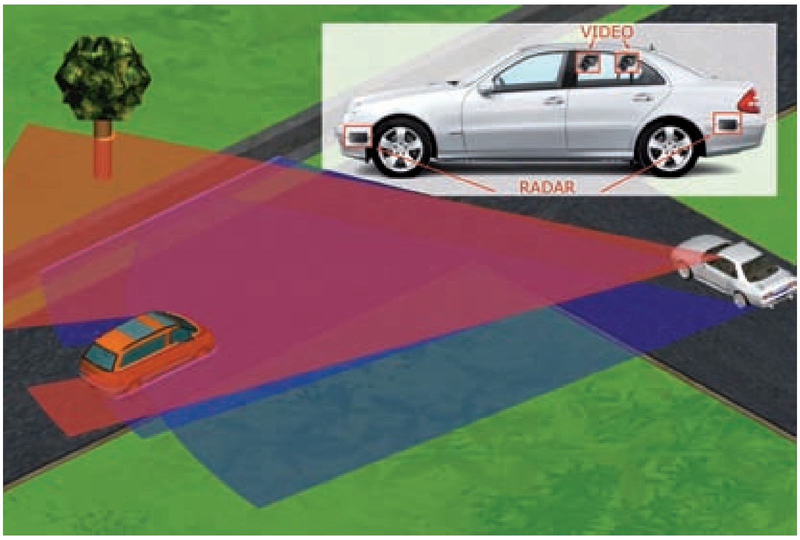

Figure 1: Installation position and surveillance field – the surveillance area lies to the side, both in front of and alongside the vehicle (blue: radar sensors, red: stereo camera); the two radar sensors are fitted below the front and rear bumpers; and the stereo camera in the region of the rear side window

The Author

Dr.
Joachim Tandler
is expert for radar and fusion systems in Continental's Chassis & Safety Division in Lindau (Germany).

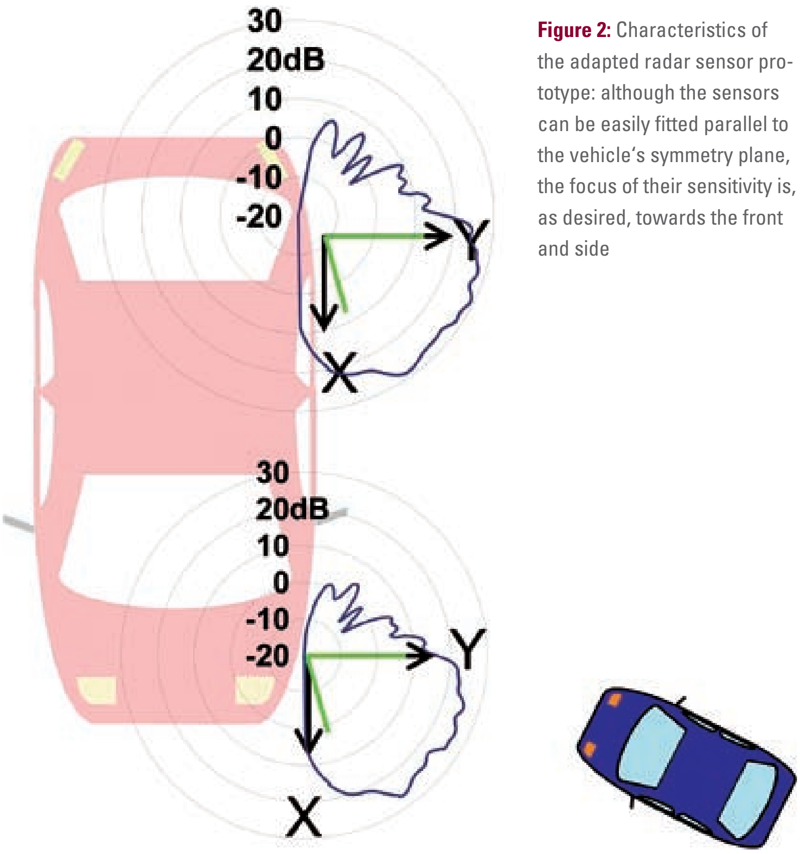

Figure 2: Characteristics of the adapted radar sensor prototype: although the sensors can be easily fitted parallel to the vehicle's symmetry plane, the focus of their sensitivity is, as desired, towards the front and side

- establish the risk of an impact and decide whether a collision was about to occur at least 200 ms before impact
- monitor an area over a range of 20 m both to the side and front of the vehicle; impacts occur most frequently at an angle of 90°, that means a classic accident due to a failure to give way, and at 60°, typical of a collision when turning off.

The task could be solved by a multi-sensor system, consisting of a radar sensor network (two sensors) and a stereo video camera on each side of the vehicle, **Figure 1**. Primarily was to process the data from each type of sensor separately. Then a fusion module collated the data before a decision module calculated the risk of an impact and finally triggered the actuator sub-system.

The short-range radar was adapted to meet the specific requirements for monitoring the side of the vehicle. It operated at a frequency of 24 GHz with a signal bandwidth of 1000 MHz. The sensors simultaneously measured the distance (accuracy: 0.1 m), angle (accuracy: 2°) and relative velocity (accuracy: 1 m/s) of an approaching object. The radar sensors were invisibly installed below the front and rear bumpers. So that it could be simply fitted parallel with the vehicle symmetry plane, the radar antenna was adapted to look forwards and sideways, **Figure 2**.

A stereo video camera was chosen to operate together with the radar network. When developing a sideways-looking video pre-crash system, a number of differences to a forward-looking perspective had to be dealt with. When the camera is oriented to the side of the vehicle, then other vehicles are mainly seen from the side, and they are so close that they are only partly seen in the video images. Consequently, a number of image properties that are successfully exploited in a forward-looking system (such as symmetry) are no longer available. In addition, lane markings are occluded most of the time, and hence unavailable to limit the area under surveillance and to identify those objects that are important more easily.

For these reasons, a more general approach had to be taken: Object hypotheses were obtained from so-called depth maps resulting from stereo analysis. Depth maps consist of three-dimensional point clouds. They are built up by finding corresponding pixels in the two video images. The distance from the camera can be calculated from the pair of pixels.

As soon as a depth map has been produced, the object's position on the road is estimated. The object points are then separated from the road points and grouped into clusters. Tracking these

Figure 3: A demanding task – raw images from a sideways-looking stereo camera; epipolar curves (magenta) for the correspondence search in the original image geometry have been drawn in

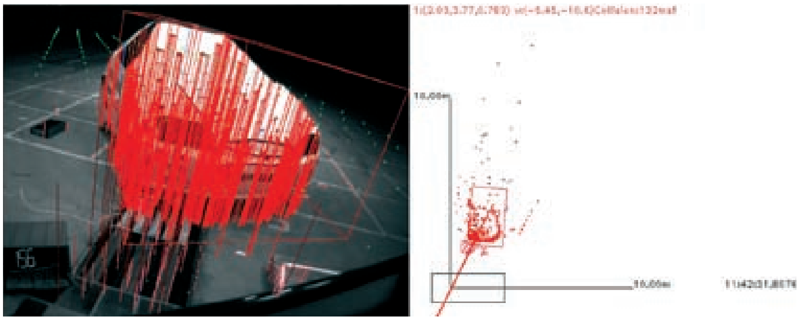

Figure 4: Results from side pre-crash detection, based on stereo analysis: on the left, an original image with the 3D points detected and their horizontal plane projection; on the right, a top view of the 3D points

clusters makes it possible to estimate how the objects being observed will move and to calculate their behavior in advance. Combining this with the estimate of one's own movement allows a collision prediction to be made.

In order to cover the surveillance area, the two cameras have wide opening angles and are arranged offset. As a consequence, the images cannot be transformed into epipolar geometry with reasonable computational effort, while this is standard in other stereo systems, **Figure 3** and **Figure 4**. The search for corresponding pixels takes place directly in the original images. During analogous features in epipolar geometry are localized on straight lines, now they have to be searched for on complex epipolar curves.

A box in Figure 4 represents the object hypothesis. The object's estimated position, relative speed and time to collision are printed in red.

Further challenges presented by a sideways-oriented pre-crash system are the short observation time and the object's generally complex trajectory. Additionally, the long period has to be mentioned, for which a prediction needs to be made.

The fusion system, **Figure 5**, joins matching video and radar objects together and transfers them to the decision module. The combination of the two types of sensor makes it possible to avoid false alarms but, at the same time, to remain highly effective as regards the early detection of imminent side collisions.

The decision module produces a risk estimate, **Figure 6**: it extrapolates from all the objects it identifies and calculates the time to collision (TTC). It decides whether it is physically possible to avoid a collision by braking or steering and calculates a collision probability. If the TTC and the collision probability exceed certain limits, the actuator system is alerted (compare also with [5]).

The lines in Figure 6 indicate, by means of linear extrapolation, where an object will be one second later. Small red squares on the test vehicle show possible impact points. In a case like this, a signal needs to be sent to trigger the actuator system.

In order to test whether the sensor and fusion system worked, trials were conducted in the crash laboratory of the company TNO, in which a test sled approached the vehicle under test at different angles at a speed of 50 km/h. Using an independent method, position and velocity of the sled were measured. The result: the system was capable of activating the additional impact protection approximately 200 ms before the expected crash – a major advantage over airbag systems, which can only be initiated 5 ms after impact.

The data diagrams a) to d) of **Figure 7** clearly show that the values calculated by the sensor system correspond to the actual positions during the crash test. A test sled approached at an angle of 37° at 50 km/h up to approximately 2 m distance to the host vehicle. Diagram e) shows the time to collision (TTC) calculated by the system's algorithms. The side impact system is only triggered if the TTC values fall below 400 ms. Diagram f) shows that the radar system achieved the additional threshold value of 80 % crash probability at the test time 160.251 s, while the video signal for the left front section detected this threshold at 160.492 s. The actuator system is only triggered, when both thresholds of both sensors are exceeded. Hence, there was still sufficient time for the side impact protection to be reliably activated. Diagram g) demonstrates that the data calculated by the sensors for the time of crash (TOC) varied only negligibly from the actual values. Lastly, the diagram h) gives a bird's eye view of the movement of the test sled with the points calculated by the video and radar sensors.

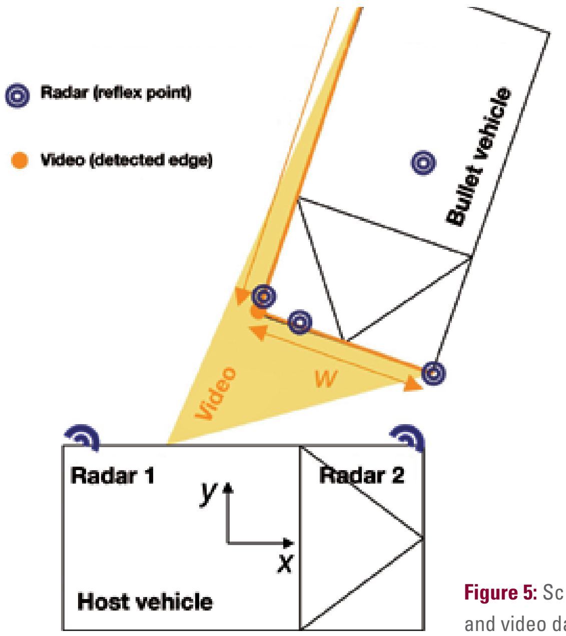

Figure 5: Scheme of the separate radar and video data before fusion

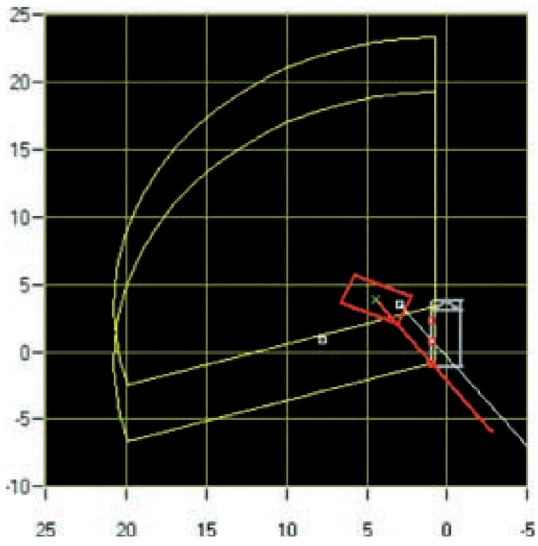

Figure 6: The decision module's view of the traffic situation: the test vehicle fitted with the sensors is shown as a gray rectangle; the red rectangle is an object, which the video system has detected; the small white square is a radar reflection object (all distances in the diagram are given in m)

forcing the B-pillar and directing the impact forces to those rigid vehicle structures not affected by the impact [7]. The latter concept turned out to be most effective. Diverting the impact forces actively opens up a new energy path during the initial contact phase and, as a consequence, relieves the load on the B-pillar and in areas where occupant is seated.

The active device (actuator) realised in this concept is located on the impact side and consists of two parts. The first part is a self-rotating door post, normally in a vertical position. Before the vehicle becomes involved in an accident, the door post moves in a horizontal position, filling the whole door frame. The second part is a tube containing a spring-loaded bolt, fitted crosswise in the seat, directly underneath the seat surface. When the sensors report an imminent crash, the spring-loaded bolt makes a rigid connection between the door and the transverse tube fitted in the seat.

3 Actuator Sub-System

Fatal injuries from a side impact normally occur within the first time segment (70 to 80 ms). These injuries are mainly caused by hard contact between the passenger and the interior fittings. There are narrow limits to what conventional protection systems such as side airbags can achieve because the side structure has only a small energy-absorbing zone.

Reducing the severity of a side impact required a two-pronged strategy. First, there had to be less structural deformation of the bodywork in the area where the occupant's life is at risk. Secondly, contact between the passenger and the interior fittings had to be gentler. In the context of Aprosys the developers concentrated on the first objective, that means on devices, which restrict penetration and thus reduce the deformation of the vehicle structure.

The aim was to evaluate the actuator sub-system through side impact tests with a deformable barrier. For this reason, a test of this nature was carried out at the very start of actuator development both for reference purposes and to optimize the simulation models (Chrysler Neon vehicles, model years 1994 to 1999, were used due to the availability of simulation models). As a result of this study, important structures, which encourage deformation (B-pillar, rocker panels, roof, floor pan, doors), were identified and analyzed.

Various concepts for reducing penetration depth were examined: These included among other things using strong bolts to join the doors to the bodywork, rein-

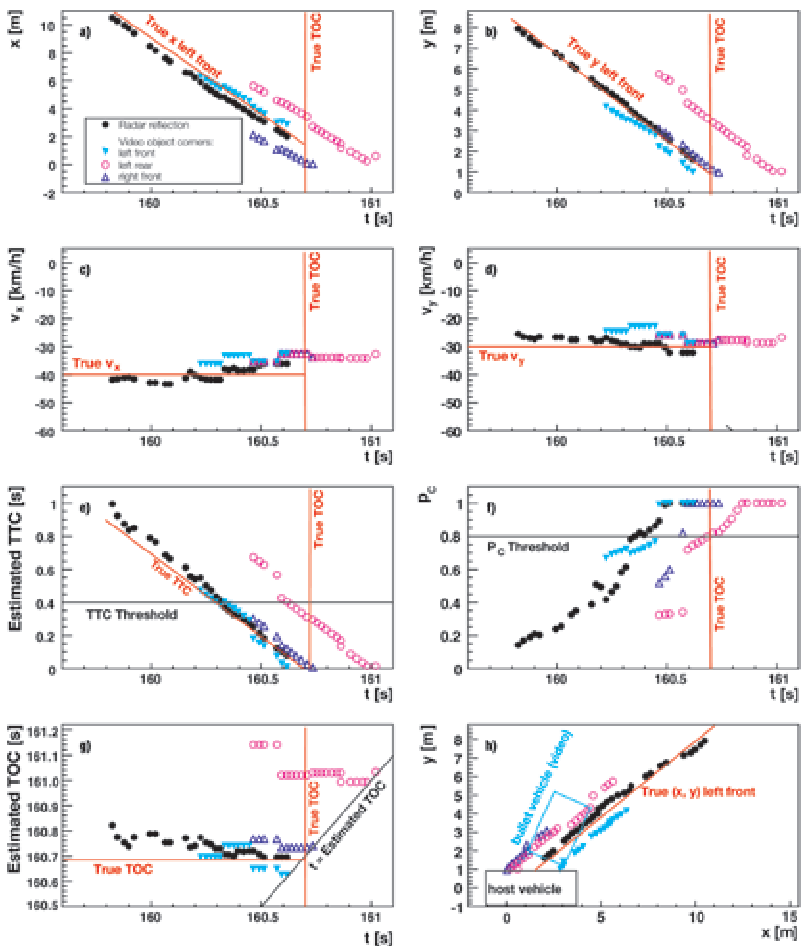

Figure 7: Data diagrams (explanations see text)

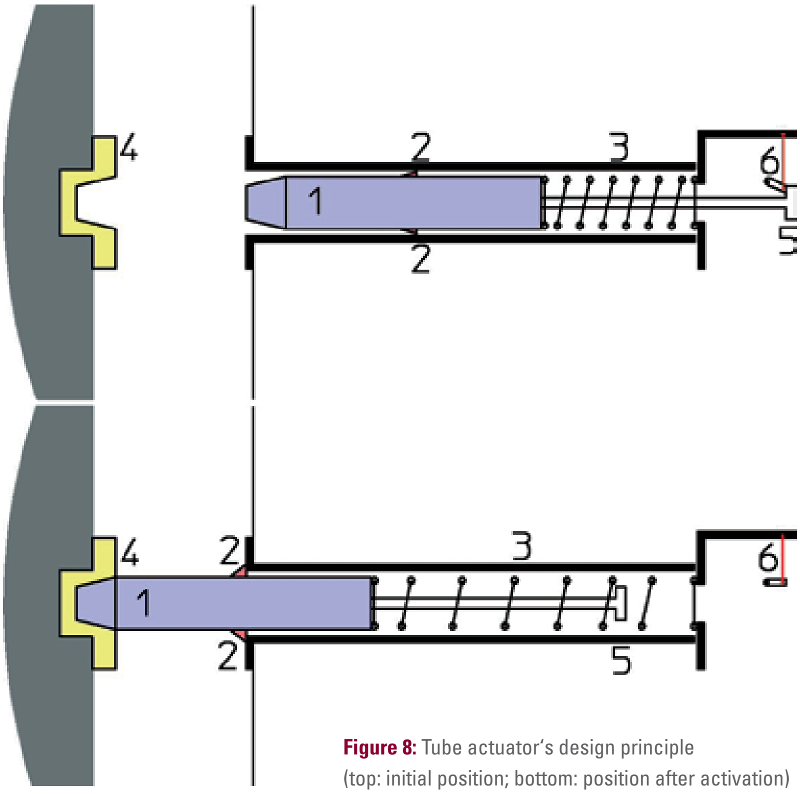

Figure 8: Tube actuator's design principle (top: initial position; bottom: position after activation)

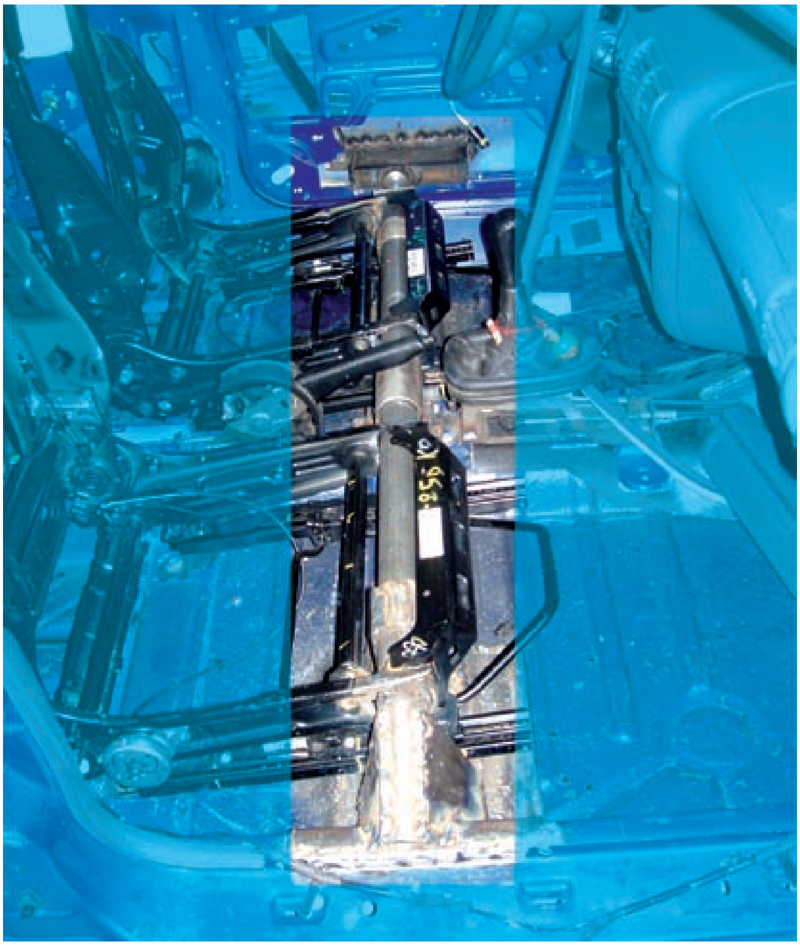

Figure 9: The actuator system, installed in a test vehicle

This seals all the gaps between the outer metal skin and the seat.

Figure 8 shows the tube actuator's design principle. A bolt (1), normally seated in a housing, can be propelled by a preloaded steel spring (3) from its original position (in the seat frame) to its activated position. In this activated position, the point of the bolt is guided by a mating piece in the door paneling (4). Small radially-mounted, expandable components (2) lock the bolt into position and prevent it from being pushed backwards. The trigger mechanism, which initiates the movement of the bolt, consists of two main parts: a small lever arm, which interacts with the rear end of the bolt (5), and a shape memory alloy wire (6), which, when activated, pulls the lever arm so as to release the bolt.

The transverse tubes of the actuator sub-system in the seats and the reinforcement in the center tunnel area can be clearly seen in **Figure 9**. The gap between the driver's seat and the reinforcement in the driver's door is sealed by the actuator; on the front-passenger side, the impact energy is diverted to the rocker panel.

3.1 Shape Memory Alloy Principle

Once both the concept and design for the actuator system had been established, the final actuator prototype was produced. It is fitted with a release mechanism, consisting of a shape memory alloy (SMA) wire [6]. It is well suited to the Aprosys project's time-critical safety application. Smart materials like sheet-like shape memory alloys or piezo-ceramics are not yet used as standard in crash applications.

The design principle of SMA is based on regrouping the molecular lattice. When heated, the material distorts; when cooled, it returns to its original shape. Several ways of heating an SMA module were examined. Using the vehicle's coolant, engine oil or chemicals was rejected due to safety risks. It was therefore decided to heat the module using electricity from a capacitor, which is charged by the vehicle's battery. A microcontroller realises the communication with the sensor system via the CAN bus and controls the activation of the SMA wire.

3.2 Actuator's Performance

The actuators and all the system components were installed in test vehicles and

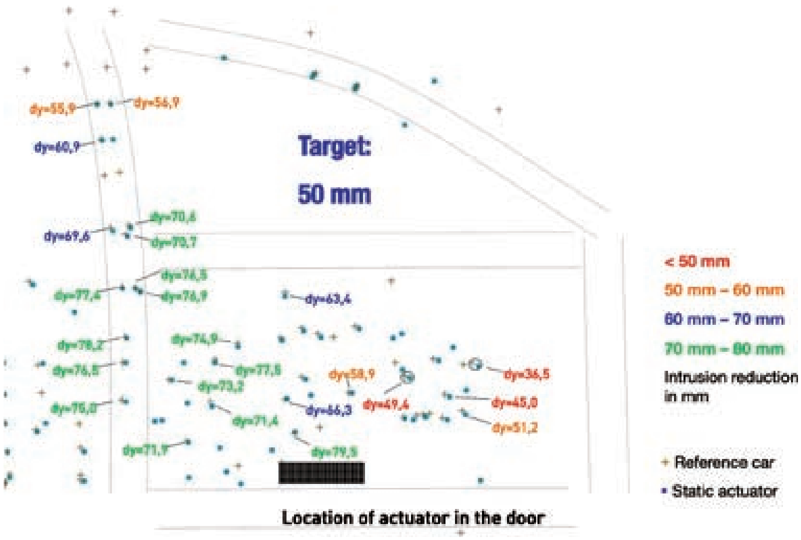

Figure 10: Crash analysis in detail: over a wide area, the penetration depth is reduced by more than the target of 50 mm

the development process was greatly assisted by simulation. The component tests evaluated the SMA actuator's mechanical performance and response time. The tests demonstrated the desired response time and clear repeatability; the actuator moved the bolt (approximately 400 g) 115 mm in 60 ms.

Four side crash tests with deformable barrier based on EuroNCAP, produced reference and improvement values for penetration depth at the B-pillar. The values for a production vehicle without actuator were 488 mm; and 418 mm for a vehicle with optimized actuator. With an actuator, the penetration depth, **Figure 10**, was significantly less, especially in the passenger seat area. During simulation runs in a variety of collision scenarios (collisions with vehicles or poles, at different impact angles and speeds), the actuator system showed itself to be robust, reducing the penetration depth in every case.

The essential gain produced by the actuator system is a reduction in the depth and velocity of penetration over a large area of the door. Interior protection systems (airbags) are given more time and space to deploy more effectively; the impact against the occupant is delayed, thus enabling the impact forces and other biomechanical values to be reduced. The depth of penetration is reduced precisely at the spot where the occupant is seated; survival space and time are won.

Project Participants and Co-authors

Several companies and institutes have collaborated on the Aprosys Sub-Project No. 6:

Dr. Dieter Willersinn, Michael Grinberg; Fraunhofer-IITB (Germany): development of the stereo camera system

Eric Zimmerman, Vlad Muntean; Faurecia (France): actuator subsystem integration, coordination of actuator development

Björn Seipel, Thorsten Koch, Dr. Tobias Melz; Fraunhofer-LBF (Germany): shape memory alloy technology, actuator development

Monica Diez; CIDAUT (Spanien), Jorge Ambrosio; Instituto Superior Técnico (Portugal): simulation and crash test analyses

Tomasz Dziewonski; Warsaw Technical University (Poland): study into driver behavior in side collisions

Richard Schram, Ronald de Lange; TNO (Netherlands): accident statistics analysis, pre-crash tests

Christian Mayer; Daimler (Germany): test coordination, test execution

Author and co-authors like to thank the European Commission for co-funding this Aprosys Sub-Project (TIP3-CT-2004-506503).

4 Evaluation of the Side Pre-Crash System

The final project phase saw an intensive series of tests for the side pre-crash system carried out using an evaluation methodology developed by Aprosys [8]:

- Evaluation of system behavior under normal driving conditions (false alarm rate and comfort aspects) using set maneuvers and a field trial: This test cluster concentrated on the sensor and decision system. The field trial was conducted over a distance of 2000 km through France, Italy, Austria and Germany and produced a total of 60 system false alarms. Although the system under consideration is reversible, this number of false alarms is too high for a series production product. However, the number can be reduced to an acceptable level by further optimization.
- Evaluation of the impact detection rate: the test conditions were based on the most important accident scenarios, taking system and test laboratory restrictions into account. Here, too, the focus was on the sensor and decision system.
- Evaluation of crash performance: a test protocol, based on the EuroNCAP side impact test, was chosen for this. Penetration depth and velocity were measured.

The whole integrated system was subjected to a performance test as the final crash trial. It should be borne in mind that the radar system's impact detection rate might possibly have been smaller due to the test environment in an enclosed hall. In addition, the floodlights installed for the high-speed cameras reduced the effective range of the stereo camera by more than half. Instead of a surveillance range of 20 m, a range of only 8 m was in effect available. The sensors needed to be adjusted to compensate for these disadvantages. Despite the unfavorable conditions, the sensors identified the imminent accident approximately 321 ms before the collision and triggered the side impact protection system in good time.

5 Conclusion

Over the next few years, more and more cars on our roads will be equipped with environmental sensors, making pre-crash data available in good time. SMA actuators will also have a place in automotive engineering.

The conventional passive safety systems in vehicles can be significantly improved by using environmental sensors. Knowing that an accident is about to happen and where the impact will occur opens up many possibilities for providing vehicle occupants with better protection. Once there is a growing market for systems, which give early warning of rear-end collisions or of the vehicle leaving the road, systems for detecting side collisions will be available shortly afterwards.

References

[1] Ambrósio, J.: Improved Protection of Vehicle Occupants in Side Impacts by Using Active Structural Devices. Proceedings of the II International Conference on Computational Biomechanics, 2005, pp 989–1002

[2] Zimmerman, E.; Muntean, V.: Generic FE Simulation Model for the Layout of Pre-Crash Actuators in Side Impact. Proceedings of the Transfac Conference San Sebastian, Spain, 2006

[3] Matusiak, K.; Dziewoński, T.; Lozia, Z.; Guzek, M.: Assessment of Driver's and Passenger's Behaviour when Facing an Imminent Side Crash. Proceedings of the Ircobi Conference, 2005

[4] Tandler, J.; Preis, C.; Willersinn, D.; Grinberg, M.: Side Pre-Crash System Specification. Proceedings of the IEEE Intelligent Vehicles Symposium, Tokyo, Japan, June 13–15, 2006

[5] Tandler, J.; Willersinn, D.; Grinberg, M.: Data Analysis of the Aprosys Side Pre-Crash Sensing System. Proceedings of the IEEE Intelligent Vehicles Symposium, Istanbul, Turkey, June 13–15, 2007

[6] Seipel, B.: Smart Material Based Actuator for an Intelligent Safety System. In: ATZautotechnology 7 (2007), No 6, December 2007

[7] Zimmerman, E.; Muntean, V.: Pre-Crash Actuator to Improve Car Structural Performance in Side Impact. Proceedings of the EAEVC Conference, Budapest, Hungary, 2007

[8] Lange, R. de: Proposal of Generic Procedures for an Assessment of Pre-Crash Systems. Public Aprosys Deliverable D6.5.1, 2007

IMPRINT

ATZ WORLDWIDE

www.ATZonline.com

11|2008 · November 2008 · Volume 110
Springer Automotive Media | GWV Fachverlage GmbH
P. O. Box 15 46 · 65173 Wiesbaden · Germany
Abraham-Lincoln-Straße 46 · 65189 Wiesbaden · Germany

Managing Directors Dr. Ralf Birkelbach, Albrecht Schirmacher
Senior Advertising Thomas Werner
Senior Production Ingo Eichel
Senior Sales Gabriel Göttlinger

EDITORS-IN-CHARGE

Dr.-Ing. E. h. Richard van Basshuysen
Wolfgang Siebenpfeiffer

EDITORIAL STAFF

Editor-in-Chief
Johannes Winterhagen (win)
Phone +49 611 7878-342 · Fax +49 611 7878-462
E-Mail: johannes.winterhagen@springer.com

Vice-Editor-in-Chief
Dipl.-Ing. Michael Reichenbach (rei)
Phone +49 611 7878-341 · Fax +49 611 7878-462
E-Mail: michael.reichenbach@springer.com

Chief-on-Duty
Kirsten Beckmann M. A. (kb)
Phone +49 611 7878-343 · Fax +49 611 7878-462
E-Mail: kirsten.beckmann@springer.com

Sections

Body, Safety
Dipl.-Ing. Ulrich Knorra (kno)
Phone +49 611 7878-314 · Fax +49 611 7878-462
E-Mail: ulrich.knorra@springer.com

Chassis
Roland Schedel (rs)
Phone +49 6128 85 37 58 · Fax +49 6128 85 37 59
E-Mail: ATZautotechnology@text-com.de

Electrics, Electronics
Markus Schöttle (schoe)
Phone +49 611 7878-257 · Fax +49 611 7878-462
E-Mail: markus.schoettle@springer.com

Engine
Dipl.-Ing. (FH) Richard Backhaus (rb)
Phone +49 611 5045-982 · Fax +49 611 5045-983
E-Mail: richard.backhaus@rb-communications.de

Heavy Duty Techniques
Ruben Danisch (rd)
Phone +49 611 7878-393 · Fax +49 611 7878-462
E-Mail: ruben.danisch@springer.com

Online
Dipl.-Ing. (FH) Caterina Schröder (cs)
Phone +49 611 7878-190 · Fax +49 611 7878-462
E-Mail: caterina.schroeder@springer.com

Production, Materials
Stefan Schlott (hlo)
Phone +49 8191 70845 · Fax +49 8191 66002
E-Mail: Redaktion_Schlott@gmx.net

Service, Event Calendar
Martina Schraad
Phone +49 212 64 232 64
E-Mail: martina.schraad@springer.com

Transmission, Research
Dipl.-Ing. Michael Reichenbach (rei)
Phone +49 611 7878-341 · Fax +49 611 7878-462
E-Mail: michael.reichenbach@springer.com

English Language Consultant
Paul Willin (pw)

Permanent Contributors
Christian Bartsch (cb), Prof. Dr.-Ing. Peter Boy (bo), Prof. Dr.-Ing. Stefan Breuer (sb), Jens Büchling (jb), Jörg Christoffel (jc), Prof. Dr.-Ing. Manfred Feiler (fe), Jürgen Grandel (gl), Erich Hoepke (ho), Prof. Dr.-Ing. Fred Schäfer (fs), Bettina Seehawer (bs)

Address
P.O. Box 1546, 65173 Wiesbaden, Germany
E-Mail: redaktion@ATZonline.de

MARKETING | OFFPRINTS

Product Management Automedia
Sabrina Brokopp
Phone +49 611 7878-192 · Fax +49 611 7878-407
E-Mail: sabrina.brokopp@springer.com

Offprints
Martin Leopold
Phone +49 2642 9075-96 · Fax +49 2642 9075-97
E-Mail: leopold@medien-kontor.de

ADVERTISING | GWV MEDIA

Key Account Manager
Elisabeth Maßfeller
Phone +49 611 7878-399 · Fax +49 611 7878-140
E-Mail: elisabeth.massfeller@gwv-media.de

Ad Sales
Sabine Röck
Phone +49 611 7878-269 · Fax +49 611 7878-140
E-Mail: sabine.roeck@gwv-media.de

Heinrich X. Prinz Reuß
Phone +49 611 7878-229 · Fax +49 611 7878-140
E-Mail: heinrich.reuss@gwv-media.de

Display Ad Manager
Sandra Reisinger
Phone +49 611 7878-147 · Fax +49 611 7878-443
E-Mail: sandra.reisinger@gwv-media.de

Ad Prices
Price List No. 51

SUBSCRIPTIONS

VVA-Zeitschriftenservice, Abt. D6 F6, ATZ
P. O. Box 77 77, 33310 Gütersloh, Germany
Renate Vies
Phone +49 5241 80-1692 · Fax +49 5241 80-9620
E-Mail: SpringerAutomotive@abo-service.info

SUBSCRIPTION CONDITIONS

The emagazine appears 11 times a year at an annual subscription rate of 269 €. Special rate for students on proof of status in the form of current registration certificate 124 €. Special rate for VDI/ÖVK/VKS members on proof of status in the form of current member certificate 208 €. Special rate for studying VDI members on proof of status in the form of current registration and member certificate 89 €. The subscribtion can be cancelled in written form at any time with effect from the next available issue.

PRODUCTION | LAYOUT

Kerstin Gollarz
Phone +49 611 7878-173 · Fax +49 611 7878-464
E-Mail: kerstin.gollarz@gwv-fachverlage.de

HINTS FOR AUTHORS

All manuscripts should be sent directly to the editors. By submitting photographs and drawings the sender releases the publishers from claims by third parties. Only works not yet published in Germany or abroad can generally be accepted for publication. The manuscripts must not be offered for publication to other journals simultaneously. In accepting the manuscript the publisher acquires the right to produce royalty-free offprints. The journal and all articles and figures are protected by copyright. Any utilisation beyond the strict limits of the copyright law without permission of the publisher is illegal. This applies particularly to duplications, translations, microfilming and storage and processing in electronic systems.

Springer Automotive Media is part of the specialist publishing group Springer Science+Business Media.

personal buildup for Force Motors Ltd.

New Airbag Technologies
Micro Module by Vacuum Folding

The development of airbag modules requires safe fulfillment of legal standards and technical specifications. In many cases this means a limitation to the realization of new designs. With its vacuum folding technology and micro module concept, Takata-Petri offers an innovative approach to realize revolutionary or retro designs not alone in vehicle studies but also to bring them onto the streets as series applications.

1 Market Requirements

Studies introduced at the IAA or the Geneva Motor Show show more and more airbag modules with grossly reduced packages. The presented designs often remind us of steering wheels from times when there were no airbags yet. If we want to fulfill such design wishes of steering wheels that come from almost every car manufacturer all over the markets, it will be necessary to reduce the package dimensions for airbag modules significantly. Here, challenging demands are made on the developers as in terms of performance of the airbag where no cut backs can be allowed. Takata-Petri took up this challenge and developed vacuum-folded airbags in a classical pre-development project from the idea to readiness for start of production. Meanwhile, the technology has left the status of pre-development and is being developed for several customers in application projects intended for the next generation of vehicles.

While the reduced package on the driver side mainly results in design benefits, the additional space on the passenger side is especially valuable for bigger glove boxes, cable channels, ventilation ducts, etc. The requirements a vacuum-folded airbag system has to meet do not differ from the ones that a conventionally folded module has to offer.

Hence, the respective crash load cases in legal and consumer tests should be met with best ratings. Thus, it becomes necessary to provide the protection potential of the system as soon as possible on the one hand. Filling times for the airbag of the driver side are between 25 ms and 30ms and on the passenger side between 35 to 40 ms. On the other hand, the system has to fulfill its task as a lifesaver for all sorts of occupants. To do so, several dummies are applied to adapt the frontal restraint system to the respective conditions. The 95-ile dummy (which corresponds to a big and heavy-weight man), the 50-ile dummy (which represents the average citizen) the 5-ile dummy (which corresponds to a small and lightweight woman) and the child dummies mirror nearly the complete spectrum of possible vehicle occupants.

First, this becomes true for occupants sitting correctly in the vehicle. But also occupants being so-called “out-of-position” must not be put at any risk by a modern airbag system.

The function of the component “airbag” is mostly defined by the Statement of Requirements issued by the different car manufacturers. This means, e.g., that an airbag module has to guarantee its full function over a period of at least 15 years. Full functionality includes that the airbag has to show an almost identical deployment behavior in a temperature range from -35° C to +85° C. After firing the airbag, no fragments or parts must peel off from the airbag module. Additional tests with the airbag exposed to salt spray, humidity, heat, vibrations, electromagnetic rays, etc. must not re-

Figure 1: Size comparison between a conventional airbag module and a vacuum folded airbag module

The Authors

Claus Rudolf
is head of the Core Engineering Front and Numerische Simulation at the Takata-Petri AG in Aschaffenburg (Germany).

Frank Sauer
is head of the Core Engineering Front Airbags at the Takata-Petri AG in Aschaffenburg (Germany).

Tobias Fechner
is project leader Vacuum Folding Technology and specialist for passenger airbags in the division Core Engineering Front Airbags at the Takata-Petri AG in Aschaffenburg (Germany).

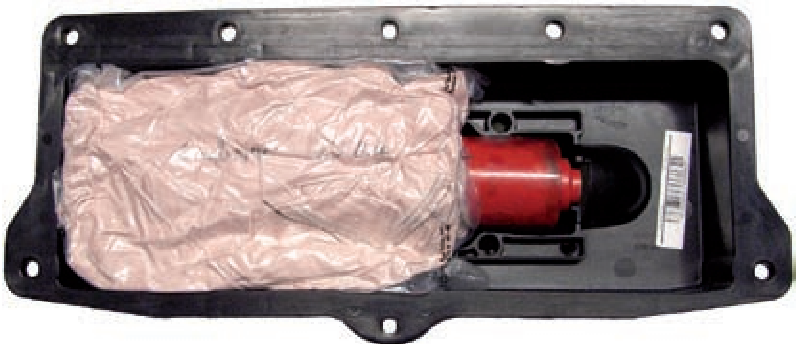

Figure 2: Design space potential for a passenger airbag by using vacuum folding technology

sult in any functional failures. All these requirements are fulfilled with the newly developed folding method just as well as with conventional modules.

2 Vacuum Folding – Description and Application

For integrating an airbag into the available package space, it is necessary to fold it. For the performance of the system the deployment kinematics of the airbag are of outstanding importance. Kinematics can be controlled by the airbag folding and this is the reason why vehicles meanwhile saw a variety of folding schemes for their airbags. These foldings are adapted to the airbag size, the requirements of the restraint system and the size of the car interior- only to mention some of the criteria to consider. For many years now, the fully automated slider folding patented by Takata-Petri, the so-called Petri folding for driver and passenger airbags, has proved its value. Many millions of cars are already equipped with airbags folded like this.

Conventional folding methods need about 0.6 l folding volume for a standard airbag (siliconized fabric, integrated tethers) with an operating volume of 60 to 65 liters on the driver side. Vacuum-folded airbags are able to reduce the folding volume for the same airbag to approximately 0.35 liters. On average, a reduction of the folding volume of 35 to 50 % can be achieved, depending on the design of the bag. **Figure 1** shows a conventionally folded airbag module compared to a vacuum-folded module. On the passenger side, package reductions of up to approximately 50 % are possible. In **Figure 2** we can see a vacuum-folded passenger airbag in a housing designed for an identical airbag but without vacuum folding.

In order to achieve such package sizes, the airbag is first laid flatly on a folding table. Then four sliders form the airbag into the desired basic shape. A punch showing the same dimensions as the basic area presses the reduced package into the cup-shaped underlay foil. Afterwards, a vacuumization unit integrated in the folding machine evacuates the ambient air so that the underlay foil can be welded with the upper foil. The return to the original condition of the ambient pressure produces the final shape of the airbag package. **Figure 3** gives an impression of a driver airbag welded into a foil and folded by machine. This technology is used by default in the pharmaceutical and food industry so that we had an approved technology to rely on. The focus of development was on the integration of the vacuum technology into the existing folding machines and to adapt the design of the folded package according to automotive criteria. This made it necessary to develop new foil technologies. The development was aimed at reaching the required 15 years of functionality of the vacuum package and at making sure the robustness of the module over the temperature range during the highly dynamical airbag deployment process. The foil is not allowed to produce any delays in the deployment behavior of the system. All these challenges have been mastered and meanwhile there is already the next generation of upper foils available.

On their surface they have imprinted warnings thus allowing the substitution of softcovers which have been used so far. If necessary, the upper foils can also be equipped with integrated opening contours. They simulate the course of the airbag cover split-lines and do thus provide a synchronous opening behavior of cover and foil even for complicated airbag cover designs. Production lines which allow for the integration of this technology into the existing folding process are available in manufacturing. A highly automated folding process combined with an easy-to-mount micro module concept guarantees that the increase of cycle times in production does not have any adverse effects on the efficiency at all. This makes it possible to provide the technology for vehicles coming in high quantities.

Figure 3: Vacuum folded standard driver airbag

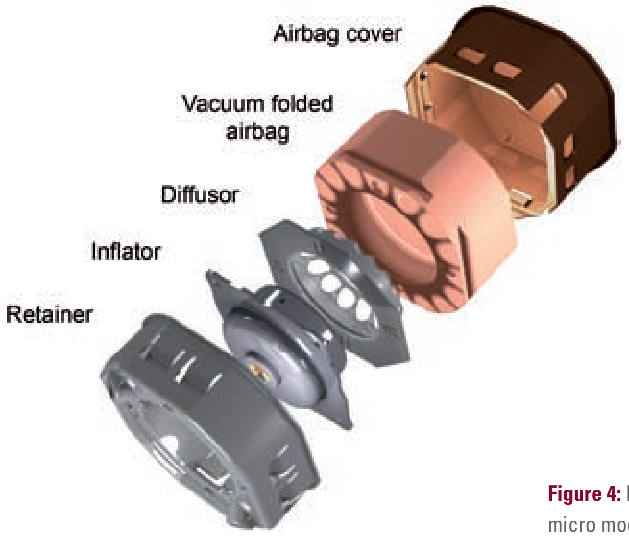

Figure 4: Exploded view of a micro module

Figure 5: Height reduction of an airbag module by vacuum folding

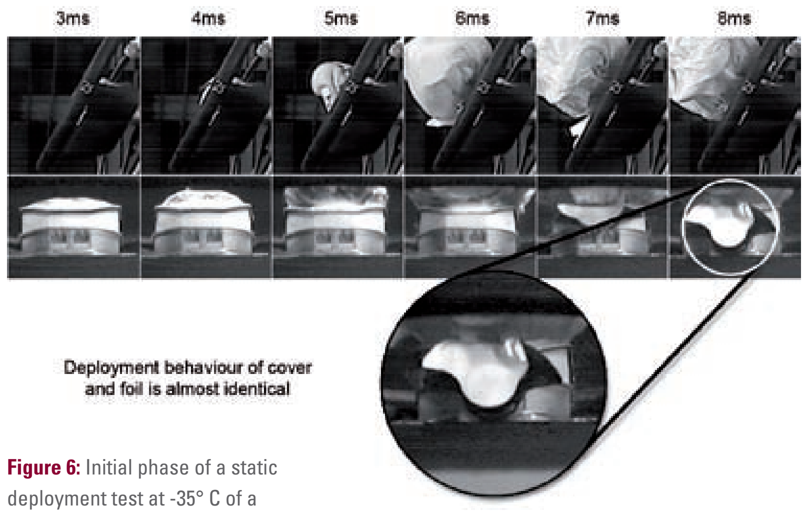

Figure 6: Initial phase of a static deployment test at -35° C of a driver airbag

3 Micro Module Concept – Driver Side and Passenger Side

The micro module unites technical innovations such as vacuum folding technology, new and lightweight gas inflators, lighter airbag fabrics with the current standards like 64-liter airbag and oop-optimized opening concepts of the airbag cover. Moreover, a mounting concept free of screws and rivets corresponds to the requirements of highly automated and perfect production processes. **Figure 4** shows the exploded view of an airbag module concept "optimized footprint" with vacuum-folded airbag. This driver module consists of standard components that are already available. Provided the module has a square footprint, the design allows a side length of 97 mm and a module height of 100 mm. Additional package optimizations such as lighter fabric (235 dtex) e.g., make it possible to reduce the side lengths under 90 mm and the heights to 80 mm. Package-optimized modules can achieve minimal heights of 40 mm if the side lengths are about 102 mm. The micro module concept, however, is not restricted to angular cross-sections. It can also serve for round module shapes as well as for concave or convex-bent outside surfaces. **Figure 5** gives an example of how much the height of an identical airbag module can be reduced if vacuum folding is used.

The airbag cover which is optimized in terms of weight and performance consists of thermoplastic material developed by Takata. This material stands out due to its low density and constant material characteristics at high and low temperatures. Due to its quality features it is already used in series production. The retainer is made of steel as it has thinner walls than the cover. A thermoplastic version, however, is possible too when it comes to bigger dimensions. The gas inflator used is a pyrotechnical, single-staged variant from the Takata-Petri product portfolio. Diffuser and airbag form a joint package. The several components are connected by bond clamping. The fixation with the steering wheel can be realized by screwing or snapping-in. Additional equipment like dual-staged inflator, vibration absorber or adaptivity can be integrated by modules when it is required. The driver airbag variant displayed in Figure 4 has a total weight of 820 g.

The concept for the passenger side essentially corresponds to the bond clamping on the driver side. Here, the shrink-wrapped airbag package is clamped by attachment strips to the housing. The smaller airbag package may reduce the weight of the housing by up to 35 % as shown in Figure 2. Due to the modular concept, the system might be adapted according to the requirements as well; i.e., mounting of single or dual-staged inflators with different performance is possible without changing the design, and a

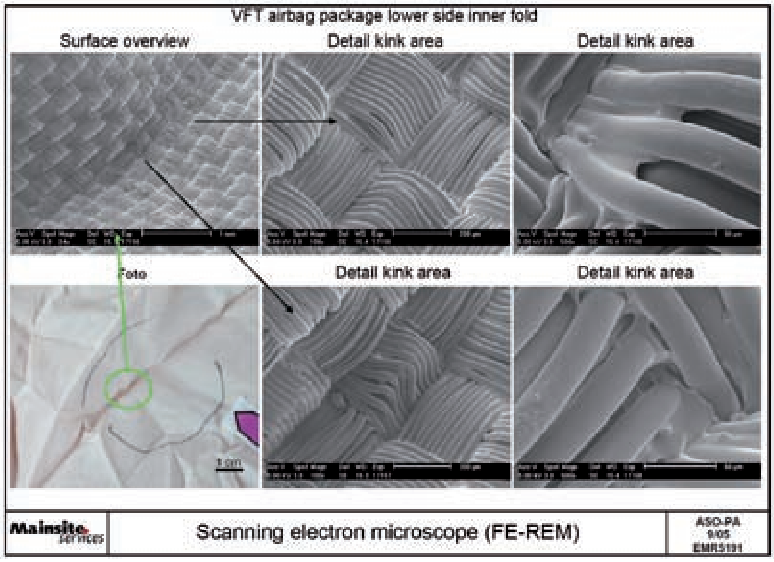

Figure 7: Microscopic analysis of a vacuum folded airbag fabric

variety of airbag sizes and shapes as well as adaptivity is individually applicable.

4 Component Performance

The vacuum folding developed by Takata does not lead to any delay in the airbag deployment behavior, nor does it change the performance of the component. Highest capability has been proven in both trigger tests and environmental simulations. Altogether, about 200 static deployment tests have been conducted over the complete temperature range. **Figure 6** shows the initial phase of an airbag trigger test at -35°C. Depending on the customer's Statement of Requirements, this means for instance testing for heat aging, humidity, dust, or salt spray. But also standardized tests such as environmental simulations according to AKLV 01 have been successfully conducted. Not only new and undamaged airbag packages have been mounted into the modules, but also damaged and perforated ones in order to detect possible damages in the fabric caused by penetrating humidity. All tests conducted were not only passed successfully but it was also possible to prove an increased protection potential for the airbag as it is additionally protected against humidity and dust by the foil.

Discussions with car manufacturers and the growing experience with the new product resulted in further examinations. One of the biggest concerns of quality managers was, for example, what would happen to the appearance of the airbag if the vacuum package lost its density over the years. Is the escalating airbag able to exert so much force on the airbag cover that the split-off lines of the covers might become visible to the customer? To answer this, airbag packages in mounted modules have been destroyed at defined moments. The forces the damaged airbag package develops to press against the cover were measured on test benches specially developed for this purpose. The results showed that just after less than two weeks the airbag kept its micro shape and, hence, there is no loss of quality to expect. Further investigations should reveal if the high packing density in such a small package might bend or fold the airbag fabric in such a way that it might be damaged. For this, microscopic analyses have been done with new and aged fabrics, **Figure 7**. With exceptions on single filament level, no damages at the airbag fabric could be detected. Also in this case, any customer's concern could be allayed.

The robustness of the clamping connections and the strength of the module have already been tested and optimized by numerical simulation before the first prototype had been available. Therefore, the geometries have been modeled with maximum accuracy on the basis of Finite Elements. All used components are modeled with the respective materials and connecting elements and fully deformable. A virtual folding process displaying the real process in any detail led to an airbag package that in terms of size and draping of the folds is almost identical to the real package. The model even considers the foil used for the folding package, **Figure 8**.

Both the opening behavior of the airbag cover and the integrity of the module

Figure 8: Explosion view of a FEM model from a micro module incl. foil and pictures of a simulated deployment behaviour

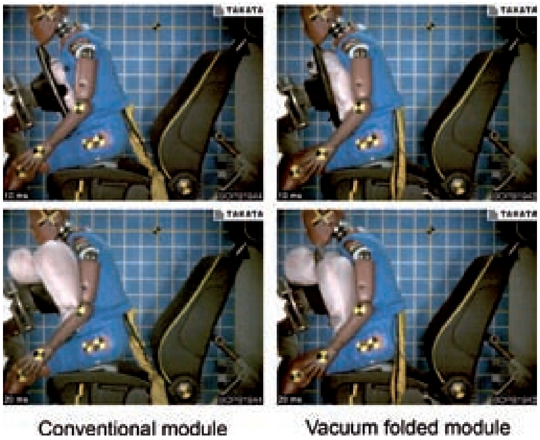

Figure 9: Out of position behaviour (Position 2) comparison between a conventional airbag module and a vacuum folded airbag

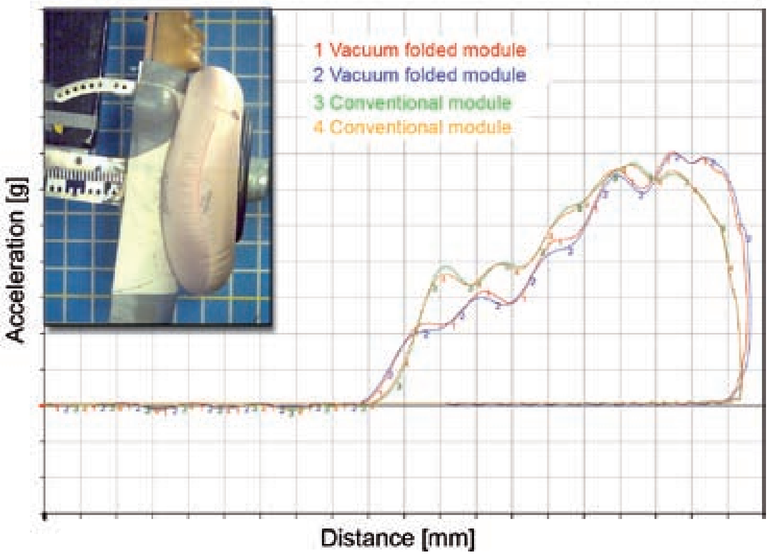

Figure 10: Identical energy absoption performance of a standard airbag module and a vacuum folded module at a pendular test

as well have been analyzed by computer for several temperatures. The airbag simulations have been performed by standard solvers for the automotive industry.

5 Restraint System Performance – In and Out of Position

A small and compact airbag module does not automatically mean compromises for the performance of the restraint system in so-called in- and out-of-position cases. The present concept is even able to significantly fall below legal and customers' requirements. The small airbag footprint and the resulting smaller cover segments offer the airbag enough space to deploy free in out-of-position situations. The reduced package volumes allow for large-scale dished module concepts. The upper edge of the module is located as distant as possible under the steering wheel rim level and thus fulfils one of the basic conditions for a very good behavior when being out-of-position. Studies using the smallest possible modules did not show any irregularities that could have adverse effects compared to conventional modules. **Figure 9** shows a comparison of the deployment process between a conventional module and a micro module in an out-of-position case. The vacuum-folded module, however, has a quite better deployment behavior because the airbag does not expand too much into head direction and, hence, neck forces and moments can be held on a lower level. The values achieved in position I and II are below the 70 to 80 % of the sharp American limits according to FMVSS208 that are required by the car manufacturers.

As mentioned in chapter 4, conventional modules and vacuum-folded modules reach identical filling times in static deployment tests. This is why there are no differences between the two module types when used in restraint systems. The energy absorbing behavior does not show any differences between them, **Figure 10**. The occupant protection values achieved in different in-position configurations (normal occupant positions) in full scale and sled tests correspond to those of conventional modules. The vacuum folding evidently does not result in any disturbance of the system performance.

6 Outlook

Apart from spectacular new steering wheel designs, **Figure 11**, the integration of small and compact airbag units also offers the chance of generating more space to integrate further functions such as vibration motors for warning the driver, additional switches, etc. On the other hand, a small, package- and weight-optimized airbag module contributes to the weight reduction of the vehicle finally leading to less gas consumption and CO^2 -emissions. Within t has proven that the vacuum folding technology has reached the necessary maturity degree for series production. This has already been awarded by some car manufacturers by placing concrete application orders at Takata. Thus, a new era has begun for frontal airbags. An adaptation of this technology for side airbags is under way. ■

Figure 11: Future steering wheel design

The Dynamic Performance Control from BMW

The new BMW X6 is the most sporty member of the BMW X model family. As well as having xDrive, the intelligent four-wheel drive system, it is the first car to be equipped with torque vectoring technology (Dynamic Performance Control) as standard, for targeted optimisation of driving dynamics.

1 Introduction

The innovative Dynamic Performance Control system in the BMW X6 opens up a new dimension combining powerful drives and sports chassis. It continues the xDrive idea of variable drive torque distribution in order to optimise driving dynamics: Torque is distributed to the rear wheels according to requirements, thereby increasing not only driving safety and traction, but in particular, the car's agility. Therefore, Dynamic Performance Control represents the logical and consistent further development of xDrive four-wheel drive technology at BMW, based on controllable torque distribution systems. A revolutionary architectural approach has been taken for integrating this in conjunction with driving dynamics control systems. The final drive is the modern form of a patent filed in the 1930s.

2 Functional Characteristics and Customer Benefits in Terms of Driving Dynamics

The primary development targets were to achieve excellent driving dynamics and maximum driving safety. In addition to the driving dynamics control systems familiar from the X5 (Dynamic Drive, Electronic Damper Control (EDC), Active Steering, Dynamic Stability Control (DSC) and distribution of drive torque between the front and rear axles according to requirements by xDrive), the rear axle of the X6 is the first to feature Dynamic Performance Control as standard. This torque vectoring system (TV system) makes it possible to impress a yaw moment on the car by means of a variable differential torque which can be set independently of the drive torque. In terms of the car, this allows both agility and stability to be increased as well as traction.

2.1 Functional Characteristics of Dynamic Performance Control in Terms of Driving Dynamics

The yardstick for the Dynamic Performance Control application is neutral self-steering properties right up into the limit range of driving dynamics. Right from the start of steering from straight-ahead travel, a differential torque between the rear wheels establishes a veering-in yaw moment that causes the car to spontaneously follow the steering angle specified by the driver, **Figure 1**, driving situation 1. This allows the agility of the car to be improved irrespective of the friction coefficient conditions. When taking a bend, the drive torque is sent to the rear axle by xDrive. In conjunction with a differential torque that is higher according to the lateral acceleration, the neutral self-steering properties are retained throughout the entire lateral acceleration range, Figure 1, driving situation 2. The car responds more directly to steering commands when taking a bend, due to the reduced tyre slip angle on the front axle. Directional accuracy increases significantly when a small steering angle is required, **Figure 2**.

Thanks to Dynamic Performance Control, the car displays neutral self-steering properties under all friction coefficient conditions and across the entire lateral acceleration range, agile steering properties and increased steering precision.

2.2 Driving Safety with Dynamic Performance Control

As well as increasing lateral dynamics, Dynamic Performance Control in the X6 is also used for stabilising the driving properties. Similarly to DSC, a corrective yaw moment is generated in dynamically critical driving situations, without however having to brake a wheel using the service brakes and thereby losing forward momentum, Figure 1, driving situations 5, 6 and 7.

Cushioning of load change responses is an example of this. When taking a bend with high lateral acceleration, a load change in the drive torque leads to a veering-in yaw reaction, which can result in oversteer under certain circumstances depending on the friction coefficient condition, car speed and load. In this situation, xDrive shifts the drive torques to the front axle. It is possible to impose any yaw moment on the car with Dynamic Performance Control, both when under traction, without load or in overrun condition, thereby establishing a veering-out TV moment on the rear axle. This stabilising differential torque results in a yaw reaction that is always consistent, with a slightly veering-in effect, but one which always remains controllable and therefore safe.

The Authors

Dipl.-Ing. Christian Billig is head of department of Longitudinal Dynamics System Testing at BMW AG in Munich (Germany).

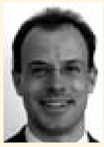

Dipl.-Ing. Harald Boedrich is a project consultant for transfer case development at BMW AG in Munich (Germany).

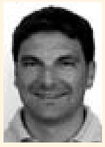

Dipl.-Ing. Jürgen Brack is a development engineer for functional integration of driving dynamics at BMW AG in Munich (Germany).

Dipl.-Ing. Bertram Höll is a development engineer at Semcon München GmbH for transfer case development at BMW AG in Munich (Germany).

Dr.-Ing. Michael Holle is the project leader of ICM longitudinal dynamics at BMW AG in Munich (Germany).

Dr.-Ing. Frank Kimmich used to be project leader for E/E gearboxes at BMW AG in Munich (Germany).

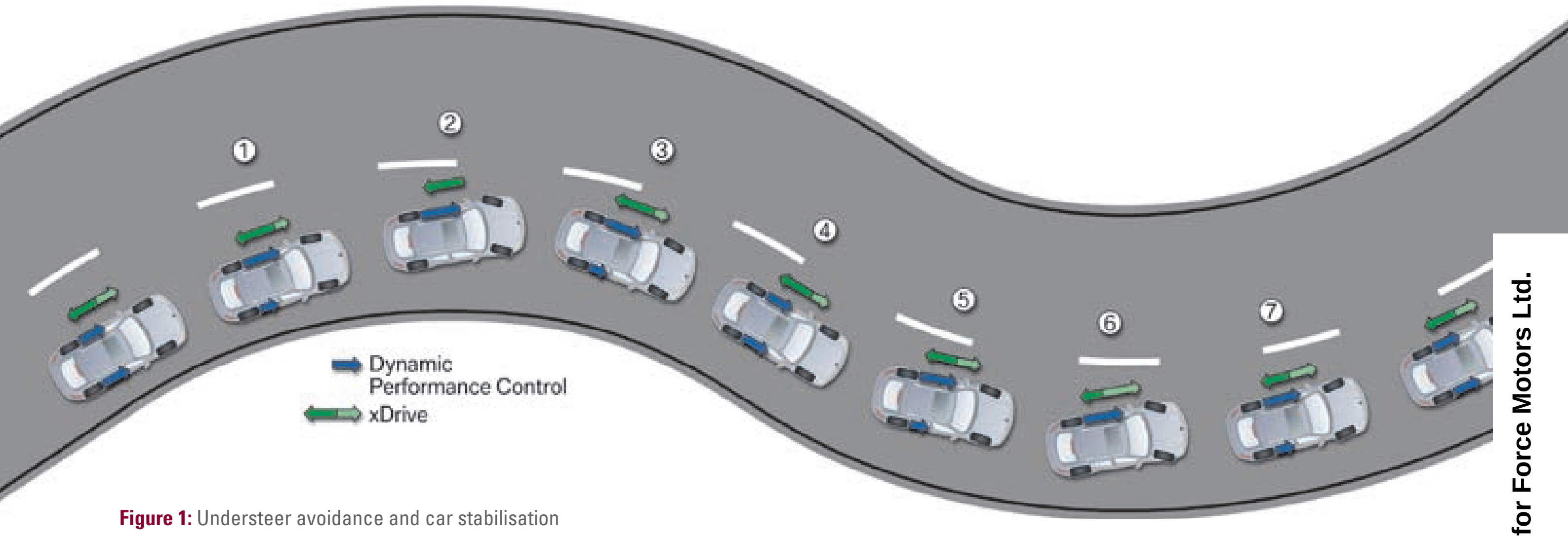

Figure 1: Understeer avoidance and car stabilisation

Close to the dynamic driving limit range, but before reduction in drive torque or brake intervention, Dynamic Performance Control achieves stable and therefore safe driving properties. When approaching the dynamic driving limit range, the veering-in differential torque is reduced and a stabilising yaw moment is established. Even in these driving situations, the car remains predictable and safe.

2.3 Traction

The X6 with Dynamic Performance Control also possesses the functional benefits of a self-locking differential. If differential slip occurs between the two wheels of the rear axle, Dynamic Performance Control is used for improving traction. This applies both when accelerating on different friction coefficients and when the load on the wheel at the inside of the bend is reduced when taking a bend at speed. In both cases, more drive torque is supplied to the wheel with the higher friction coefficient. The car accelerates significantly faster compared to a car with a conventional final drive and brake intervention. Excess drive slip is avoided, therefore the lateral force potential increases significantly and driving safety is further enhanced.

3 Control System and Functional Integration in the ICM

Parallel operation of several driving dynamics control systems requires an integrative approach in which the driving dynamics potential is exploited to the full in every control system combination. For this purpose, a central ICM (Integrated Chassis Management) control unit is used in the X6 for the first time. It controls the available actuators so that optimum driving properties can be achieved in all configurations.

The most important precondition for functional integration in the ICM is decoupling the function from the actuator. For this purpose, an architecture has been developed for simultaneous and co-ordinated control of all systems. Functional integration of the available actuators and coordinated use of the effectively expanded adjustment potential has made it possible to achieve the driving dynamics targets specified for the X6. **Figure 3** shows part of the entire functional architecture, the central driving dynamics module. The most important functional blocks are the modules of pre-

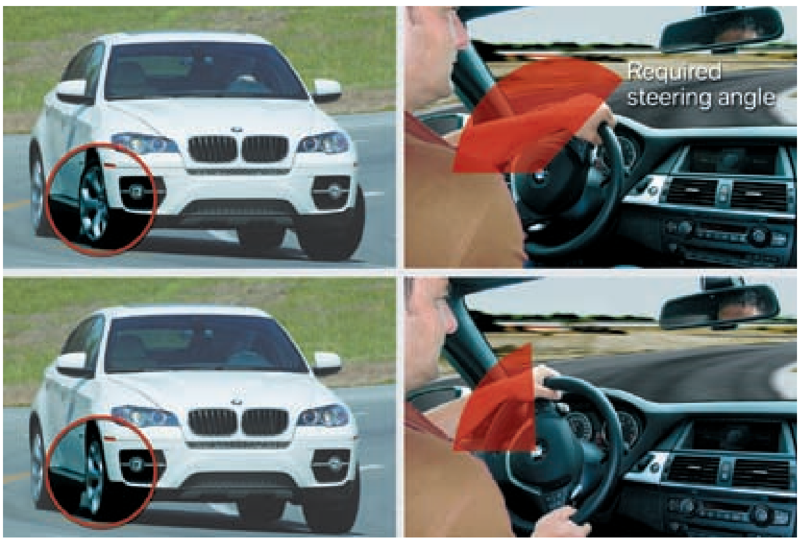

Figure 2: Reduced steering angle requirement and improved directional accuracy. Understeering car without Dynamic Performance Control (top left), steering precision and steering angle requirement when taking a bend without Dynamic Performance Control (top right), neutral cornering with veering-in differential torque by Dynamic Performance Control (bottom left), steering precision and steering angle requirement with Dynamic Performance Control (bottom right)

control, reference evaluation and driving situation detection, disturbance intrusion, lateral and longitudinal dynamics controllers as well as prioritisation and allocation.

3.1 Pre-control

Pre-control slices for Active Steering and Dynamic Performance Control are calculated in this module in order to improve directional accuracy and reproducibility. The specifications show a straightforward dependency between driver input and driving speed.

3.2 Reference Evaluation and Driving Situation Detection

The nominal value for the controller is calculated in the reference evaluation and driving situation detection function module, based on the pre-control values. Furthermore, indicators for different driving situations such as understeer or oversteer are calculated in this module. Based on the indicators, intervention criteria for the various actuators are calculated in subsequent function modules.

The nominal yaw rate calculated using the car model is not only used inside the ICM as a central reference variable, but is also used as a communal reference variable by external partner control units, specifically DSC.

3.3 Control: Lateral and Longitudinal Dynamics

The control slices required for optimising driving properties in the normal and transitional ranges are calculated in this module. The control functions are divided into longitudinal and lateral car dynamics. The objective is, firstly, to minimise deviations between the actual and nominal yaw rates using Dynamic Performance Control and Active Steering. Secondly, a TV moment for improving traction is requested in the ICM via the longitudinal controller. The first step in prioritisation between lateral and longitudinal dynamics control is performed by means of wheel slip monitoring.

The output signals are the parameters of target yaw moment (lateral dynamics) and wheel differential torque (longitudinal dynamics). These are communal and can be converted into actuator-specific control variables for all systems.

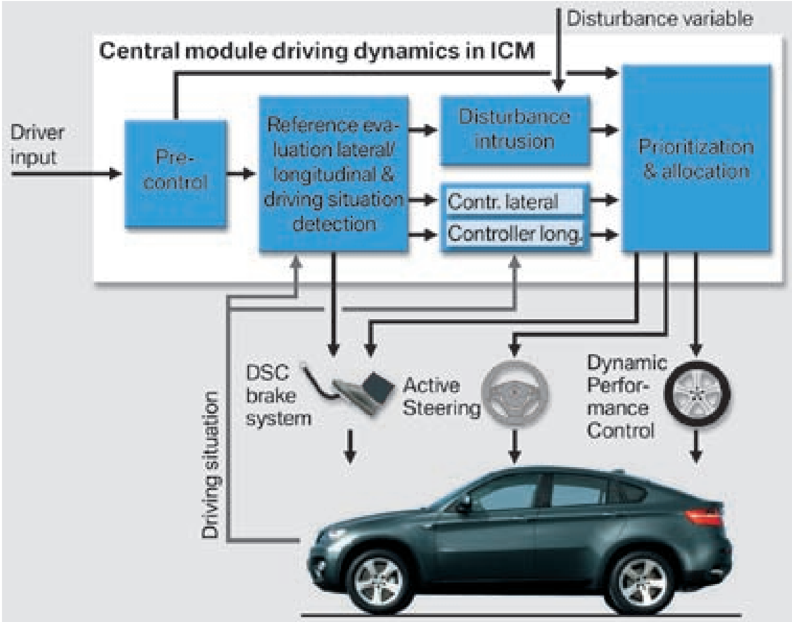

Figure 3: Functional structure of the central driving dynamics module

In addition to the TV moment, brake intervention at the front axle is required in order to assist traction in some driving situations, e.g. µ-split moving off, in order to ensure traction and component protection, **Figure 4**. In special cases, a braking torque is also superimposed on the TV moment on the rear axle.

The brake control system takes over the task of drive stabilisation in the dynamic driving limit range.

3.4 Disturbance Intrusion

Disturbance influences on the car, e.g. a yaw moment caused by longitudinal dynamics effect, can typically only be par-

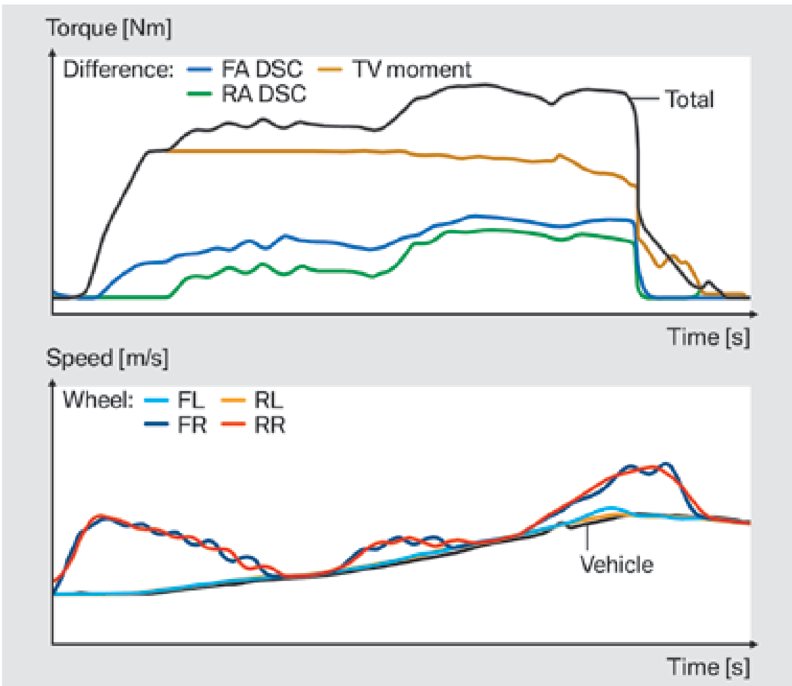

Figure 4: Superposition of TV and brake control for µ-split moving off

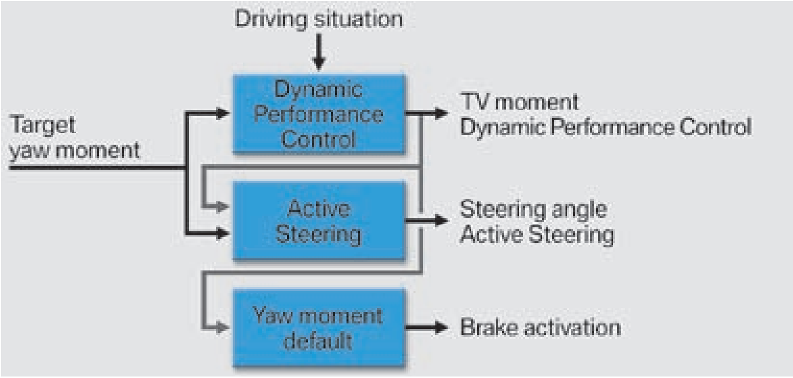

Figure 5: Simplified functional logic for the distribution between Dynamic Performance Control, Active Steering and target yaw moment

tially compensated for by a controller. In accelerated cornering, dynamic axle load distribution leads to a stronger tendency for the car to understeer. To achieve the required neutral self-steering properties in this situation as well, the veering-in differential torque is increased on the rear axle according to the longitudinal acceleration.

3.5 Prioritisation and Allocation

The task of this module is to prioritise and allocate actuation requests to the driving dynamics actuators. The target yaw moment and wheel differential torque is divided up according to the following criteria:

- car equipment (car dynamics control systems)
- system availability
- driving situation
- range of action of the driving dynamics control systems.

Complete implementation of the input request is aimed for in this case, from a functional perspective.

One aspect of the distribution logic will be explained taking the example of the division of tasks between Dynamic Performance Control, Active Steering and the target yaw moment. The functional logic is shown in a simplified form in **Figure 5**.

The target yaw moment to be set by the Dynamic Performance Control is transferred to the actuator as a differential torque. If complete implementation of the TV moment cannot be achieved due to the aforementioned intervention criteria, then the remaining stabilisation task is taken over by Active Steering. This can apply the remaining target yaw moment by means of steering intervention, following corresponding transformation of the control variable.

A comparable transfer of the TV moment to another actuator takes place when narrow bends are involved. Due to the design of Dynamic Performance Control, it cannot transfer any further torque to the wheel on the outside of the bend at high wheel differential speeds (see 3.3), therefore the TV moment is converted into a target yaw moment for the brake control system, based on a geometrical model in the ICM. To maintain a balanced distribution of longitudinal torque, the DSC not only applies a brake torque to selected wheels, but also increases the engine torque. In special situations (such as ABS braking), DSC can also suppress the TV moment for an individual direction in part or in full by means of an interface.

4 The Dynamic Performance Control Final Drive

More than 100 principles for superposition gears were analysed in the process of finding the concept. More than 40 criteria were taken into account in the concluding technology evaluation.

The basic preconditions are compatibility with other driving dynamics systems, compliance with safety requirements and a robust structure in terms of mechanical, actuator, electric/electronic systems and the oil circuit. It is strategically relevant to have a scalable basic concept in terms of size, ratio range and functional requirements. The factors which have the greatest importance in terms of function are dynamics, accuracy and reliability of positioning procedures throughout the entire lifecycle, followed by the ability to withstand the widest possible range of temperatures. Component weight and efficiency in straight-ahead driving are the dominant mechanical criteria for concept selection.

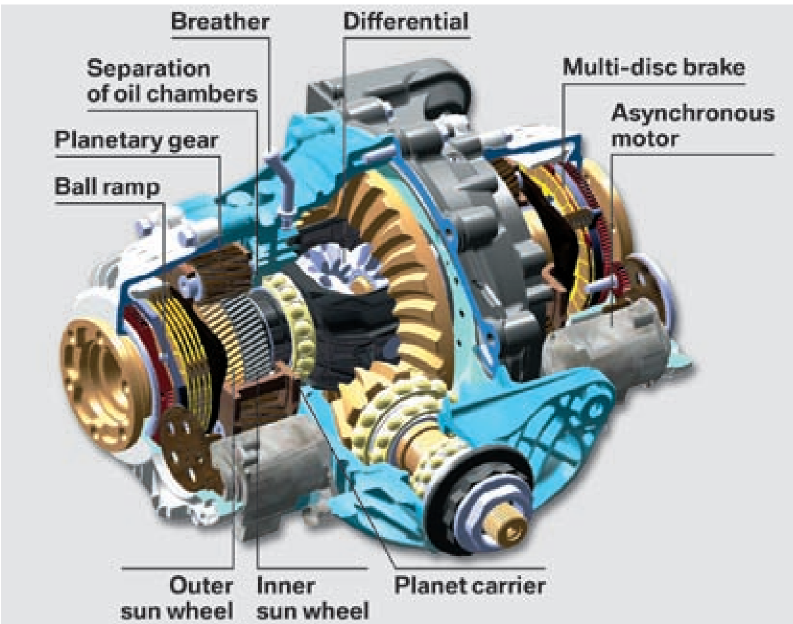

Figure 6: Final drive of BMW Dynamic Performance Control

4.1 Concept Characteristics

The basic gearbox with hypoid gear set and bevel gear differential is arranged in the middle of the aluminium housing. The gear set is mounted in angular-contact ball bearings, thereby delivering a significant contribution to achieving the best possible efficiency.

The superposition units are arranged on both sides. Each of these comprises a double planetary gearbox and multi-disc brake actuated by electric motor, **Figure 6** and **Figure 7**.

The gearbox is filled with two different synthetic oils, formulated to match the total car lifecycle. The basic gearbox is filled with a hypoid oil, while the oil used in the superposition units is optimised in terms of the friction behaviour in the multi-disc brakes. The separation of the oil space permits oil distribution throughout the basic gearbox so as to optimise efficiency, combined with an independent, function-oriented oil circuit in the superposition units. See [1] for more information.

4.2 Functional Principle

The system behaves like a final drive with open differential in driving situations without torque transfer. When there is no speed difference between the left and right wheels (driving straight ahead), the planetary drives of the superposition units circulate in a block. The inner discs, which are fixed to the planet carrier, rotate with the speed of the wheel, in contrast to the outer discs that are fixed onto the housing. When there is a speed difference between the left and right rear wheels (taking a bend) then the differential compensates for the speed difference. In response to the speed difference between the inner and outer sun wheels, the planet gears roll and the planet carriers rotate without load.

In driving situations with torque superposition, the planet carrier is braked in relation to the housing by means of the multi-disc pack. As a result, the corresponding outer sun wheel is accelerated in favour of the output end due to the selected ratio of 10 % in the planetary drive, thereby establishing a torque flow from the differential cage via the planetary drive onto the wheel. Both wheels are driven with different torque levels.

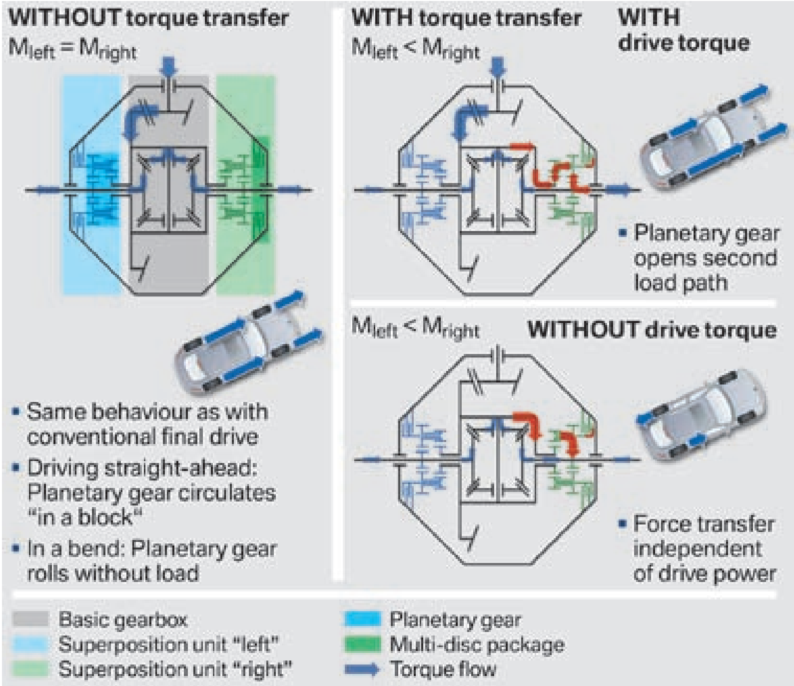

Figure 7: Summary of torque flow

Even without input torque, rolling of the planetary drive can be forced by means of the multi-disc pack. The outer sun wheel turns faster than the differential housing, therefore causing a positive torque flow to the actuated end due to the summation effect of the differential, Figure 7.

4.3 Differentiation from the Competition

Several aspects differentiate Dynamic Performance Control from other technologies available on the market for individual wheel drive torque distribution. Lockable final drives – which are

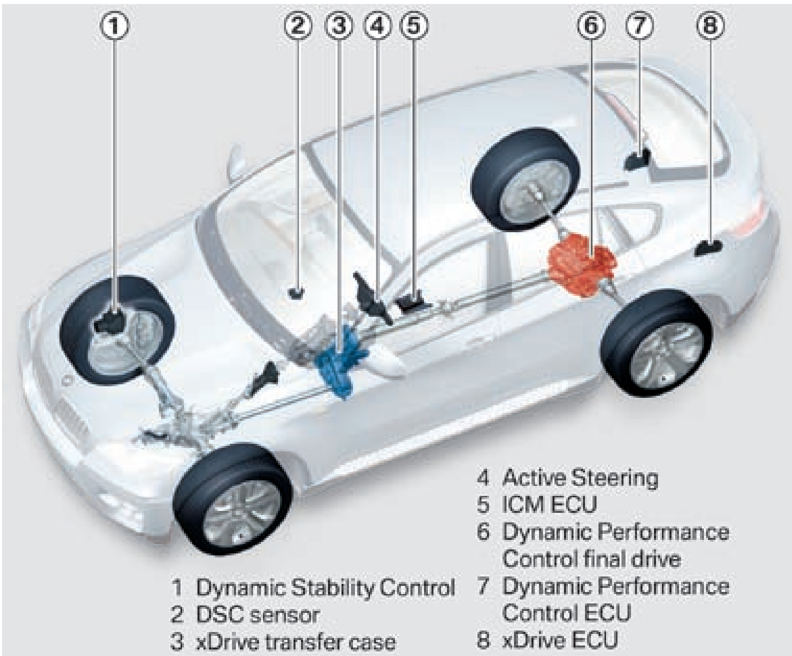

Figure 8: System overview – Components in the car

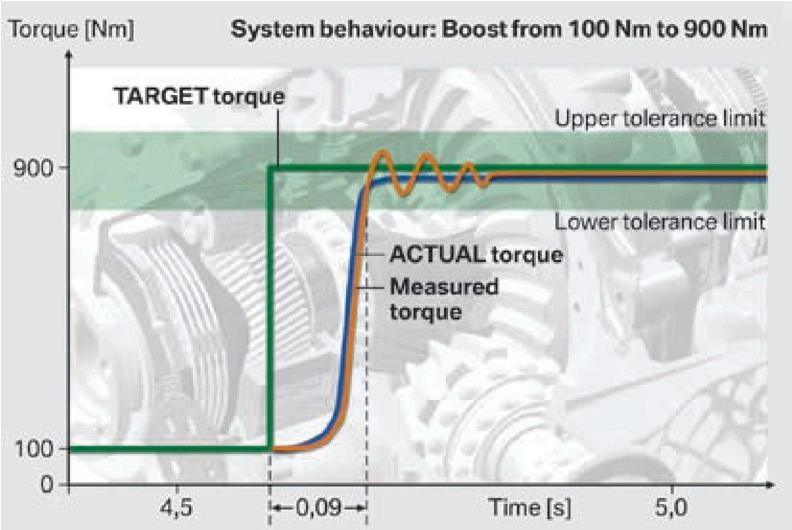

Figure 9: Torque jump

sometimes incorrectly put into the group of TV systems – do not make it possible to set a torque difference between the driven wheels. A lock limits the differential effect by equalising the speeds of the wheels with the objective of increasing traction, whereas a TV gearbox on the driven axle permits active yaw moment imposition on the car similarly to intervention at the wheel brake, however without incurring its decelerating effect.

The advantage compared to clutch-based torque distribution systems without a differential lies in the lack of dependency between torque distribution and drive torque. This means control over the car is boosted even when there is a load change during a bend or when driving downhill.

Compared to versions with a „stepped up" clutch which transmits the entire superposition torque, the main customer benefit in terms of efficiency lies in the lower losses when driving straight ahead. This driving situation is particularly relevant for everyday use, and in it the planetary drive circulates in a block without rolling the gearing. This minimises the torque losses caused by the superposition units, and creates the basis for an axle gearbox concept that offers optimum efficiency.

The selected ratio of 0.9 in the planetary drive covers all situations that are relevant in terms of driving dynamics. Cornering radii close to the turning circle limit are deliberately excepted. Covering this range would entail a greater relative speed between the inner and outer discs, thereby not only worsening the efficiency but also leading to greater heat input.

Both in terms of gearbox weight and for the positioning dynamics, it is advantageous for the brake torque to be boosted by the transmission ratio of the planetary drive, thereby allowing the disc pack and the corresponding actuation device to be designed for lower maximum torques.

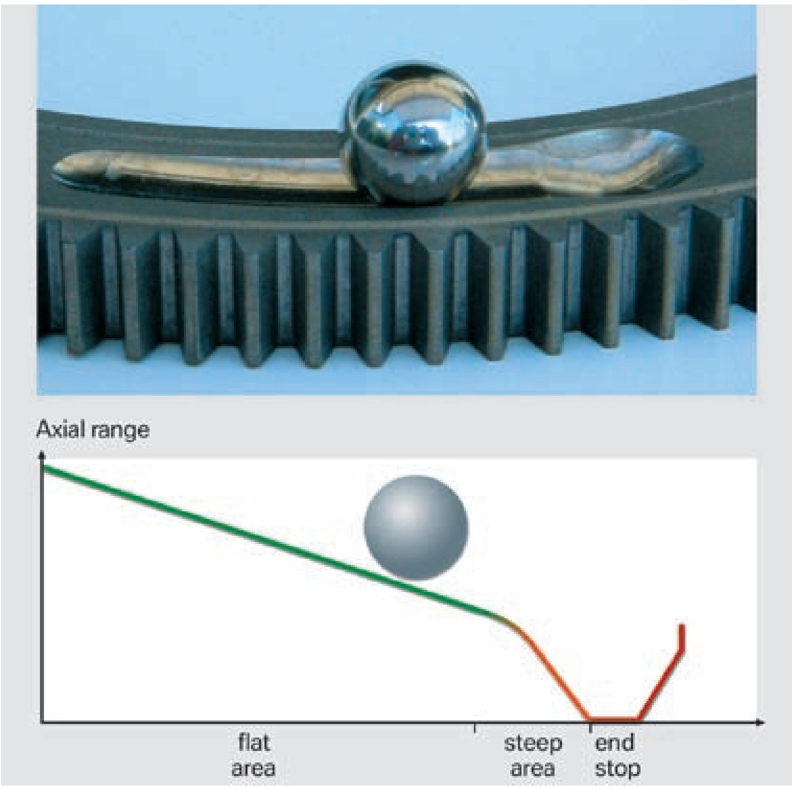

Figure 10: Ball-in-ramp track

5 Fulfilment of the Required Driving Dynamics Functions

The actuator control unit of Dynamic Performance Control converts the nominal value specification from the ICM into a corresponding command for the electric motors of the final drive, **Figure 8**.

5.1 Representation of Torque Distribution

It is a precondition of harmonious driving that the torque should be distributed between the rear wheels quickly, accurately and individually.

The system meets this requirement because the actual torque follows the nominal torque throughout the entire range of action in less than 100 milliseconds, with an accuracy of at least ±10 %, **Figure 9**.

The hardware preconditions for high dynamic performance are based on asynchronous electric motors operated using field-oriented control.

The motor position is detected by an angle sensor and assigned to the brake torque by means of a characteristic curve.

The rotational movement of the electric motor is transferred to the ball-in-ramp by means of a spur gear stage. The ball-in-ramp converts the rotational movement into an axial stroke, thereby closing the multi-disc brake and generating the brake torque.

The ball-in-ramp is configured with two different gradients: The steep range is used for rapidly covering the air gap between the discs, whereas the low gradient permits the required TV moment to be set precisely, **Figure 10**.

5.2 Overrunning Calibration

It is necessary to know all influencing factors (including hysteresis, temperature, wear) to achieve consistent positioning accuracy throughout the entire service life.

Determining the „0 Nm point“ (kiss point of the multi-disc brake) and the ball-in-ramp gradient in the working range are of central importance. The kiss point and ball-in-ramp gradient are determined after each journey as part of wear adaptation. The values are stored in the Dynamic Performance Control unit and used the next time the engine is started.

5.3 Component Load

The rotation speed and TV moment are monitored to avoid damage to the planetary drives in special situations with intensive loadings, and in case of misuse. If there is a large speed differential between the rear wheels, the speed of the slipping wheel is reduced by means of the lock functions of the final drive. If this is not sufficient, the engine torque is reduced and the wheel brake is applied in order to prevent damaging rotation speeds on the planetary gears.

6 Functional Reliability

Because the Dynamic Performance Control function intervenes in the lateral dynamics of the car, ensuring functional safety in accordance with the currently valid safety standards [2] was a central aspect of product development. All activities to be performed for this purpose during the concept and implementation phase were based on the functional safety process specified at BMW.

6.1 Safety Categorisation and Safety Concept

At the beginning of concept development, danger and risk analyses were used as tools for systematically finding all situations that could occur due to faults in Dynamic Performance Control, and evaluating them based on their effect on driving properties. This resulted in the safety categorisation of Dynamic Performance Control with ASIL D (SIL 3). Classification ASIL D corresponds to the categorisation of stability systems or active steering. Based on the safety categorisation, the safety requirements for configuring the function and HW architecture were systematically established as well as the software functions for detecting and overcoming faults. One of the measures taken in order to meet the exacting requirements on functional reliability was to configure all control units involved in Dynamic Performance Control as dual processor systems. The redundant implementation of safety and diagnostic functions ensures that the system automatically goes to a safe status in case of a failure (conventional final drive with open differential such as BMW X5) and the car also has stable driving behaviour even without Dynamic Performance Control.

6.2 Software Development and Safeguarding

In addition to safety requirements on the hardware architecture, ASIL D classification of Dynamic Performance Control imposed high requirements in terms of software development and safeguarding processes. Methods for systematic design of system and function architecture as well as of software modules were required for this purpose. The majority of the software used for safety-critical functions was generated automatically using function modules by means of a certified code generator. This made it possible to avoid errors, in contrast to manual software preparation. Integration and safeguarding of electronics and software were performed step-by-step as part of integration stages: Both SIL and HIL tests were performed at the component level. At the subsystem level, this was followed by first verification of the driving dynamic system group, before the function group was definitively accepted in the car.

7 Conclusion

Dynamic Performance Control, other driving dynamics control systems and functional integration in the ICM allow the X6 to achieve previously unparalleled levels of manoeuvrability and agility for a four-wheel drive car in this class. Tracking stability, steering precision and the associated feeling of great safety when driving are characteristic features of the X6. The result for the customer is effortless and masterful driving under all friction coefficient conditions. Dynamic Performance Control therefore makes a significant contribution to experiencing the driving dynamics of a BMW not only in the limit range, but also in the normal and transitional ranges, at the same time as increasing driving safety.

References

[1] Denzler, R.; Granzow, C.; Peter, R.; Spieß, M.: The Vector Drive final drive. In ATZ 109 (2007), no. 12, pg. 1106-1115

[2] Norm IEC61508, Part 0-7. Functional safety of E/E/PE safety-related systems

Acknowledgements

Development of BMW Dynamic Performance Control demanded close interdisciplinary co-operation between driving dynamics and drive development staff at BMW AG. A whole range of colleagues worked with great commitment to define the functional architecture, establish the concept and push ahead with series development. We would like to express our gratitude specifically to the following people, amongst others: Dipl.-Ing. Eduard Ginglas, Dipl.-Ing. Holger Felix Mayer, Dipl.-Ing. Werner Pfau and Dipl.-Ing. Gerd Riedmiller.

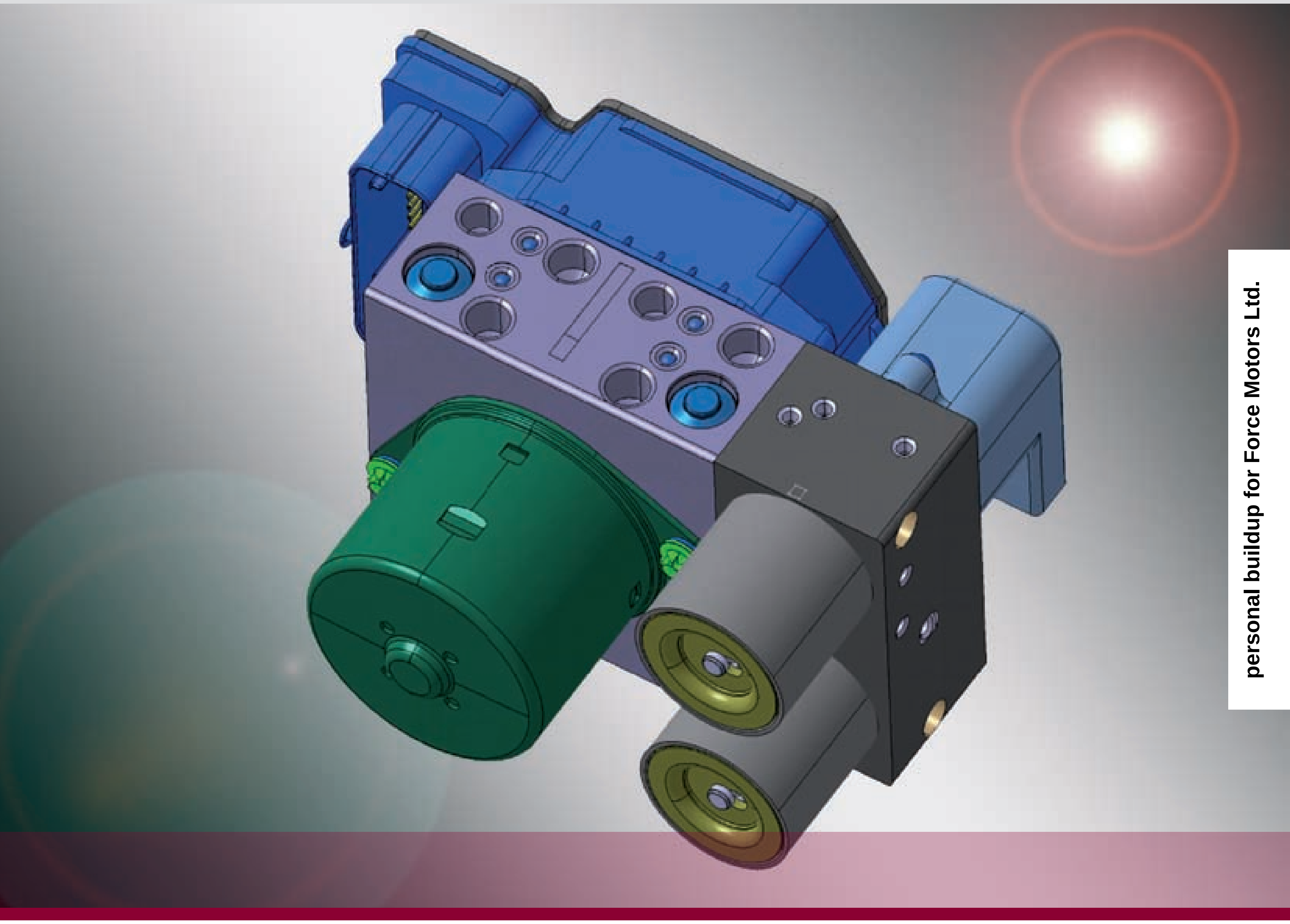

Fuel Savings through Steering and Braking Technologies

Technical discussions about effective means of addressing reduction in fuel consumption and lower CO_2 emissions are often centred on elaborate and costly drive train modifications. The automotive supplier TRW shows how, independent of the selected drive train concept, steering solutions and leading-edge braking technologies can help to optimise consumption levels. For example, TRW can quickly adapt the electro-mechanical and electro-hydraulic steering system, the electronic stability control with a regenerative braking function ESC-R and the electro-hydraulic braking system SCB to different models and platforms.

1 Introduction

Cutting vehicles' fuel consumption is an increasingly important consideration for both manufacturers and drivers, not only due to the rising cost of fuel, but also to the current debate in the European Parliament on new and tougher draft legislation. National CO_2 levies, such as a bonus/malus system in France or special taxes on automobiles in Finland and Ireland, have already come into force. **Figure 1** shows the increase in emission-related costs attributable to the tougher legislation involved, as exemplified by a vehicle with emissions of 161 g CO_2/km. Against this background, all initiatives helping to reduce CO_2 emissions have assumed a considerably higher level of importance. The technical measures involved here range from highly complex and costly engine and drive train modifications (starter-generator, hybrid drive, electromotor, etc.) and electric-motor-driven auxiliaries (oil pump, water pump, etc.) to friction-optimised sub-components such as tyres, bearings and shaft seals.

TRW's product portfolio includes various technologies, that besides their contribution to vehicle safety also significantly reduce fuel consumption. One core product is electrically powered steering (EPS and EPHS), which in it's various base configurations is in series production already. A major role in reducing consumption levels is also played here by new braking concepts for hybrid drive vehicles, like regenerative braking (ESC-R and SCB). For enhanced comprehension, the paper begins by describing how the steering and braking technologies function, before proceeding to detail the advantages of the systems in regard to fuel savings and reducing CO_2 emissions.

2 Selection of Different Electrical Steering Systems

In its range of electrically powered steering systems, TRW offers electrically powered hydraulic (EPHS) and electrically powered mechanical steering variants (EPS). With the aid of electronic control systems and a combustion-engine independent, electro-motor driven, energy source, current and future requirements for low fuel consumption, high steering dynamics and fine-control capabilities are fully met. Electrically powered hydraulic steering systems were developed in the early 1990s especially for the B and C segment. So far, more than 15 million vehicles have been fitted with this technology. These steering systems with electro-hydraulic energy supply offer the advantage of re-use of existing hydraulic steering components (hydraulic power steering, HPS) and high packaging flexibility. The achievable CO_2 reduction is, compared to an electro-mechanical system at a comparable drive cycle and on a vehicle with a 1.6-l engine, at about 85 %. In view of the demands for cutting CO_2 emissions, conventional mechanical-hydraulic steering systems are increasingly being replaced by EPHS in vehicles with higher axle loadings as well. TRW's fam-

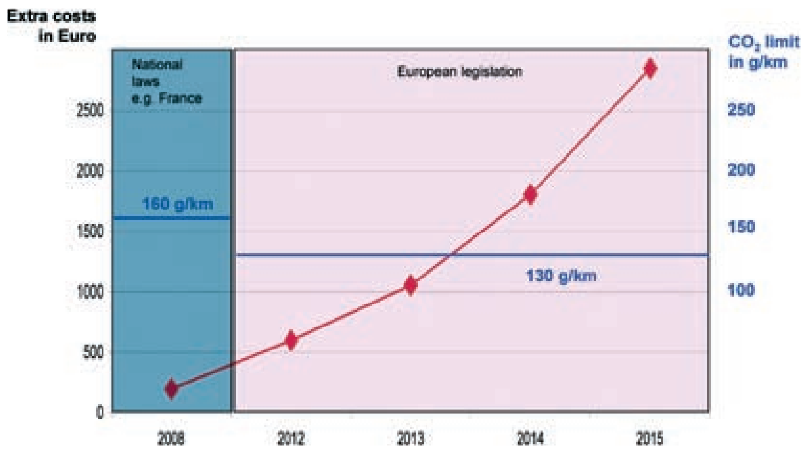

Figure 1: Exemplified depiction of the additional costs entailed by tougher European legislation for a vehicle with emissions of 161 g of CO_2 per km

The Authors

Dipl.-Ing. Frank Lubischer is Vice President Steering Engineering at TRW Automotive in Dusseldorf (Germany) and Washington, Michigan (USA).

Dipl.-Ing. Josef Pickenhahn is Vice President Brake Engineering at TRW Automotive in Koblenz (Germany).

Dr.-Ing. Jochen Gessat is Engineering Manager Systems Layout Electrically Powered Hydraulic Steering Systems at TRW Automotive in Dusseldorf (Germany).

Dipl.-Ing. Leo Gilles is Chief Engineer Advanced Control Systems, New Products, Braking, at TRW Automotive in Koblenz (Germany).

ily of electromotor-pump assemblies from the latest product generation, called EPHS GenC, now includes six power gradations (from 580 to 1000 W of hydraulic output). With this choice of ratings, the electro-hydraulic steering systems from TRW can be used in all vehicle categories, from small cars up to luxury limousines, SUVs and light commercial vehicles (up to 18 kN rack load).

In the category of electro-mechanical steering systems, TRW offers two system architectures that by virtue of their modularised construction, shared subsystem utilisation and high installation-space flexibility meet the disparate application requirements of the vehicle segments involved: the Column Drive EPS and the Belt Drive EPS. In the case of the Column Drive EPS, the drive torque is applied via an electromotor/worm-gear system located at the steering column, while in the Belt Drive EPS this is done using an electromotor with a belt and recirculating-ball transmission arranged in parallel to the steering rack. The main differentiating criterion in choosing between the two systems for a particular application will usually be the power requirement for the steering system concerned. Lower steering-system power requirements permit the use of column drive EPSs in vehicles of the A, B and lower C-segments, while Belt Drive EPS meets premium requirements for a broad spectrum of vehicle platforms, extending to the D-segment, small SUVs and crossover models.

2.1 Advantages of Electro-hydraulic and Electro-mechanical Steering Systems

For mechanical-hydraulic steering systems, supplied by the internal combustion engine, there is a conflict involved in system dimensioning: whereas during parking high power levels are briefly required by the steering system at low engine rpm (> 500 W), the average amount of power required for steering support while motoring at high engine rpm is very low (< 50 W when driving straight ahead). The temporal component in this load case with a low power demand for the steering system is more than 90 % both for real driving cycles and for consumption test cycles for automobiles (NEDC, FTP75, etc.). In the case of the pump designs typically used for mechanical-hydraulic systems, this leads to substantial power losses in the steering system.

In the case of electrical steering systems (EPHS and EPS), by contrast, the power for steering support is provided independently of the vehicle drive's operating state. This is depicted diagrammatically in **Figure 2**. The steering power is controlled electronically in line with demand, utilising the steering angle speed and the vehicle speed with the EPHS, and the steering torque and the vehicle speed with the EPS, **Table**. Using electrical steering systems offers OEM an opportunity to optimise the efficiency of steering support and to avoid parasitic losses for the engine. In addition, an electrical steering system scores in terms of an excellent cost/benefit ratio, meaning that the cost increase at the vehicle per gram of CO_2 reduction is low compared to other consumption-cutting measures. If we take a possible reduction of 7 g CO_2/km from using an electrical steering system in place of a mechanical-hydraulic one, this corresponds to a cost benefit in 2015 of up to 665 euros, under the legislation currently being planned. Another significant advantage of electrical steering systems is that they can be easily integrated into different drive concepts (conventional internal combustion engines, engines with an automatic start-stop system, hybrid drives, and fully electrical drive trains).

2.2 Energy-economical Alternatives

There are currently some alternative energy-economical hydraulic solutions on the market that reduce the power loss by regulating the pump's delivery volume in dependence on the speed (varia-

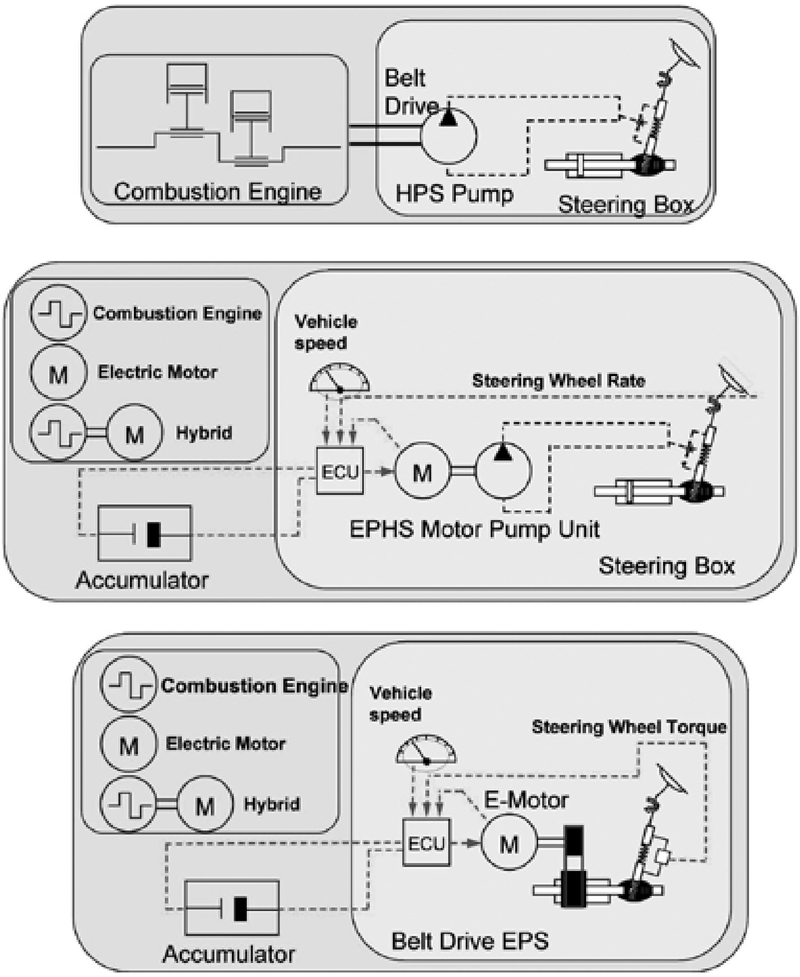

Figure 2: Simple integration of an electrical steering system in vehicles with different drive concepts, without a mechanical interface to the drive (top: conventional system, centre: EPHS system, down: Belt Drive EPS)

Table: Principles and energy consumption of various steering systems

	HPS Vane Pump	HPS ECO Vane Pump El. Controlled Orifice	HPS VDP Variable Displacement Pump	EPHS	EPS
Principle	REFERENCE	Reduced system flow	Rotational speed dependent displacement volume	Power on demand – Speed Control Input Signals: STW Rate, Vehicle Speed	Power on demand – Torque Control Input Signals: STW Torque, Vehicle Speed
Main Effect	REFERENCE	Reduced system pressure –> reduced drive torque	No bypass flow	No bypass, reduced flow level reduced system pressure	Lowest power draw option
Power Consumption	501 W	313 W	313 W	50 W	10 W

* Typical value for average power consumption at Crank Shaft in NEDC for D segment vehicle

ble displacement pump, VDP) or the pump reduces its system volume flow with a solenoid valve (electronically controlled orifice, ECO). These measures likewise reduce the power loss, but not to the same extent as a demand-responsive control system, see also the Table. This is because the load status cannot be detected, due to the absence of sensors, and the VDPs, by reason of their construction, exhibit significantly higher internal losses and are operated at comparatively higher volume flows. Due to the high circulating oil volume flow of hydraulic-mechanical steering systems even when a low level of steering power is being demanded, the pumps' power consumption will depend closely on the steering system's flow resistance. To exemplify, **Figure 3** shows the variation in steering system energy consumption at the crankshaft. In the left-hand part of the picture, the absolute additional consumption (and thus the absolute additional emissions) for various assisted steering technologies is in each case shown in a best-case (A) and a worst-case (B) system configuration. For EPHS and EPS, the grey-backed arrows show the relative savings potentials in regard to the use of standard hydraulic powered steering designed for consumption efficiency. The principal parameters influencing variation in consumption lie in the design of the hydraulic system, performance characteristic tuning, and efficiency variations in the components used, with the hydraulic losses in dependence on the volume flow accounting for the greatest power loss. The presumptive cause is the hydraulic components connected to the pump, outlined in the right-hand half of Figure 3, such as hydraulic lines and steering gear. The variation in flow resistances inside the steering system (operating points depicted) may lead to a higher power consumption by the hydraulic pump. Since the electro-hydraulic system is operated at a very much lower level of energy (in the green), this effect is hardly ever encountered in actual practice. The electro-mechanical system generates a power loss only in its electronic control unit, and thus possesses the best energetic properties.

Complementing the mentioned advantages of electrical steering systems over their conventional hydraulic counterparts in terms of energy consumption, electrical steering systems, as what are called semi-active steerings, offer the advantage that the steering torque can be adjusted by varying the servo-support. This enables speed-dependent steering support to be implemented without any additional outlay, for example. Electro-mechanical systems also possess a unique feature in that active safety or comfort functions can be implemented using torque superimposition (for example lane guidance or automatic parking).

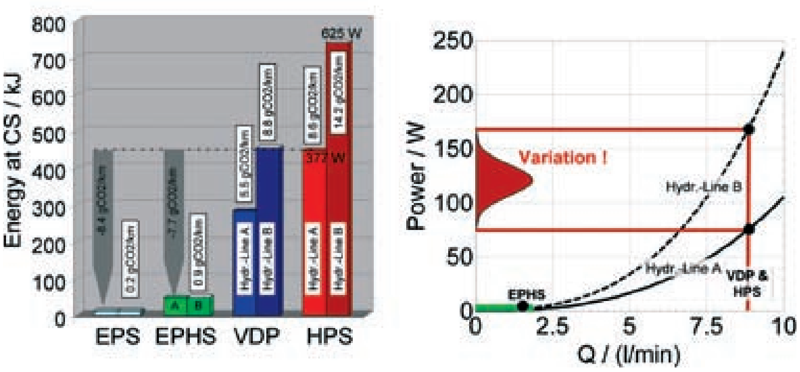

Figure 3: Energy management functionality – energy consumption in the test cycle NEDC of four steering systems EPS, EPHS, VDP und HPS (left) at the crankshaft (CS) and hydraulic power loss of a „best case" (A) and „worst case"(B) system configuration

3 Systems for Regenerative Braking

Systems for regenerative braking enable braking energy to be recovered in hybrid and electric vehicles using the vehicle's generator. While the brake is being operated by the driver, or during autonomous deceleration requests, for example from the adaptive cruise control (ACC), the aim is to recover a maximum of the available kinetic energy, in dependence on vehicle speed, driver's wish, braking deceleration and the vehicle's weight. For any additional braking deceleration required – if the driver's wish exceeds the maximum regenerative power – the friction brake is used.

3.1 Requirements

The major functional requirements posed for a regenerative braking system are:

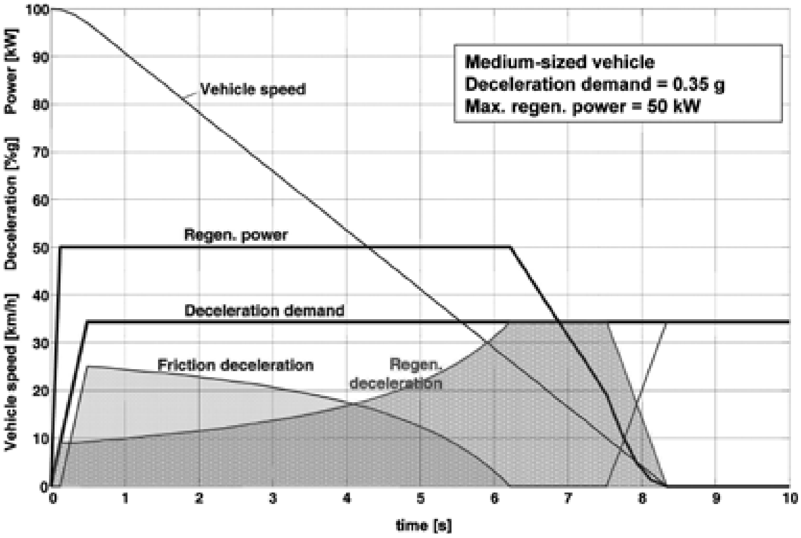

Figure 4: Simulated stop from 100 km/h for a braking deceleration of 0.35 *g* with blending of regenerative braking and friction braking

- precise adjustment and control of the braking torques in accordance with the braking request from the driver or through system requests for an active braking function
- separate control for the regenerative braking torque and the friction braking torque
- variable control of the friction braking force in accordance with the system request as a supplement to the regenerative braking torque
- the mixing of friction braking torque and regenerative braking torque should not be perceived by the driver, neither acoustically nor when operating the brake pedal
- fast take-over of braking by the friction brake should be assured by all stabilising control interventions, such as ABS/ESC; all wheel slip and stabilisation requirements are handled by the friction brake.

3.2 Brake Torque Blending

To perform the brake torque blending function (the requirements for brake torque mixing between friction and regenerative brakes), the friction brake system has to assure decoupling between the driver's wish and control of the friction braking torque for the wheel brakes, that means "by wire" functionality, or alternatively provide intermediate storage of any braking medium not required by the friction brake system. Various concepts for the construction and design of friction braking systems that meet the requirements for regenerative braking are already in series production and under development. The blending function between the friction and regenerative braking torques is derived from a torque "blender" algorithm, with the regenerative torque of the drive axle being determined from the generator's output. The sum of regenerative and applied friction braking torques corresponds to the driver's wish. **Figure 4** and **Figure 5** show examples of brake torque blending between regenerative and friction brakes at simulated stops from 100 km/h and 50 km/h. Restrictions/limitations on the regenerative power due to battery charging capacities and efficiencies have not been factored in here. As the basis for an illustrative calculation, a medium-sized car has been taken with an assumed driver's wish for a braking deceleration of 0.35 g and 0.15 g respectively, and an assumed maximum generator power of 50 kW.

3.3 Regenerative Braking Systems

To cover the global market variance in regard to complete system integration without any additional vacuum supply, plus the modularised approach as a supplement to a conventional braking system, TRW is pursuing two concepts: slip control boost (SCB) as a fully integrated system and electronic stability control-regenerative (ESC-R) as a modularised system.

3.3.1 Slip Control Boost

The slip control boost (SCB) system from TRW, mass-produced since the end of 2007 in the USA for the Chevrolet Tahoe, is an integrated hydraulic braking system that replaces the conventional brake booster, the brake master cylinder and the vacuum pump by an electro-hydraulic control unit (EHCU), and integrates a brake pedal simulator and a multi-cham-

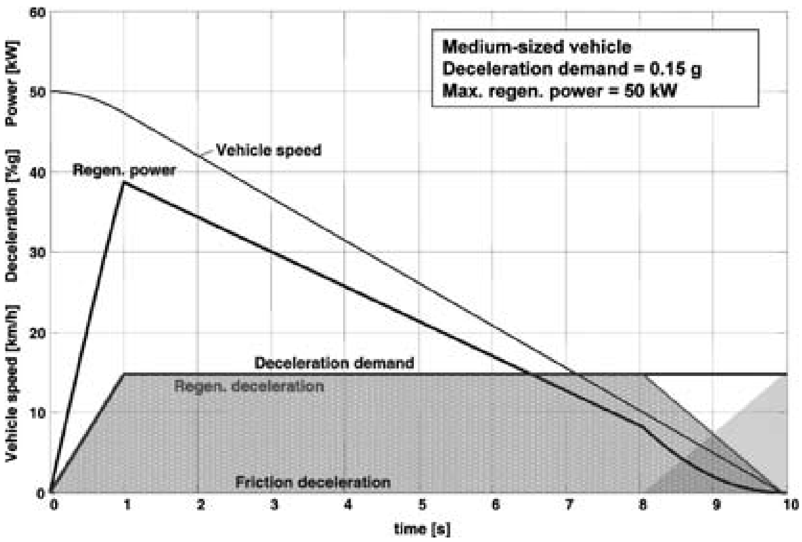

Figure 5: Simulated stop from 50 km/h for a braking deceleration of 0.15 *g* with blending of regenerative braking and friction braking

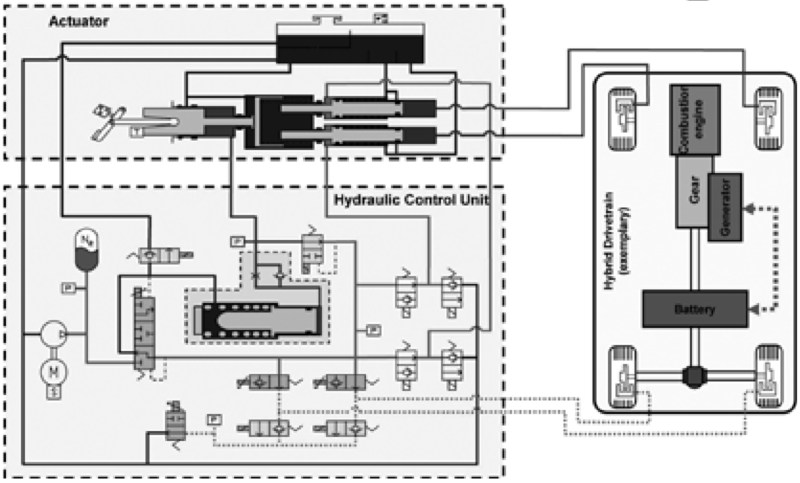

Figure 6: SCB hydraulic system architecture

ber brake master cylinder. **Figure 6** shows the construction of the SCB's hydraulic system, as exemplified by rear axle blending; **Figure 7** shows the actuating unit and the EHCU.

The system's energy source consists of a high-pressure accumulator with an integrated pressure sensor for detecting the loading state and faults, and an integrated motor/pump unit for loading the accumulator. The actuating unit incorporates a redundant travel sensor, and is linked to the wheel brakes, which in normal braking operations is separated by an open-when-deenergised safety valve. Additional monitoring of the driver's wish is assured by a pressure sensor integrated into the hydraulic unit. The pedal feel is provided by a spring/elastomer-assisted pedal simulator integrated into the hydraulic unit, which is connected at the rear to the reservoir via a closed-when-deenergised safety valve. When a braking request is received from the driver or an active pressure request from the system, the booster pressure is generated using a hydraulic proportional valve in a closed control loop with pressure monitoring only in the booster circuit from the high-pressure accumulator. Pressure is supplied to the rear-wheel brakes directly from the booster pressure via a holding and reduction valve in each case. The front-wheel brakes are indirectly actuated in hydraulically separated mode using the master-cylinder separation pistons and likewise a holding and reduction valve in each case. Features of the system include the adjustable pedal feel simulator with a low NVH level during control operations and a system construction that is fault-tolerant for electrical system or sensor errors. If the energy fails, the safety valves will switch back to the normal position, and permit a hydraulic four-wheel link to the wheel brakes without any loss of pedal travel. In response to a brake blending request, the inlet valves of the axle to be blended are closed, and the brake blending pressure request is controlled using a TC-ISO valve in "closed-loop" mode. The standardised electro-hydraulic control unit (EHCU) meets the requirements for all cars and light commercial vehicles.

3.3.2 Electronic Stability Control and Regenerative Braking System

The regenerative braking system ESC-R is a modularised, hydraulically enclosed system based on TRW's standard ESC system. In the winter of 2006/2007, TRW premiered its new electronic stability control system, with an option for recuperation of braking energy in some initial experimental vehicles. It operates with a conventional brake booster, a master cylinder, a vacuum pump (if required) and a simulator for the hydraulic braking volume requirement. For a compactly dimensioned system construction and in order to avoid additional hydraulic connections, this simulator can alternatively be integrated into the slip control system. The teaser photo shows the ESC-R hardware.

Figure 8 shows the hydraulic system of the ESC-R. In the case of conventional brake operation without a recuperation request, the hydraulic unit works like a conventional hydraulic system. For braking operations with a regenerative request, the direct link between the master cylinder and the wheel brakes is interrupted, with the friction brake torque being replaced by a recuperative-electrical brake torque. The master cylinder pressure applied by the driver acts on the simulator, while the displaced volume of liquid is put into intermediate storage in the low-pressure storage chambers of the hydraulic unit, with the conventional pedal feel being retained. The master cylinder travel is here detected, and in accordance with the driver's wish additional hydraulic brake blending pressure is provided in the circuits as needed by means of the multi-piston pump. The system operates in a closed hydraulic circuit without any additional volume, comparable to a

Figure 7: SCB hardware

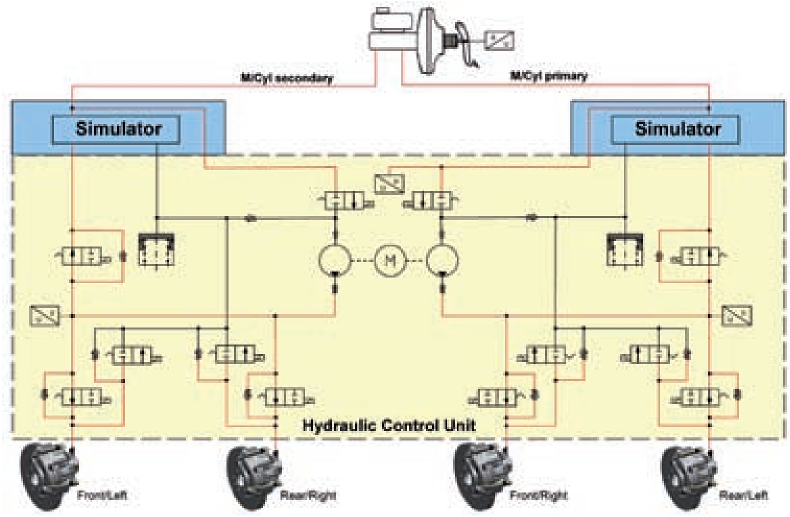

Figure 8: ESC-R hydraulic system architecture

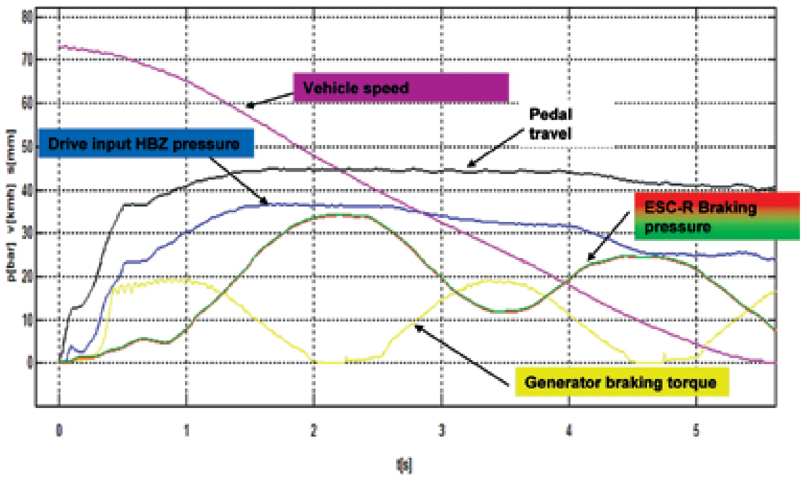

Figure 9: Vehicle recorder with sinusoidal modulation of the generator and braking torques

conventional control system and provides the advantage that in the event of a fault the hydraulic boost is retained without any loss of pedal travel. **Figure 9** shows a vehicle recorder with exemplified sinusoidal modulation of the available electro-regenerative braking torque and corresponding modulation of the hydraulic braking pressure in phase opposition by the ESC-R system.

3.4 Advantages of Regenerative Braking Systems

Regenerative braking systems constitute a solution that in conjunction with hybrid vehicles offers fuel savings and reduces exhaust gas emissions. In addition, hybrid vehicles, thanks to electrical support of the internal combustion engine, enables driving performance to be improved and safety levels enhanced by integrating active safety systems such as radar-assisted cruise control and optical (camera) systems, which produce technologies like the autonomous braking function or the emergency braking function. By recovering braking energy, potential fuel savings of between 6 and 25 % can be achieved in the NEDC driving cycle, depending on the hybrid system (Micro/Mild/Full) and the dimensioning of the generator involved. Hybrid vehicles and regenerative braking technologies thus make a crucial contribution towards reducing CO_2 emissions.

The system utilises the existing actuators and ESC components to optimum effect. It is compatible with all drive train configurations, like front, rear and four-wheel drives, and supports a wide range of different vehicle sizes – from small cars and light vans to SUVs.

4 Summary

TRW aims to support OEM in meeting the stringent requirements for CO_2 reduction, and concentrates here on off-the-shelf solutions that are efficient and, above all, swiftly available. Against this background, TRW emphasises the potential of the technologies already available, such as electrically assisted steering systems. Market analyses show that the demand for electrical steering systems will continue to rise in the years ahead. In TRW's view, electrically assisted steering systems are the technologies of the future, and will, moreover, push the integration of safety systems to a higher level. TRW also presents new concepts like ESC-R and SCB for hybrid vehicles. Rising prices for fuel and the demand for reduced CO_2 emissions will also accelerate the trend towards hybrid and electric vehicles. The SCB technology from TRW has, for example, already been adopted for mass production in some hybrid vehicle applications like the Chevrolet Tahoe. Many other models have meanwhile been announced for the years ahead. ■

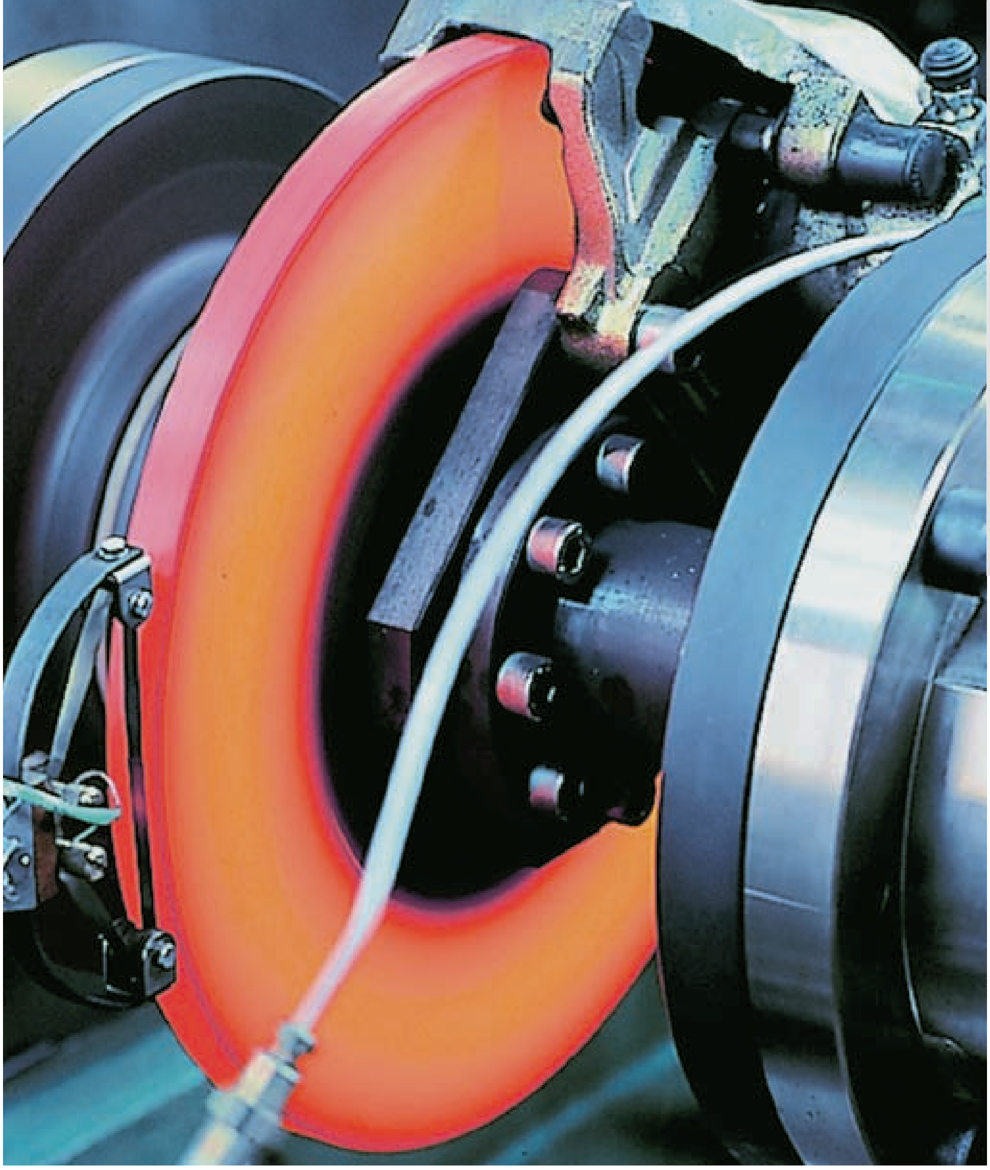

Centre Console Concept
Innovations for More Ease of Use

In its centre console concept, control system specialist Preh has integrated a multitude of innovative technologies. As a result more ease of use can be achieved. Furthermore the centre console presents expanded design options for interior design.

1 Introduction

At first glance the centre console looks elegant and simple, as while the ignition is turned off, all surfaces are smooth black and chrome. Only when the ignition is started does the console "wake up": the gear shifter, which was embedded flat into the console surface before, rises into the ideal operating position for the driver. The icons are now displayed, back-lit in ice-blue, on the surfaces of the control elements, which was a smooth high-gloss black before. This latter effect is known as black panel design and can be achieved in control systems by using a special design.

2 Black Panel Design

The design, with which a black panel effect can be achieved, always looks similar in principle and can be explained on the basis of a button. Initially, the button is produced from transparent plastic (Lexan). In comparison with conventional buttons, where the surface is coated and icons are laser-etched, the black panel button receives just a high-gloss clear coating on the surface. However, the underside of the button is coated with a black varnish that is suitable for laser-etching. Then, the icons are laser-etched onto the button's underside. So that the icons, which are only visible when back-lit, can be read well even from a distance, suitable light distribution of the illuminant is provided. All in all, a high-quality, dark-black surface with low transmission can be achieved using this procedure.

3 Preh-PVD Translucent Surface Technology

The black panel effect can also be used for metallic-look surfaces. The Preh Physical Vapor Deposition (Preh-PVD) surface technology was modified for this purpose. This distributes a very thin coating of real metal onto plastic surfaces in its standard application. The properties of this metal layer then allow laser-etching of the icons and backlighting for night design. The modified Preh-PVD translucent coating procedure is new and still not used in the full-production automotive run. The procedure entails the real metal layer being given translucent properties so that the icons on the button surface are only visible after being back-lit, **Figure 1**.

This technical advancement also has enormous potential for the ambiance lighting in a vehicle's interior, as well as use for the black panel effect for metallic control surfaces. Up to now, design accents, which worked through the targeted use of metal surfaces, could only be seen in daylight. By using the Preh-PVD translucent technology, such surfaces can also be back-lit in night design. **Figure 2** shows an example of the air conditioning control system of the centre console concept, whose frame metal surface can also be back-lit in night design.

Figure 1: Plastic buttons with a genuine-metal surface using Preh-PVD translucent technology

4 Dual-Zone Air Conditioning System with just One Control Knob

The air conditioning control system was designed in such a way that the comfort settings can be operated by the driver and passenger with the same control elements

The Authors

Dipl.-Ing. Wolfgang Küchler heads the advanced development department at Preh GmbH in Bad Neustadt/Saale (Germany).

Dipl.-Kfm. Ronald Schaare heads the marketing and product management department at Preh GmbH in Bad Neustadt/Saale (Germany).

Figure 2: Genuine-metal-look at day and ambient illumination at night, using Preh-PVD translucent technology

(control knob and buttons). One control knob regulates everything. The underlying operating principle here is simple as it is aligned to the seating position. In the initial setting, both air conditioning zones can be set together. If the passenger wants to change the temperature setting for themselves (in Germany for example, the right hand side of the vehicle), he tilts the control knob to the right. Then he selects his desired temperature for the passenger side as usual by turning the knob. If the driver wants to adjust the temperature individually for his air conditioning zone, he tilts the control knob in his direction (that is in Germany to the left).

In order to make this selection function possible, the axis of the control knob is mounted in such a way that the entire chassis of the control knob performs a tilting motion to the right or left when moved. Through appropriate contact with the chassis, the control can recognise which air conditioning zone has been selected.

In order to make even more intuitive operation possible, the design of the control knob has been modified to include an additional feature. The aim of the designers here was to provide other relevant sensory feedback for the control knob to select different functions. Different detent-steps and forces are produced. As a result, for example, when setting the temperature, both a shorter detent interval and a lesser effort is needed when setting the fan, whose detent interval is comparatively longer with a simultaneously increased force being needed to set it. When driving, the user associates a noticeably different tactile feedback with the appropriate function unconsciously after a short amount of time.

This feature was realised technically through a simple and robust mechanical design. To create the engagement, different latches are used, whose contact is controlled through a mechatronic switch. The different engagement strengths are realised using springs allocated to the latches.

5 Design of the Gear Shifter

In the construction of today's vehicles, by-wire technologies are used increasingly. This trend opens up new design options in the centre console, when the traditional mechanical coupling of the gear shifter and gears is omitted as a result. This means that different design forms on the gear shifter can be created right through to total replacement by switch paddles on the steering wheel. The Preh Con centre console concept shows a design variation of the gear shifter with integrated parking brake. In a resting position ("ignition off"), the lever is flat in the centre console and only moves into the operating position when the ignition has been started, Figure 3. The upper part of the gear shifter is used to control. This part has been designed as a rocker and uses downwards pressure and upwards pulling motions. The driver chooses between automatic

Figure 3: Left: gear shifter in resting position; right: gear shifter in operating position

and Steptronic modes using a button integrated into the rocker switch, which can be comfortably operated by thumb. The selected gear (P-R-N-D) is displayed next to the switch in the aforementioned black panel technology. When an overload force is applied to the system, it turns itself off and reverts to the operating position after these overload forces have been removed. A clamp protection provides safety when the gear shifter moves into the "at rest" position when the ignition has been turned off.

As well as an attractive design, the ergonomic formation, robustness, safety and a high-quality sensation were also important guidelines for construction. A complete metal was selected as the material for shaft and rocker. This provides the system with the necessary stability and is an important parameter to produce a "close-fitting" switch feeling. The haptic feel of the rocker was adjusted using magnetic technology for a defined calibration of the switching force. A robustly embedded worm drive ensures the gear shifter moves into the resting position and operating position when necessary.

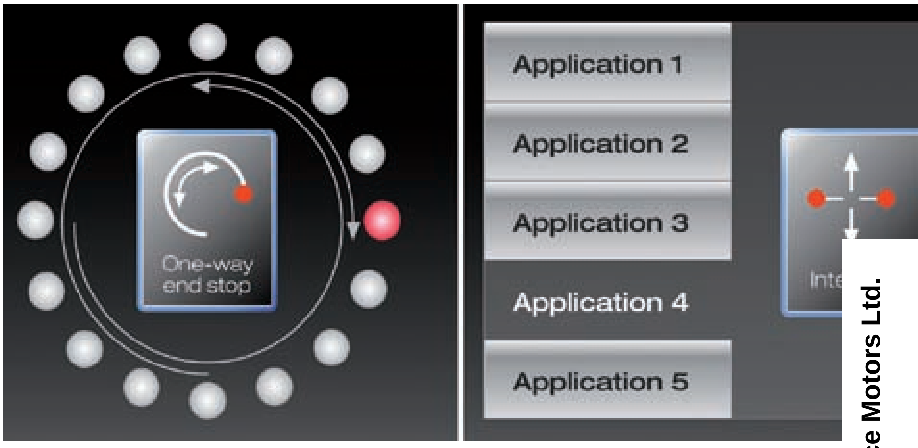

Figure 4: Left: rotating stop at end of menu; right: specific locking of tilting directions

6 Central Control System with Sensory User Guidance

With some of the systems established on the market to date, the user navigates in the different menu points using the multi-functional control element by turning, pushing and tilting. However, this does not ensure that a function is always selected during an operating step; it is necessary to check on the selection menu on the vehicle display. So that the driver can concentrate with as little distraction from the windscreen as possible, one aim of the redesign was to achieve a simplified function selection as well as largely avoiding operating errors. To achieve this, a haptic user guide was developed, which provides function-dependent mechanical locking. This makes tilting the control element into different directions possible or not possible, depending on the configuration of the selection menu. The example in **Figure 4** right shows a menu, in which five applications can be selected. Application four is highlighted, marking the position at which the control element is found at that moment. The only reasonable movement directions here are upwards in the direction of application three or downwards to application five. Therefore, an intelligent, menu-dependent locking makes sure that the control element can only move in these directions, that is neither left nor right. If menu point five is then selected, the end of the menu is reached at the same

Figure 5: Dual touchpad for operating navigation and telephone

personal buildup for Force Motors Ltd.

Figure 6: Ergonomic design

time so that another movement downwards is now blocked. The user feels this clearly as a hard mechanical locking. All in all, when using this technology, the user is only able to access those control channels which are necessary to select the function. As a result, his perception is relieved as he receives clear, tactile feedback and is no longer entirely dependable on visual checks.

In a similar way, blocks for the rotary function of the control element can also be set. For example, it is possible to prevent continued turning in the different function menus, when the end of the setting options is reached, Figure 4 left.

The technical realisation of the tilting functions relies on a mechanical design, while the haptic feel is realised using magnets. The locks for the tilting functions are based on a mechatronic concept, with which a locking element is moved under a back bracket. Also the hard rotary blocks have been implemented using a mechatronic design. As a result, a blocking element is moved and held in a defined way. The position of the controllable blocks is provided through a fixed mechanical coupling, so that an exact high-quality haptic feel can also be achieved.

7 Touchpad with Dual Function

The touchpad, which is integrated directly in front of the arm rest, is an innovation as it can be used, firstly, for the navigation selection and, secondly, as a telephone pad, **Figure 5**.

The advantages of the navigation selection in comparison with the conventional procedure are clear. To date, the place name has had to be entered letter by letter by turning and pressing. Selection via touchpad is clearly simpler and quicker. Here, the user moves a cursor – quite similar to a computer touchpad – over the map image on the vehicle display and selects his destination by clicking.

When the telephone mode is activated, a telephone keypad appears on the surface of the touchpad and on the vehicle display screen. When selecting the telephone number, the user, as he is used to from using a telephone, receives feedback on all three sensory channels: sensory, optical and acoustic.

8 Ergonomic Concept

The ergonomic design of the centre console at hand was selected after weighting the widest range of practical requirements on the innovative control features. So that the forearm and wrist can rest stably on the central arm rest, while the navigation destination or telephone number is selected, the touchpad is located immediately in front of the arm rest, **Figure 6**. In order to dial a telephone number safely even while driving, the driver does not need to look at the touchpad. Using capacitive technology, the position of the finger is detected and the appropriate icon, above which the finger is, is distinctly emphasised in the vehicle display. This means that it is even possible to dial a phone number by looking very briefly to the side at the display.

If a function selection is being made through the central control element, the rear part of the forearm rests on the arm rest, while to operate the gear shifter, the forearm is completely raised, as is generally the case in today's vehicles. ■

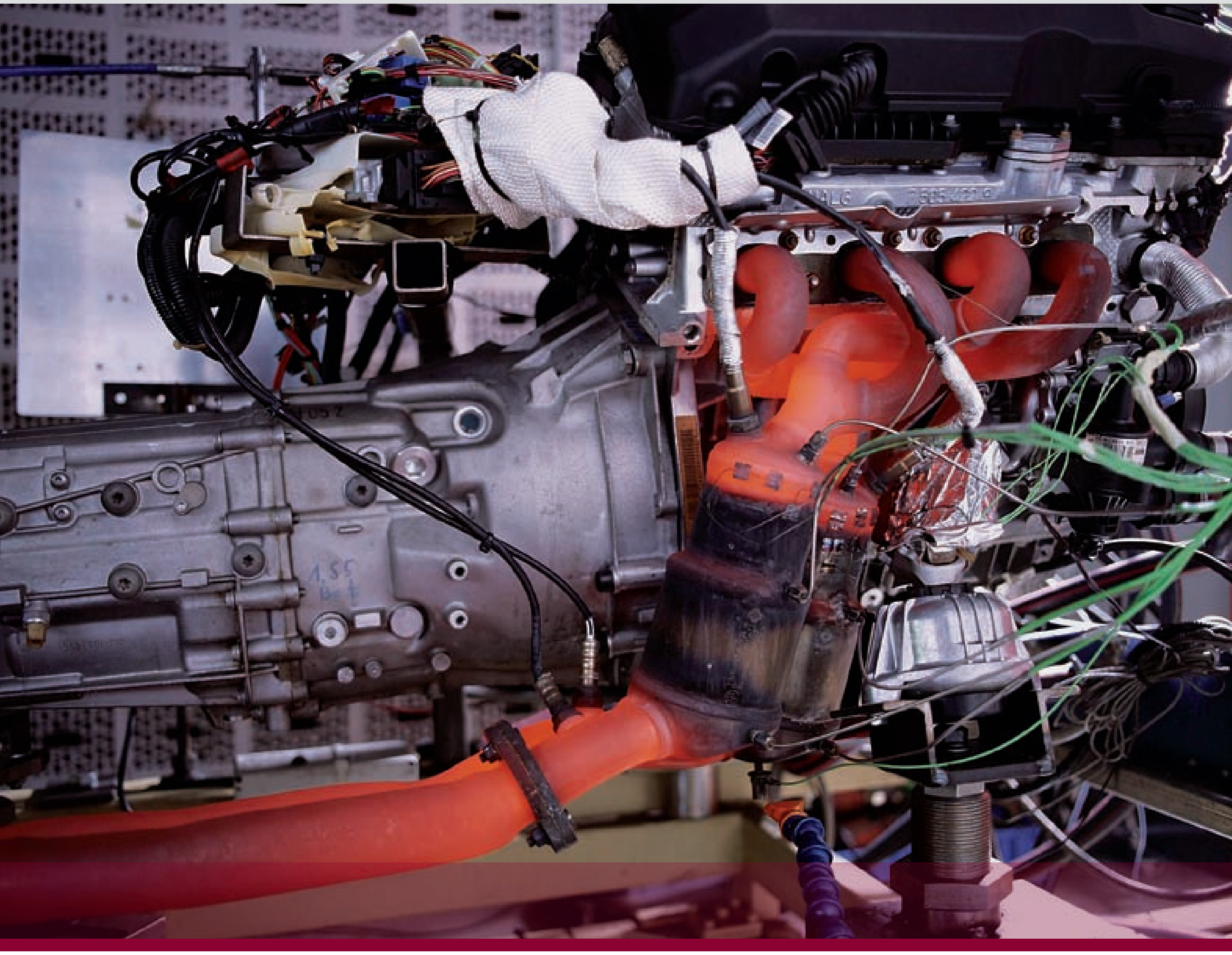

Engine Model for Dynamic Simulation of Exhaust Systems Derived from Measured Data

Nowadays, the FEA has become an indispensable tool in the durability investigation of exhaust systems. A realistic dynamic simulation requires that its boundary conditions are reproduced as closely as possible. To realize this, the excitation data is extracted from experimental measurements. Compared with the exhaust system, the powertrain (engine and transmission) is much stiffer, so it can be treated as a rigid body. Tenneco developed a tool to generate a simplified engine model and related excitation data automatically. This program optimizes computational speed and robustness.

1 Introduction

The dynamic response of automotive powertrain affects exhaust systems in many aspects, especially the lifetime durability of components. There are two ways to investigate the durability: Experimental test and numerical simulation. In consideration of costs and practicability, the FEA became an indispensable tool.

Figure 1 demonstrates a powertrain connected to an exhaust system, which is characterized by a long structure in geometry. So far, it is difficult to integrate a fully meshed powertrain into exhaust system for dynamic computations due to long computation time. Compared with exhaust system, powertrain is much stiffer. Therefore the powertrain can be assumed as a rigid body and simplified as a mass/inertia system. Besides, the engine excitations play an important role in the dynamic simulations of exhaust systems. Two kinds of excitations are used in the dynamic simulation: The force/moment and the enforced motion method. The second one is straightforward because the movements of powertrain can be measured directly by using acceleration sensors.

Thus, this method is applied both in industrial tests and numerical simulations. The purpose of the work done by Tenneco is to generate a robust and reliable engine model based on measurements of the powertrain for dynamic analysis with the FEA solver Nastran.

2 Enforced Motion Method

For the simulation of dynamic response of exhaust systems, engine excitation in the form of forces and moments is always optimal, since the excitation is induced by internal forces of engine. Thus, it can be named as primary excitation. Nevertheless the primary excitation is not straightforward, because the measurements of excitation are accelerations. They can be expanded to velocities and displacements by using the integral to time. Thus, engine excitation in the form of enforced motion can be fetched directly from experimental measurements. However, since the measurements from experiments are essentially the response of engine block and exhaust system, it is named as secondary excitation.

To realize the secondary excitation in FEA model, excitation points must be constrained, so boundary conditions of the model are changed compared with the primary excitation. This can result in change of the modal eigenvalues. Fortunately, the mass of powertrain is normally much larger than that of total exhaust system, so that the secondary excitation – enforced motion – is reasonable for the dynamic analysis of exhaust systems.

Based on the experience of Tenneco, if the mass of powertrain is ten times greater than that of the exhaust system, the dynamic responses of exhaust system by using the primary and the secondary excitations are nearly the same above 30 Hz.

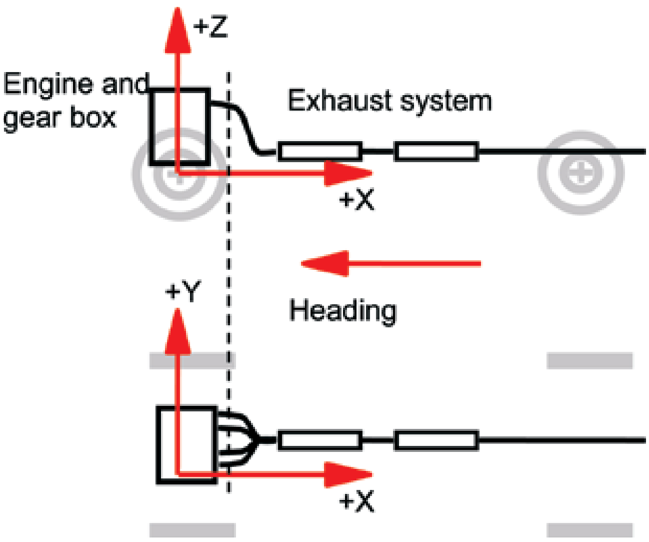

Figure 1: Schematic demonstration of layout of exhaust systems

The Authors

Dr.-Ing.
Shunxin Zhou
works as FE analyst and R&D engineer for new methods and processes in simulation at Tenneco Emission Control Europe, Heinrich Gillet GmbH in Edenkoben (Germany).

Dipl.-Ing. Yu Wang
works as FE analyst and R&D engineer for new methods and processes in simulation at Tenneco Emission Control Europe, Heinrich Gillet GmbH in Edenkoben (Germany).

Dipl.-Ing.
Peter Feisst
is responsible for durability engineering and advanced development of new methods and processes at Tenneco Emission Control Europe, Heinrich Gillet GmbH in Edenkoben (Germany).

Philipp Salomon
is responsible for linear structural dynamic FEA calculation and development of new methods and processes in simulation at Tenneco Emission Control Europe, Heinrich Gillet GmbH in Edenkoben (Germany).

With the increase of performance of computer hardware und FEA software, the application of the enforced motion method was improved and stabilized [1]. Up to 1995, relatively simple excitation models were applied with only one degree of freedom in the direction of engine piston movement. A constant excitation in the total frequency range was restricted for cold end, for example 0.1 mm in a four-cylinder engine.

From 1995 to 2003, the enforced motion was improved by the use of multi-axial excitations, nevertheless amplitudes were still assumed to be constant in total frequency range. Since 2004 with the Nastran release for advanced enforced motion, a multi-axial spectral and complex, which is defined as enforced motion, can be directly obtained from experimental measurements, so that the excitation data is able to represent the real vibration behavior of powertrain.

To measure the movement of powertrain, acceleration sensors must be equipped at least at three locations on powertrain. **Figure 2** shows schematically measuring points on a powertrain. Three points P1, P2 and P3 are spanned on the powertrain so that they can fully describe the rigid body motion of engine block. At each point, three acceleration channels are set up in x-, y- and z-directions, respectively. That is, nine signal channels are obtained simultaneously.

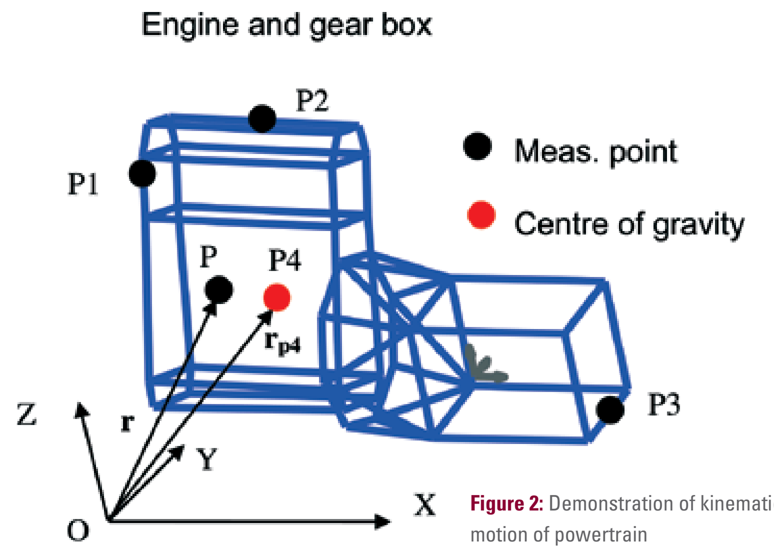

Figure 2: Demonstration of kinematical motion of powertrain

3 Reduction of Multipoint Measurements

It is known based on the theory of rigid body motion that the movement of a rigid body can be fully described by six degrees of freedom. As mentioned above, the experimental data is measured in at least nine degrees of freedom in tests. Therefore excitation can be simplified by transferring measurements from three measuring points to an arbitrary point, and the degrees of freedom can be reduced to six during this process.

To guarantee reasonable results from FEA – especially for dynamics calculation –, the model should be correlated in advance. This is done in two steps: First, the correlation of physical features of the FEA model, for example masses, material properties, and geometries. The second step is the correlation of excitation like scaling, smoothing, and peak shifting. Both steps give significant influences to MAC (Modal Assurance Criterion) values. Besides the function "correlation of measurement with FEA", the signals of engine excitation have to be elevated for the simulation in some specially load cases [2].

Figure 2 schematically illustrates a powertrain and the reduction of measurements from P1, P2, and P3 to P4. For a rigid body, the velocity at an arbitrary point P can be expressed as:

$$v = v_{P4} + \omega_{P4} \times (r - r_{P4}) \qquad \text{Eq. (1)}$$

Applying Eq. (1) to all measuring points gives:

$$Ax = y \qquad \text{Eq. (2)}$$

Here, A is the geometric matrix, x represents the rigid body motion at point P4 and y are signals from measurements. Because at least three measuring points P1, P2 und P3 are used, the equation systems in Eq. (2) are over-determined. The implemented pseudo-inverse creates an averaged solution in favor of the smallest error-square. When the magnitude of engine vibration is very small, the form of Eq. (2) can be also applied for displacement and acceleration.

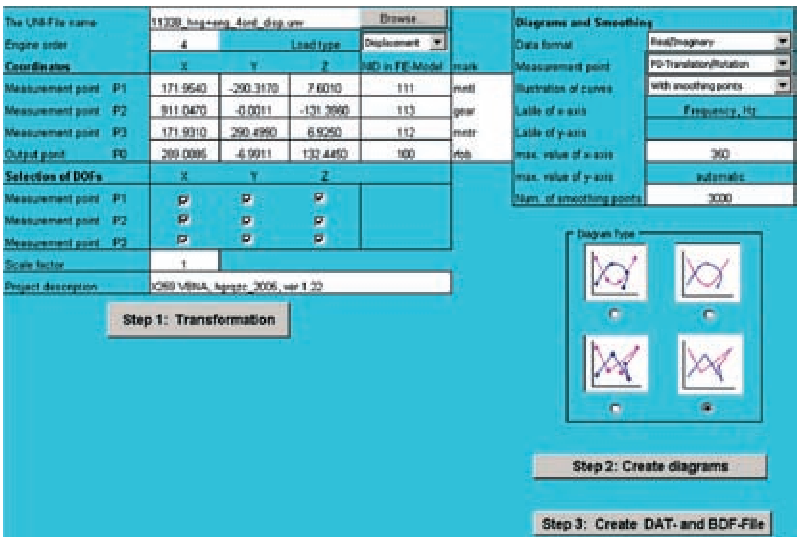

Figure 3: Software for the engine model

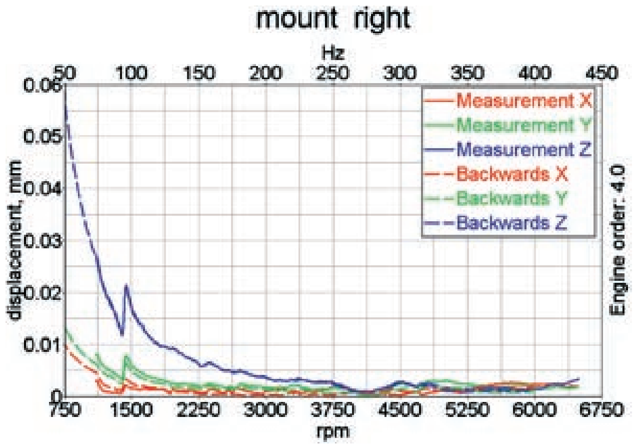

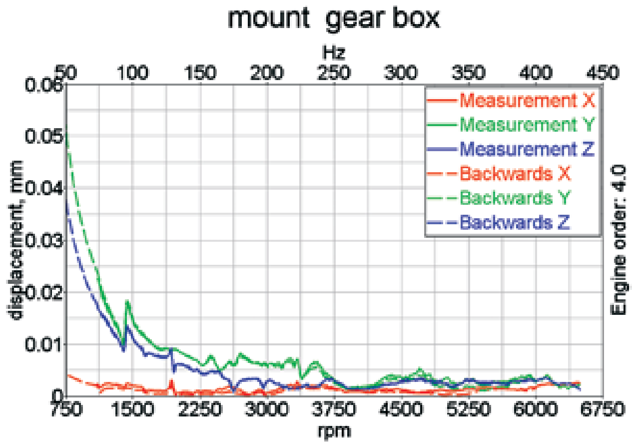

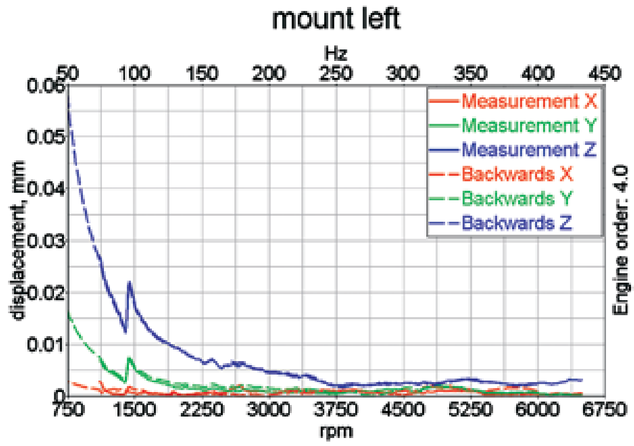

Figure 4: Verification of rigid body motion of engine block – measurement and simulation at mount right (top left), at gear box mount (top right) and at mount left (down)

4 Software for the Engine Model

Tenneco has developed a software package, which is composed of a Fortran kernel and VBA interface (visual basic application). The combination of Fortran with VBA has an advantage that mathematical options in Fortran are powerful and very fast whereas the VBA has convenient interface functions. The software includes: read-in experimental measurements, reduction of three-point excitation to single-point excitation data, and generating an engine model for dynamic simulations. The user interface of the software is shown in **Figure 3**.

4.1 Input and Data Transformation

The users' interface is quite simple. Affordable data like measurement data file (universal file format 58), coordinates of measuring points, engine order, and load type (displacement, velocity and acceleration) should be specified at first in the interface, which is done intuitively. The input in the "DOF Selection" section can be used to remove data channels, which carry wrong measured data significantly influenced by noise. In addition, the unit of measurements can be converted by using a scale factor. By clicking button "Step 1: Transformation", the original measurement data is read in and transformed to the output point P4. Two tables are generated simultaneously, which incorporate all the data in unified format.

To verify the assumption of rigid body motion for powertrain, a backward transformation by use of the solver Nastran from output point P4 to the measuring points P1, P2, and P3 was performed, as shown in **Figure 4**. The diagrams show that the FEA output from backward transformation is significantly close to measurements. That means, the transformed motion at the output point P4 can correctly describe the rigid body motion of the powertrain.

4.2 Diagrams and Data Smoothing

By using pull-down menu "Diagrams and Smoothing", different options can be selected for the illustration of output data and presentation possibilities: Data format can be used to switch the forms of excitation data to real/imaginary or magnitude/phase. Measurement point is used to specify, whether the spectra of 3-point-excitation or 1-point-excitation is to be displayed.

With the help of the menu "Illustration of Curves", it can be selected, whether the spectrum curves should be smoothed. **Figure 5** shows the difference between raw data from measurements (black curve) and the smoothed output (magenta curve). The small peak in black curve is due to the reaction from a resonance in exhaust system. When used for excitation data, this kind of peaks should be removed. By using the filter function, the peaks can be diminished, as shown by the pink curve. The curves can be further smoothed or corrected manually by dragging individual sampling points by mouse, which is a standard function in Microsoft Excel, as shown in the cut-out in Figure 5. Additionally, the scaling of

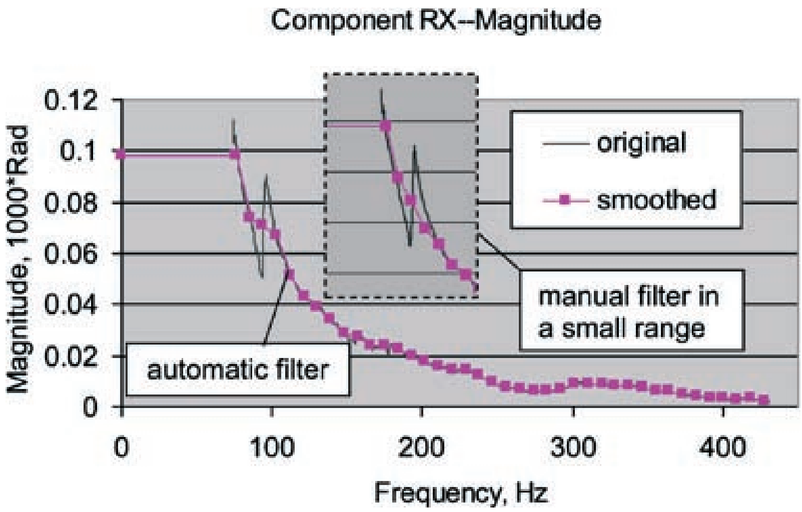

Figure 5: Data filter

diagram axes and the display type of diagram can be defined in the interface too. After accomplishing above settings, the curves of excitation spectrum can be displayed by clicking the button "Step 2: Create Diagrams".

4.3 Engine Model for the Nastran Solver

By clicking button "Step 3: Create Data and BDF File", the excitation spectra illustrated in the steps before are exported into Nastran bulk data file (Nastran BDF). A dummy engine model is generated by means of beam elements, which represent the rigid body motion of the powertrain. Additionally, a master deck for frequency response analysis in Nastran is generated simultaneously.

5 Summary and Conclusion

Based on experimental measurement data, Tenneco has developed a tool to generate a dummy engine model to apply excitation profiles for the dynamic frequency response analysis of exhaust systems. It has been proved that the powertrain can be regarded as a rigid body. The experience in practice at Tenneco encourages this topic.

Thus, the reduction of several measured distributed points with nine degrees of freedom to a single point with six degrees of freedom is allowed. The reduced measured data can be smoothed by using data filter function in the software for a better work in Nastran for easier processing and stabilization. Finally, it has to be mentioned that an easy manipulation of excitation data is possible as it is required for comparisons between measurement and simulation. In case of significant feedback of the exhaust system's dynamic movement, primary excitation based on force/moment is recommended.

References

[1] Feisst, P.: FE-Analyse in Abgasanlagen. Interner Bericht, Tenneco, Edenkoben, 2005
[2] Feisst, P.; Maier, A., Pettrich, T.: Ersatzlastbestimmung für System- und Komponententest bei Abgasanlagen. In: MTZ Motortechnische Zeitschrift 68 (2007), Nr. 9, S. 720–725

Peer Review ATZ|MTZ

Peer Review Process for Research Articles in ATZ and MTZ

Steering Committee

Prof. Dr.-Ing. Stefan Gies	RWTH Aachen	Institut für Kraftfahrwesen Aachen
Prof. Dipl.-Des. Wolfgang Kraus	HAW Hamburg	Department Fahrzeugtechnik und Flugzeugbau
Prof. Dr.-Ing. Ferit Küçükay	Technische Universität Braunschweig	Institut für Fahrzeugtechnik
Prof. Dr.-Ing. Stefan Pischinger	RWTH Aachen	Lehrstuhl für Verbrennungskraftmaschinen
Prof. Dr.-Ing. Hans-Christian Reuss	Universität Stuttgart	Institut für Verbrennungsmotoren und Kraftfahrwesen
Prof. Dr.-Ing. Ulrich Spicher	Universität Karlsruhe	Institut für Kolbenmaschinen
Prof. Dr.-Ing. Hans Zellbeck	Technische Universität Dresden	Lehrstuhl für Verbrennungsmotoren

Advisory Board

Prof. Dr.-Ing. Klaus Augsburg	**Prof. Dr.-Ing. Martin Meywerk**
Prof. Dr.-Ing. Bernard Bäker	**Prof. Dr.-Ing. Werner Mischke**
Dr.-Ing. Christoph Bollig	**Prof. Dr.-Ing. Klaus D. Müller-Glaser**
Prof. Dr. sc. techn. Konstantinos Boulouchos	**Dr. techn. Reinhard Mundl**
Prof. Dr.-Ing. Ralph Bruder	**Dipl.-Ing. Sascha Ott**
Dr. Gerhard Bruner	**Dr.-Ing. Lothar Patberg**
Prof. Dr. rer. nat. habil. Olaf Deutschmann	**Prof. Dr.-Ing. Peter Pelz**
Dr. techn. Arno Eichberger	**Prof. Dr. techn. Ernst Pucher**
Prof. Dr. techn. Helmut Eichlseder	**Dr. Jochen Rauh**
Dr.-Ing. Gerald Eifler	**Prof. Dr.-Ing. Konrad Reif**
Prof. Dr.-Ing. Wolfgang Eifler	**Dr.-Ing. Swen Schaub**
Prof. Dr. rer. nat. Frank Gauterin	**Prof. Dr. rer.-nat. Christof Schulz**
Prof. Dr. techn. Bernhard Geringer	**Prof. Dr. rer. nat. Andy Schürr**
Prof. Dr.-Ing. Uwe Grebe (enquired)	**Prof. Dr.-Ing. Ulrich Seiffert**
Prof. Dr.-Ing. Horst Harndorf	**Prof. Dr.-Ing. Hermann J. Stadtfeld**
Prof. Dr. techn. Wolfgang Hirschberg	**Prof. Dr. techn. Hermann Steffan**
Univ.-Doz. Dr. techn. Peter Hofmann	**Dr.-Ing. Wolfgang Steiger**
Prof. Dr.-Ing. Günter Hohenberg	**Prof. Dr.-Ing. Peter Steinberg**
Prof. Dr.-Ing. Bernd-Robert Höhn	**Prof. Dr.-Ing. Christoph Stiller**
Prof. Dr. rer. nat. Peter Holstein	**Dr.-Ing. Peter Stommel**
Prof. Dr.-Ing. habil. Werner Hufenbach	**Prof. Dr.-Ing. Wolfgang Thiemann**
Prof. Dr.- Ing. Roland Kasper	**Prof. Dr.-Ing. Helmut Tschöke**
Prof. Dr.-Ing. Tran Quoc Khanh	**Dr.-Ing. Pim van der Jagt**
Dr. Philip Köhn	**Prof. Dr.-Ing. Georg Wachtmeister**
Prof. Dr.-Ing. Ulrich Konigorski	**Prof. Dr.-Ing. Henning Wallentowitz**
Dr. Oliver Kröcher	**Prof. Dr.-Ing. Jochen Wiedemann**
Dr. Christian Krüger	**Prof. Dr. techn. Andreas Wimmer**
Univ.-Ass. Dr. techn. Thomas Lauer	**Prof Dr. rer. nat. Hermann Winner**
Dr. Malte Lewerenz	**Prof. Dr. med. habil. Hartmut Witte**
Dr.-Ing. Markus Lienkamp	**Dr. rer. nat. Bodo Wolf**
Prof. Dr. rer. nat. habil. Ulrich Maas	

Scientific articles in ATZ Automobiltechnische Zeitschrift and MTZ Motortechnische Zeitschrift are subject to a proofing method, the so-called peer review process. Articles accepted by the editors are reviewed by experts from research and industry before publication. For the reader, the peer review process further enhances the quality of ATZ and MTZ as leading scientific journals in the field of vehicle and engine technology on a national and international level. For authors, it provides a scientifically recognised publication platform.

Therefore, since the second quarter of 2008, ATZ and MTZ have the status of refereed publications. The German association "WKM Wissenschaftliche Gesellschaft für Kraftfahrzeug- und Motorentechnik" supports the magazines in the introduction and execution of the peer review process. The WKM has also applied to the German Research Foundation (DFG) for the magazines to be included in the "Impact Factor" (IF) list.

In the ATZ/MTZ Peer Review Process, once the editorial staff has received an article, it is reviewed by two experts from the Advisory Board. If these experts do not reach a unanimous agreement, a member of the Steering Committee acts as an arbitrator. Following the experts' recommended corrections and subsequent editing by the author, the article is accepted. *rei*

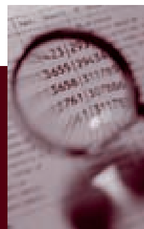

ATZ Peer Review
The Seal of Approval for scientific articles in ATZ.
Reviewed by experts from research and industry.

Received ....
Reviewed ....
Accepted ....

Seal of Approval – this seal is awarded to articles in ATZ/MTZ that have successfully completed the peer review process

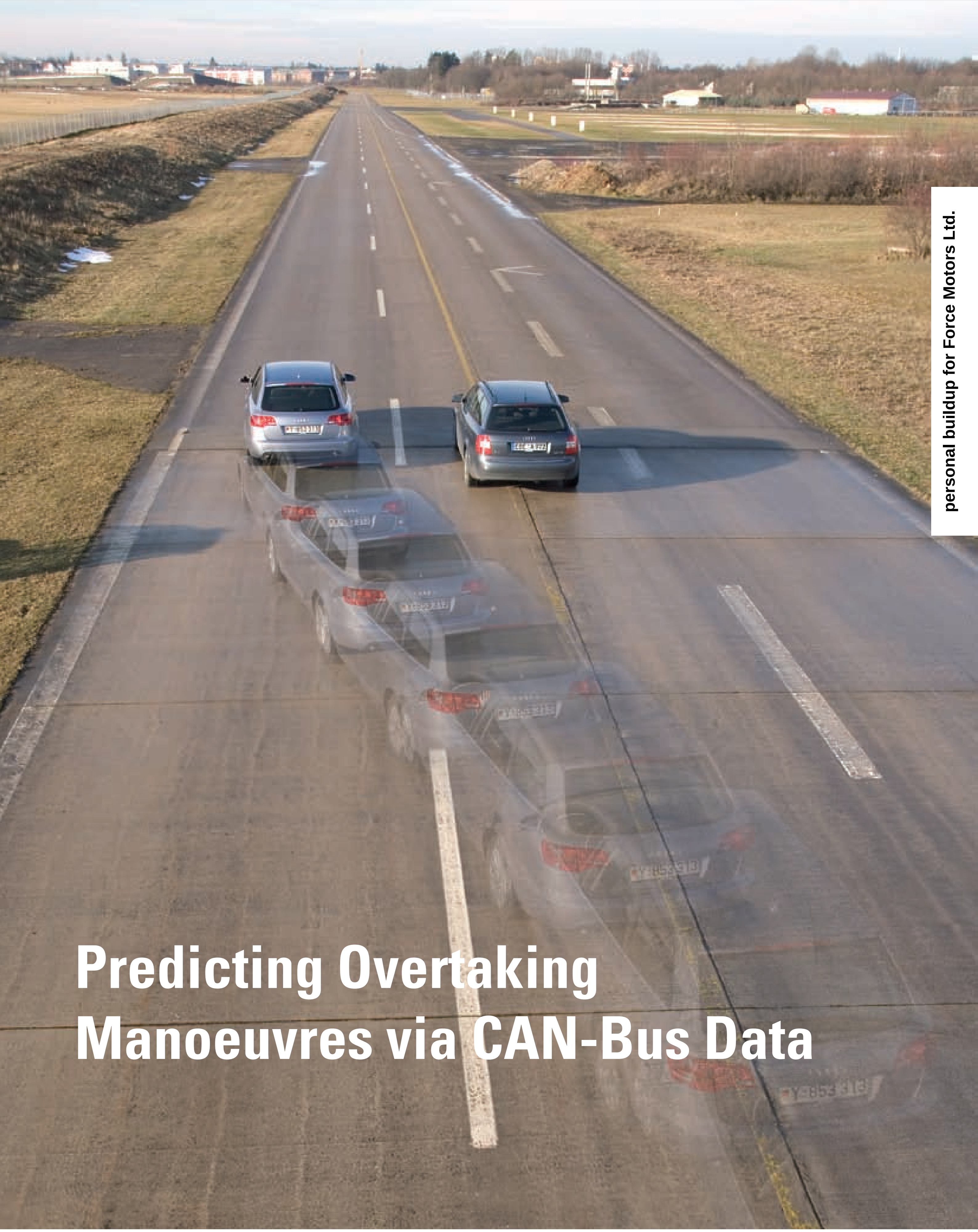

Predicting Overtaking Manoeuvres via CAN-Bus Data

In order to resolve the conflict between the support and autocracy of advanced driver assistance systems (ADAS), system control must incorporate the driver him/herself. At the Human Factors Institute of the Bundeswehr University Munich, research is therefore being conducted on the prediction of driver intention, which can greatly increase the specificity of driver assistance. This article describes the development of an algorithm which is based on currently available vehicle sensors and which is able to predict overtaking manoeuvres with a high level of reliability.

1 Introduction

The development of ADAS in the area of longitudinal and lateral control is increasingly leading to a take-over of the driving task on the part of systems. While conventional cruise control systems were only able to maintain a pre-set speed, modern adaptive cruise control (ACC) systems detect and adjust to vehicles ahead and enable vehicle control across the entire speed spectrum. In the near future, further functions ranging from longitudinal acceleration to emergency braking will also be possible, **Figure 1**.

Similar qualities and aims can be seen when examining the development of ADAS in the domain of lateral control. With the evolution of adequate lane tracking, lane departure warning (LDW) systems which attract drivers' attention upon lane departure were introduced onto the market. Development progressed from direction-unspecific warning signals to heading-control systems which take over part of the lateral control task via directed steering torques on the steering wheel. Depending on parameterisation, this take over can occur exclusively at the edge of the lane (e. g., VW Passat CC) or as a permanent supporting feature (e. g., Lexus LS 460).

It is, however, becoming increasingly apparent that the driver assistance provided by these systems does not automatically bring relief to the driver. While lane-keeping assistants offer a certain amount of support, the driver must continually check that the system is functioning correctly and intervene whenever the system fails to operate in line with his/her notion of lateral control. A similar problem also applies to LDW. Current systems require the driver to either indicate or actively work against the system when changing lanes. Traffic observations [1] show, however, that drivers only indicate in half of lane changes on the motorway and one third of inner-city lane changes.

According to this a study by LeBlanc et al [2] demonstrated 26 % of lane departure warnings due to lane changes. The participants of the study by Alkim et al. [3] judged the lane departure warning system as effective but, because of too many warnings, also as annoying. False alarms not only lead to an acceptance problem among "lazy indicators"; they also reduce the warning nature of system alerts which in turn reduces not

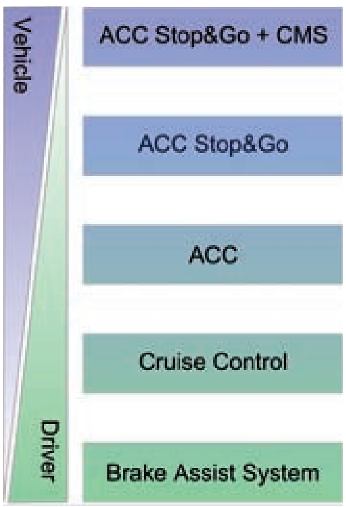

Figure 1: Division of longitudinal control between driver and vehicle

The Authors

Dipl.-Psych.
Christoph Blaschke
is research assistant in the area of research "driver intention recognition and driver state recognition" at the human factors institute at the Bundeswehr Universität in Munich (Germany).

Dipl.-Ing.
Josef Schmitt
is research assistant in the area of research "advanced driver assistant systems" at the human factors institute at the Bundeswehr Universität in Munich (Germany).

Prof. Dr.
Berthold Färber
is head of the human factors institute at the Bundeswehr Universität in Munich (Germany).

ATZ Peer Review
The Seal of Approval for scientific articles in ATZ.
Reviewed by experts from research and industry.

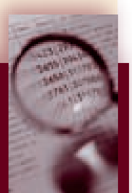

Received .... July 14, 2008
Reviewed .... August 22, 2008
Accepted .... September 2, 2008

only driver reactions [4] but also the potential increase in safety provided by such a system. ADAS are designed to support and not unduly dictate or issue unnecessary warnings to the driver. Kompass & Huber [5] summarized the idea in No. 3 of their 10 golden rules of driver assistance: "Driver assistance should preserve a driver's sovereignty by being supportive, but not patronizing, in operating such system. The driver should not be inadvertently controlled by the driver assistance system".

The basic problem is often to be found in the input parameters of the respective system control. Given that driving constitutes an interaction between environment, vehicle and driver, control should not be restrictively based on vehicle and environment data. Instead, the driver him/herself should be integrated into the data fusion in the form of sensor data or, at the very least, be able to configure system behaviour to meet her/his own needs. This could be accomplished in a variety of ways: by accounting for driving style, driver intention, or driver state. With respect to the first of these, an increasing number of driver settings already take driving style into account, including, for example, preferred distance settings in the case of ACC and variable warning times in the case of LDW.

In the context of "driver state", the first drowsiness warning systems (e. g., Volvo's "Driver Alert Control") which aim to recognize drops in driver performance over a more extended period of time are already on the market. Research is underway on possibilities of recognizing short-term attention deficits due to distracting activities [6].

The recognition of driver intention offers a particularly large range of possibilities for improvement with respect to the problems mentioned above. Driver intention is to be found in all three levels of vehicle guidance, although it plays only a subordinate role at the navigation level in the form of route planning. Driver intention is considerably more important at the guidance level (i. e., intended driving manoeuvres) and the vehicle control level. Some simple driver intention predictions have already found implementation, for example "braking" in brake assist systems. The high speed with which the accelerator pedal is released represents a typical indicator of braking intention on the part of the driver. This indicator reliably implies braking intention with very little additional information [7].

Lateral and longitudinal assistance systems might also be adapted based on driving manoeuvre prediction at the guidance level. The prediction of an ensuing overtaking manoeuvre may, for example, enable a lane departure warning signal to be overridden independently of unreliable driver-intention recognition based on whether the driver indicates. A system of this kind would be considerably more driver-friendly. However, it is not only the extended time frame which makes predictions of overtaking manoeuvres difficult. The primary problem lies in the fact that there are no universally valid or singular behavioural indicators for overtaking manoeuvres, such as the sudden release of the accelerator pedal in the case of emergency braking. Overtaking is rather characterized by the interplay of various environmental and driver-related factors which must be identified and interpreted.

As a result of this complexity, two different approaches to predicting driving manoeuvres are to be found in the respective literature. The first of these approaches encompasses studies in which machine-learning algorithms are used [8-10]. Oliver and Pentland [8], for instance, used Hidden Markov models to predict overtaking manoeuvres with a high level of reliability approximately one second before their performance. As also applies to many other studies, the authors failed to assess false-positive predictions of overtaking manoeuvres (i. e., the number of overtaking manoeuvres predicted which did not occur). Furthermore, the algorithm was not validated for other situations or drivers, so that no conclusions can be drawn concerning the generalizability of the findings. The second group of studies found in the literature apply a theoretically oriented approach [11,12]. Salvucci (e. g., [11]), for example, was able to recognize 85 % of lane changes based on cognitive driver models. This investigations were, however, conducted exclusively in simulators.

In the following, the development of an algorithm for the prediction of overtaking manoeuvres is described. This algorithm can be used to override unwarranted lane departure warnings independently of whether the driver indicates.

2 The Good Passenger as Prototype

The theoretical prototype used for the structural composition of the algorithm is that of a "good passenger" who is able to distinguish between lane departures due to inattentiveness and as preparation for overtaking manoeuvres. The good passenger is highly reliable in making very few false predictions. The pertinent question is therefore how passengers recognize driver intentions to overtake.

The information which the driver requires when deciding to perform an overtaking manoeuvre predominantly relate to the traffic situation; information which is also available to the passenger in making manoeuvre predictions. An assessment of relevant traffic situation indicators via vehicle sensors should thus enable automatic predictions of driver intentions to overtake.

Psychological action models such as the Rubicon Model [13] aid understanding of how people form action intentions, make action decisions, and finally execute these actions. Potential indicators which – from a technical view point – might prove useful for prediction were therefore first determined based on the phases of this action model. In a next step, the list was reduced to indicators for which sensors in luxury-class vehicles were already available.

It was then necessary to collect representative data on driver behaviour in overtaking manoeuvres and driver behaviour when following the road without overtaking. To this end, a field experiment was conducted in which 28 participants aged between 22 and 65 years drove with varying speeds along a country road. A vehicle ahead drove partly at the same speed and partly 30 km/h slower than the recommended speed limit. Participants were instructed that they were permitted to overtake vehicles ahead. This procedure generated data on 43 overtaking manoeuvres. Vehicle data stemming from those journeys in which the vehicle ahead was not overtaken or in which the test vehicle complied with instructions to turn off were used as a point of reference.

Table 1: Linguistic variables of Fuzzy Sets

Indicator	Fuzzy Set
Distance between ego and vehicle ahead	small – normal – high
Difference in speed: ego to vehicle ahead	high – medium – near zero – negative
Brake pressure ego vehicle	no breaking – small – medium – high
Accelerator pedal value ego vehicle	near zero – small – medium – high – very high
Accelerator pedal speed ego vehicle	negative – normal – kickdown

Table 2: Examples of rules in the Fuzzy-System – the parts of the premise are connected with „and"-operations; permutations of all linguistic variables can be summarized to 100 meaningful rules (same-weighted)

Premise					Conclusion
Distance	Difference in speed	Break pressure	Accelerator pedal value	Accelerator pedal speed	
…					
normal	near zero	no breaking	small	normal	following the road
normal	medium	no breaking	high	normal	overtaking
small	medium	medium	near zero		following the road
high	high	no breaking	very high	kickdown	overtaking
…					

Frequency distributions for the various indicators were derived according to manoeuvre. The following indicators proved relevant for overtaking:
– distance between ego vehicle and vehicle ahead
– difference in speed between ego vehicle and vehicle ahead
– brake pressure ego vehicle
– accelerator pedal value ego vehicle
– accelerator pedal speed ego vehicle.

Continuing with the analogy of human prediction processes, the connection between information and the process of inferring driver intention, Zadeh's Fuzzy Logic [14] was used to integrate individual indicators. Similar to human inference processes, fuzzy input variables (e. g., normal to small distance from vehicle ahead) were connected via a set of rules which determined degree of membership for various initial conditions and subsequently provided predictions.

The Fuzzy-System was constructed using the Matlab software package (The MathWorks). Fuzzy Sets were compiled for all indicators, **Table 1**. The distance from a vehicle ahead was, for example, classified as "high", "normal", or "small". Via the above named frequency distributions, it was then possible to define membership functions for these linguistic variables. All meaningful Fuzzy-Set permutations were additionally combined to form a body of 100 same-weighted rules which distinguished between the conclusions "following the road" and "overtaking", **Table 2**. "Mamdani"-method was used as Inference System („Minimum"-Implication, „Maximum"-Aggregation, „Centroid"-Defuzzification).

This Fuzzy System was subsequently applied to the field experiment driving trials. **Figure 2** depicts various examples of CAN-signals and the algorithm-based prediction during an overtaking manoeuvre.

Two measures were used to determine the accuracy of prediction. First, the number of overtaking manoeuvres correctly predicted from the 43 actual manoeuvres performed (operationalized as lane departure). A high level of accuracy was found with accurate system predictions being provided for 41 of the 43 (95 %) manoeuvres. In contrast to previous studies, the occurrence of false predictions (i. e., overtaking manoeuvres predicted in cases of no overtaking) was also examined based on the data of those drivers who "followed the road". Wrong predictions occurred in only 4 of the 55 trial drives (7 %).

In order to employ information on overtaking intention in LDW systems, however, a certain length of time is required in advance of manoeuvre performance – in this case, predictions must be made before the driver departs from his/her lane. The second measure of ac-

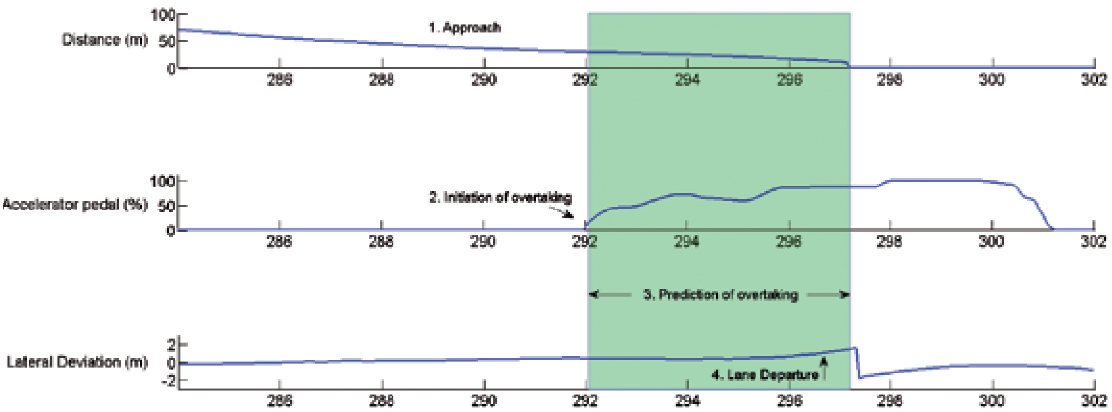

Figure 2: Example of an overtaking prediction

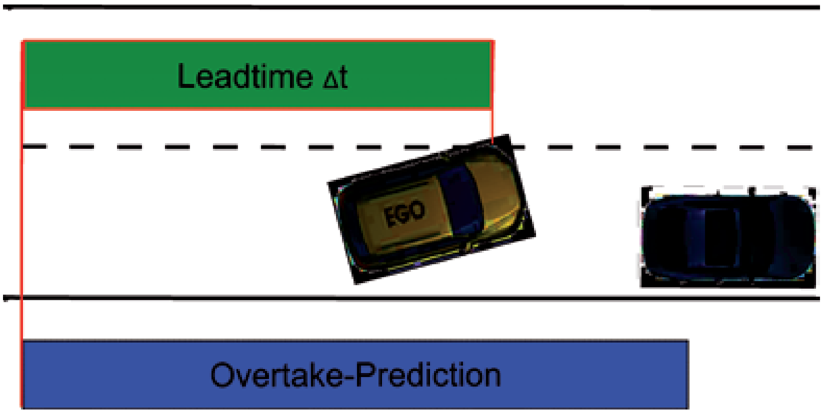

Figure 3: Measure of accuracy: leadtime

curacy therefore determined the length of time between stable prediction of correctly classified overtaking manoeuvre and lane departure, **Figure 3**. The algorithm was able to predict overtaking manoeuvres an average of 2.3 seconds prior to lane departure.

In summary, the algorithm under examination provided good results. Nonetheless, it remains to be seen whether this performance was due to the standardized driving situation employed or whether the Fuzzy System is also able to deliver similar predictions on other types of roads and with other drivers.

3 Validation

In order to validate the algorithm developed above, a second field study was conducted. 28 participants aged between 22 and 59 years drove an approximately 71 km-long route over country roads, the motorway, and in city traffic. On this route, sensor data required for the algorithm were permanently logged from CAN-Bus and video recordings of driver and scene observation cameras were made. During driving, a slower-moving target vehicle which provided opportunity to overtake repeatedly appeared. A study investigator in the ego vehicle noted all overtaking manoeuvres performed. Following route completion, the algorithm was applied to all time points at which drivers had driven at a speed above 60 km/h in order to account for the operational scope of an LDW system. Using the study investigator's notes and video data, it was possible to identify all correct and "false positive" predictions.

Table 3 presents absolute frequencies of overtaking manoeuvres on country roads correctly and incorrectly predicted at the point of lane departure. As can be seen, the Fuzzy Logic System correctly predicted 147 of a total of 156 (94.2 %) overtaking manoeuvres. Three overtaking manoeuvres were not identified and six manoeuvres were only recognized after lane markings had been crossed. This resulted in a total of nine unrecognized overtaking manoeuvres. In 16 cases, overtaking manoeuvres were predicted without actually taking place. Analysis of video and vehicle data revealed that these situations were often characterized by drivers strongly approaching the vehicle in front. Whether these drivers prematurely abandoned their intention to overtake remains unclear.

In line with the first study, the length of time between prediction and lane departure was also computed. For 117 of the 147 overtaking manoeuvres, the quality of lane tracking was so high that an exact calculation of this time span was possible, Figure 3. Calculations showed that overtaking manoeuvres were predicted on average 2.1 seconds prior to lane departure. **Table 4** presents the distribution of overtaking manoeuvres according to the time span between prediction and lane departure.

As mentioned above, for six overtaking manoeuvres, prediction only began following lane departure. In 30 of a total of 123 cases (24.4 %), overtaking manoeuvres were predicted up to one second prior to lane departure. In 87 cases (70.7 %), predictions were made at least one second prior to lane departure.

While the Fuzzy System was developed based on country road data, the algorithm was also applied to motorway and city traffic. Since these environments do

Table 3: Overtaking manoeuvres and overtaking predictions on country roads

		Manoeuvre	
		Overtaking (156)	Followed the road (16)
Prediction	Overtaking	147	16
	Followed the road	9	

Table 4: Overtaking leadtimes on country roads

	Absolute	Percent
< 0,0 sec	6	4,8
0,0 - 1,0 sec	30	24,4
1,0 - 2,0 sec	28	22,8
> 2,0 sec	59	48,0
All	123	100

not allow a clear distinction between lane changes and overtaking manoeuvres, an exact classification of unpredicted overtaking manoeuvres is not possible. Therefore, a complete examination of all predictions must be conducted. Of a total of 128 predictions, 108 (84.4 %) were correct (i. e., the driver clearly overtook a vehicle). In 20 cases (15.6 %), a prediction was made although no apparent overtaking manoeuvre was observed.

4 Discussion and Future Prospects

The results of the present studies give rise to optimism. Using currently available vehicle sensors and based on the human as prototype, the Fuzzy Logic algorithm was able to predict 94.2 % of overtaking manoeuvres on country roads. In 70.7 % of overtaking manoeuvres, the time span of more than one second between predictions and the crossing of lane markings would appear sufficiently long. Depending on the parameterisation of an LDW system, overtaking information less than one second prior to lane departure may also prove useful.

These findings are even more notable when considering that both prediction reliability and the time span between prediction and lane departure can be further optimized. To date, membership functions are based on data from the first experiment and are yet to be adapted to data from the second experiment. In addition, the use of further indicators which may increase prediction reliability is conceivable. Indicating has, for example, yet to be included in the algorithm. Three of the six cases in which manoeuvres were belatedly predicted would, for instance, have been detected at an earlier stage if driver indication had been included. In the remaining three cases, steering wheel angle may have represented potentially useful information for predictions.

Results on motorway driving reveal a considerably greater number of prediction errors and also suggest that an even larger number of unpredicted lane changes are to be expected. Given that the algorithm was developed based on country road data, this is not particularly surprising. False predictions are, however, not necessarily critical, since the overriding of lane departure warnings is almost never noticed by the driver. In order to assure transparency of function, improvements in the domain of unrecognized lane changes are, however, necessary. Further studies in which similar algorithms are developed for lane changes on the motorway must therefore follow. When considering that the number of false alerts issued by LDW systems can be greatly reduced with the help of modern hardware and little software, cost-benefit calculations already prove extremely positive.

In improving ADAS, the prediction of driver intention is a field of great potential. In addition to the case example of LDW, improvements in "Blind Spot Warning" or overtaking assistants are also conceivable. Predictions of other manoeuvres such as, for example, "turning off" may also prove useful in the development of crossing assistants.

Until vehicles completely and autonomously take over lateral and longitudinal control, the conflict associated with the division of roles between driver and vehicle will continue to reign. As vehicles progressively take over more and more of the driving task, adapting assistance systems to the driver is likely to become absolutely essential. At the end of the day, a good passenger does not simply stare through the window screen, but also pays attention to the actions of the driver.

References

[1] Moetsch, M.: Blink mal wieder. AutoBild, 2005, 19, pp. 18-20

[2] LeBlanc, D., Sayer, J., Winkler, C., Ervin, R., Bogard, S., Devonshire, J., Mefford, M., Hagan, M., Bareket, Z., Goodsell, R. & Gordon, T.: Road departure crash warning system field operational test: Methodology and results. Technical report, The University of Michigan Transportation Research Institute, 2006. http://www-nrd.nhtsa.dot.gov/pdf/nrd-12/RDCW-Final-Report-Vol.1_JUNE.pdf

[3] Alkim, T.P., Bootsma, G. & Hoogendoorn, S.P.: Field Operational Test „The Assisted Driver". Intelligent Vehicles Symposium, pp.1198-1203, 13-15 June 2007, Istanbul, Turkey

[4] Zabyshny, A.A. & Ragland, D.R.: False Alarms and Human-Machine Warning Systems. UC Berkeley Traffic Safety Center, 2003. Paper UCB-TSC-RR-2003-07. http://repositories.cdlib.org/its/tsc/UCB-TSC-RR-2003-07

[5] Kompass, K. & Huber, W.: Advanced Driver Assistance: Chances and Limitations on the Way to Improved Active Safety. SAE Technical Paper, No. 2007-01-1738, 2007

[6] Blaschke, C., Färber, B. & Limbacher, R.: Online-detection of driver distraction. Proceedings of the 4th International Conference on Traffic and Transport Psychology, Washington D.C., USA, 1.- 4. September 2008

[7] Schmitt, J. & Färber, B.: Verbesserung von FAS durch Fahrerabsichtserkennung mit Fuzzy Logic. In: Fahrer im 21. Jahrhundert, VDI-Bericht 1919, Düsseldorf: VDI-Verlag 2005

[8] Oliver, N. & Pentland, A.P.: Graphical models for driver behavior recognition in a SmartCar. Proceedings of IEEE Conference on Intelligent Vehicles, Dearborn (MI), USA, 2000, pp. 7-12

[9] Kuge, N., Yamamura, T., Shimoyama, O. & Liu, A.: A driver behaviour recognition method based on a driver model framework. Proceedings of the 2000 SAE World Congress, Detroit (MI), USA, 2000, pp. 469-476

[10] Ohasi, K., Yamaguchi, T. & Tamai, I.: Humane automotive system using driver intention recognition. Proceedings of the SICE Annual Conference in Sapporo, Japan, 2004, pp. 1164-1167

[11] Salvucci, D.D.: Inferring driver intent: A case study in lane-change detection. Proceedings of the Human Factors Ergonomics Society 48th Annual Meeting. Santa Monica, USA, 2004, pp. 2228-2231

[12] Dagli, I., Brost, M. und Breuel, G.: Action recognition and prediction for driver assistance systems using dynamic belief networks. Proceedings of the Conference on Agent Technologies, Infrastructures, Tools and Applications for E-Services, Erfurt, Deutschland, 2002, pp. 179-194

[13] Heckhausen, H., Gollwitzer, P.M., Weinert, F.E.: Jenseits des Rubikon: Der Wille in den Humanwissenschaften. Berlin: Springer Verlag 1987

[14] Zadeh, L.A.: Fuzzy Sets. Information and Control, 8 (3), 1965, pp. 338-353

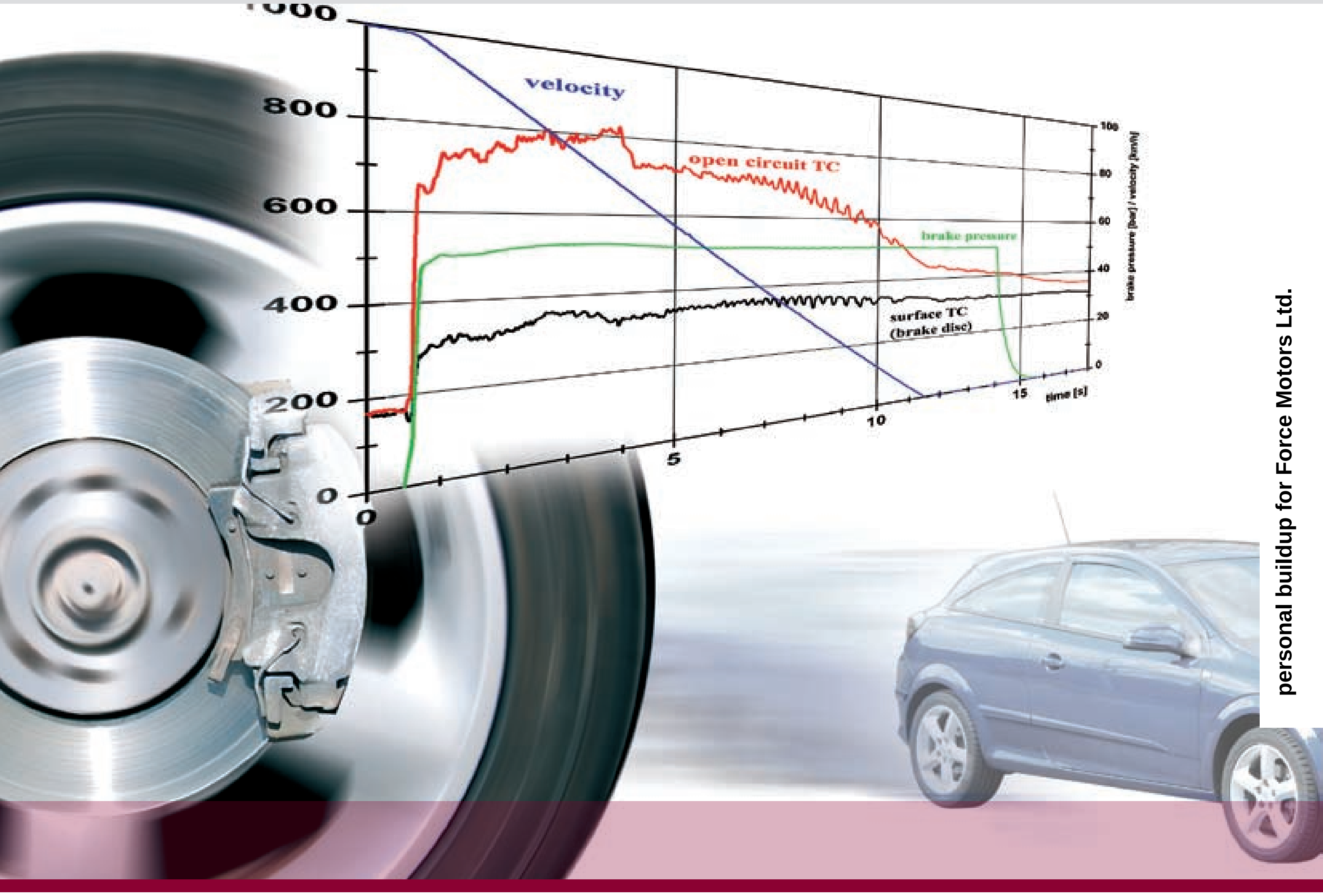

personal buildup for Force Motors Ltd.

Measuring Methods for Analysing the Braking Process in Disc Brakes

For the analysis of friction procedures in a disc brake during the braking process, no measuring methods have until now existed for determining the clamping forces, the active friction radius and the temperature acting in the friction area between the pad and the disc on disc brakes with short response times. Within the framework of studies carried out by the Chair of Automotive Engineering at the Technical University of Darmstadt (Germany) and the TMD Friction Group, two measuring devices have been developed, and examples of their measurement results are introduced in the following.

1 Introduction and Motivation

The measuring device presented in the following enables the clamping forces that act during a braking process in the friction area between the pad and the disc to be measured for the first time. In this area, the amount and the contact point are determined on the finger and piston sides at the same time. Furthermore, a measuring device that enables the temperature in the friction area between the brake pad and the disc of a vehicle wheel disc brake to be measured during the braking process is shown. It features open-ended thermocouples embedded into a brake pad, thus providing a response time that is several times faster than that of a standard thermocouple.

The reason for measuring these quantities is that many of the processes in the brake are unknown. This is reflected in the large number of research and development papers on the subject of braking torque and variations in the friction coefficient in the following specific areas: the occurrence of an increase in disc thickness variation (DTV), squeal, brake judder, the occurrence of hot spots, and comfort and performance features. In many approaches, processes are studied during a braking process by simulating the wheel brake, while the occurrence of DTV is examined by means of a multi-body model. The input of the simulation model is generally the brake's clamping force as a causal effective quantity. Thus, the information about the clamping force can serve to validate the simulation model. However, as both the amount and the point of application of the clamping force are not available, the piston force is generally used instead (the differences between piston and clamping force will be discussed later).

2 Force Measurement

2.1 Analysis of a Disc Brake und State of the Art

The basic quantities of the forces in a brake are presented in **Figure 1**. The hydraulic pressure p and the piston surface A_p result in the clamping force F_C. The latter causes the tangential force $F_T = F_C \cdot 2\mu$ on both friction areas. Together with the active friction radius r_a, the tangential force causes the braking torque $T_B = F_T \cdot r_a$. After all, the braking torque, with the help of the dynamic tyre radius in the contact patch of the tyre, is the quantity that causes the desired braking force, and thus the deceleration of the vehicle. Detailed research has shown that some simplifications are assumed in this model of forces [1]. **Figure 2** left observes the forces acting on a brake pad more exactly.

The support of the tangential force on the stator results in a force $F_{C,red}$ opposite to the brake piston. Thus, it shows that the clamping force does not correspond to the piston force during a braking process. Furthermore, this also shows that one cannot start with a uniform surface pressure (compare ΔF_C). What is more, the point of application of the load shifts during braking, corresponding to $F_{C,m}$, and does not lie on the same function line as the piston force.

A further phenomenon is presented on the right-hand side of Figure 2. The calliper can be an assumed model. It is likely to have a u-profile, which inevitably expands under the high clamping forces. Because of this, the shifting of the points of application of the load and therefore a larger active friction radius can be expected. Furthermore, the assumption that no identical shifting will appear on the finger and piston sides

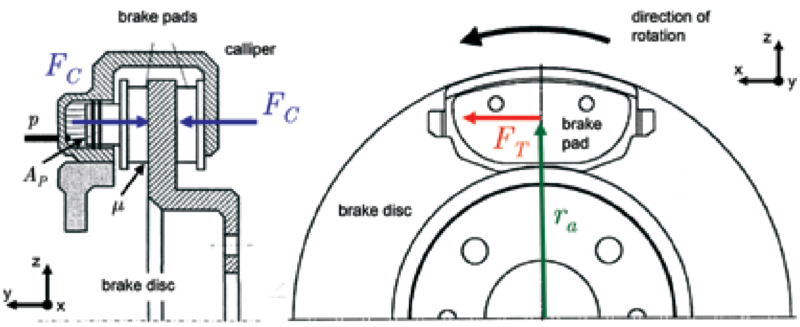

Figure 1: Forces acting on a disc brake [1]

The Authors

Dr.-Ing.
Thomas Degenstein
is project engineer in the advanced technical work group chassis, General Motors Europe. The research results presented were gained during his time as a Scientific Assistant at the Chair of Automotive Engineering at the Technical University of Darmstadt (Germany).

Prof. Dr. rer. nat.
Hermann Winner
is Director of the Chair of Automotive Engineering Department at Technical University of Darmstadt (Germany).

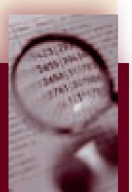

ATZ Peer Review
The Seal of Approval for scientific articles in ATZ.
Reviewed by experts from research and industry.

Received .... May 20, 2008
Reviewed .... July 16, 2008
Accepted .... August 1, 2008

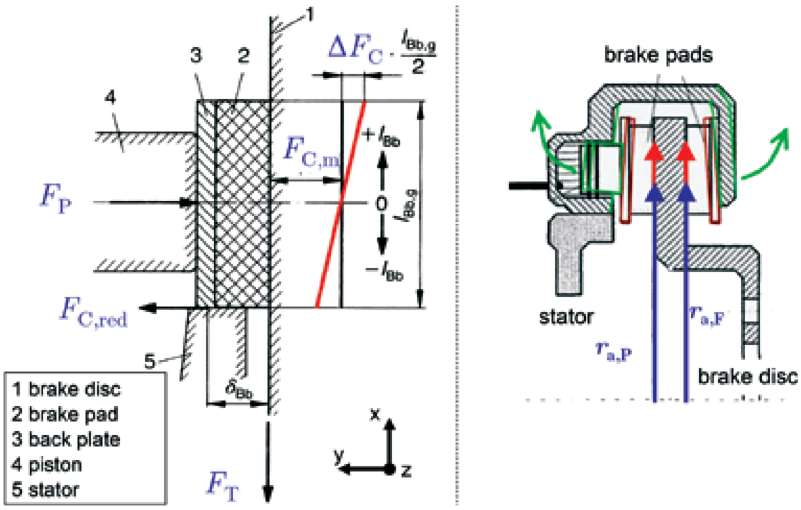

Figure 2: Left: forces acting on a brake pad during a braking process [1]; right: calliper expansion under brake pressure

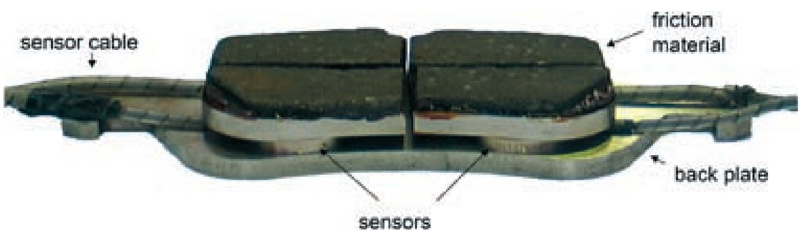

Figure 3: Measuring brake pad (iPad)

seems reasonable, since the finger side has, due to its design, more elastic qualities than the piston side. Analyses of the brake disc also show that the distribution of the surface pressure will change as a result of run-out or DTV. Thermal effects such as the shielding of a brake disc may also result in changes in the surface pressure of the clamping force.

From this, it follows that inconsistent or non-uniform surface pressure can be expected in a disc brake. According to [1], this would lead to slanted, uneven wear of the brake pads. Furthermore, a higher energy expenditure is required at those positions with a higher surface pressure, which leads to higher temperatures. On the other hand, according to [2], higher temperatures result in lower friction coefficients and this reduces the efficiency of the brake. According to [1], the comfort of the brake is also reduced, since unevenly worn pads increase the sensitivity to squealing.

In order to determine the influence of these measures and the actual surface pressure, various methods were developed. The state-of-the-art methods are the tension-optical ball pressing process [1], pressure indication films from the company Fuji and electrical pressure indication films from the company Tekscan [3], for example. Beside their limited accuracy (for example Tekscan fault indication > 10 % [3]), all these methods have the disadvantage that they can be only applied by a static brake disc. As can be seen in Figure 2, however, it appears that, during the braking process, other distributions lead to the clamping force by the support of the tangential force. In these methods, the effect of calliper expansion can be primarily examined, but this will not behave in the same manner during the actual braking process as during a test with a static disc. Measuring methods for determining the clamping force during a braking process do not exist to date. The focus of this study lies on determining the point of application of the clamping force of the finger and piston side during the braking process.

2.2 Structure and Model of the Measuring Brake Pad

An analysis of the force lines in a calliper (a Continental Teves type 2 FNR-Al42 was chosen as an example) shows that the best measurement point is to be found in the friction material before the forces are split (details in [4]). Comparing different sensor principles with the requirements resulted in the use of the piezoelectrical effect.

For the measurement of the point of application of the load of the clamping force, four piezo quartz sensors were installed between the back plate and a support plate, **Figure 3**. In the following, the measuring brake pad is referred to as the iPad.

Figure 4 shows the model concept of the measuring brake pad. In order to determine the acting clamping force, the

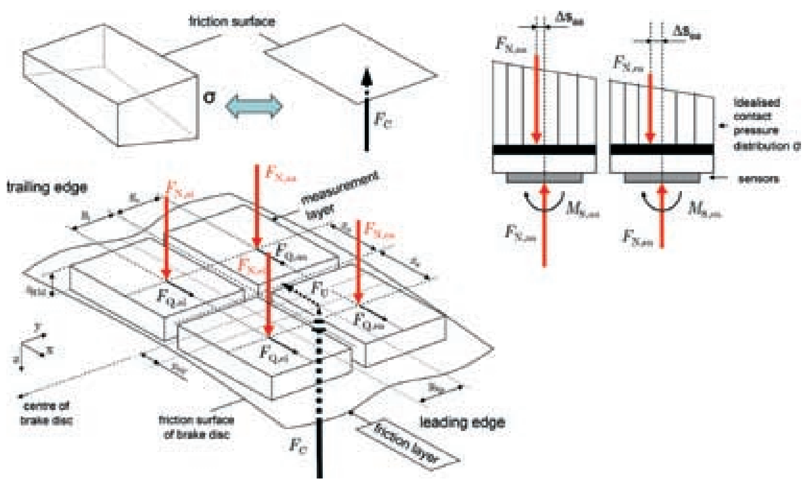

Figure 4: Model concept of the measuring brake pad (details in [4])

aggregated signal of the four single forces is formed. The point of application of the load is determined by a moment balance in the sensor measuring level.

2.3 Specification and Measurement Uncertainty

The iPad is of the same size as the original brake pad. The friction material layer is 4 mm thick, which is equivalent to a lifetime in a series-production vehicle of approximately 10,000 km. The clamping forces F_C can be measured in a range from 1.2 kN to 16.5 kN.

In consideration of potential measurement errors for example by reason of drift (change of the signals due finite resistance of the measurement chain) changes of temperature and hysteresis, the uncertainty of the measurement with a static brake disc assumes a maximum of 1 %. Whereas the maximum uncertainty of the measurement during the braking process was 1.7 % (explanation and proof in [4]).

2.4 Results

The indications of the positions of the sensors in the brake pad for the following results correspond to **Figure 5**. The curve of the four sensors of the piston-side pad is presented as an example in **Figure 6** left at a braking pressure of 40 bar and with a static brake disc. Figure 6 right shows the curve during a braking process with an initial speed of 15 m/s (425 rpm).

It can be derived that the outer sensors transfer greater forces. This increases further with increasing braking pressure – corresponding to the model concept of expanding the calliper at increasing pressure. The right-hand side clamping force variations are visible. These are the result of brake disc thickness variations and will be analysed later.

Figure 7 summarises the results of the measurements for the static brake disc and for braking at an initial speed of 15 m/s (425 rpm) at the finger-side and piston-side pad.

It can be derived that the point of application of the load moves by 10 mm on the piston side to the outside with a static brake disc when the braking pressure rises from 10 bar to 60 bar. This effect is approximately 12 mm greater on the finger side, which can be explained by the design of a brake, Figure 2, since the brake is connected to the suspension on the piston side and is stiffer than the finger side, which has to be led over the brake disc. During a braking process, the points of application of the load shift in the direction of the leading edge. This corresponds to the model concept according to [1], Figure 2. If these results are transferred to the change in the friction radius, there is a rise in braking torque by approximately 7 % for this brake at a braking pressure of 60 bar.

In the following, the brake torque variation and the clamping force variation shown in Figure 6 are analysed with the iPads. The braking parameters are 40 bar brake pressure and the initial speed is 30 m/s. The disc thickness varia-

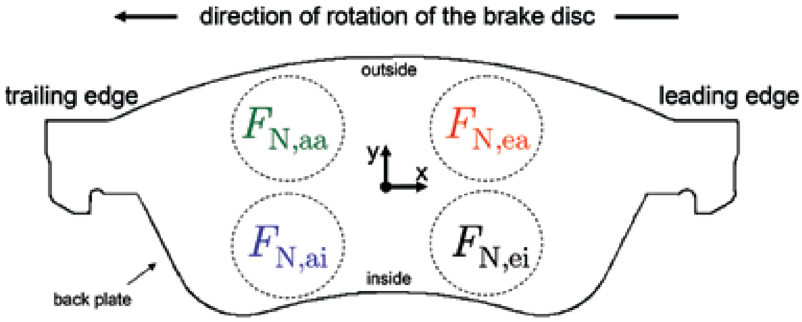

Figure 5: Indication of the sensors in the brake pad

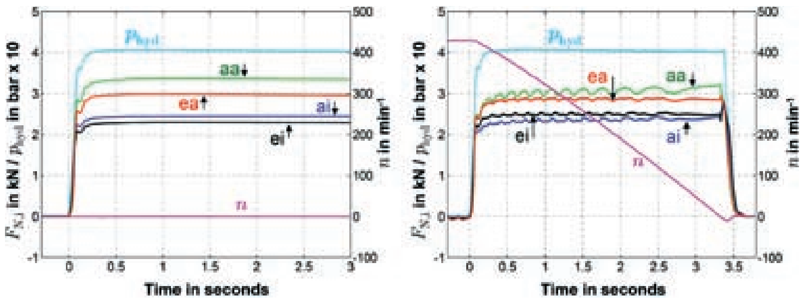

Figure 6: Left: curve of the normal force of the single sensors of the piston-side pad, static brake disk; right: during the braking process

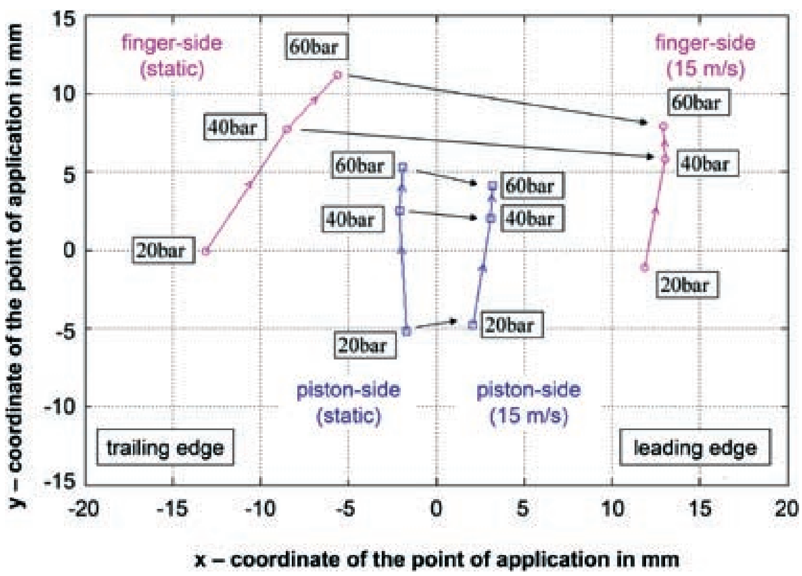

Figure 7: Shift in the point of application of the load during a braking process

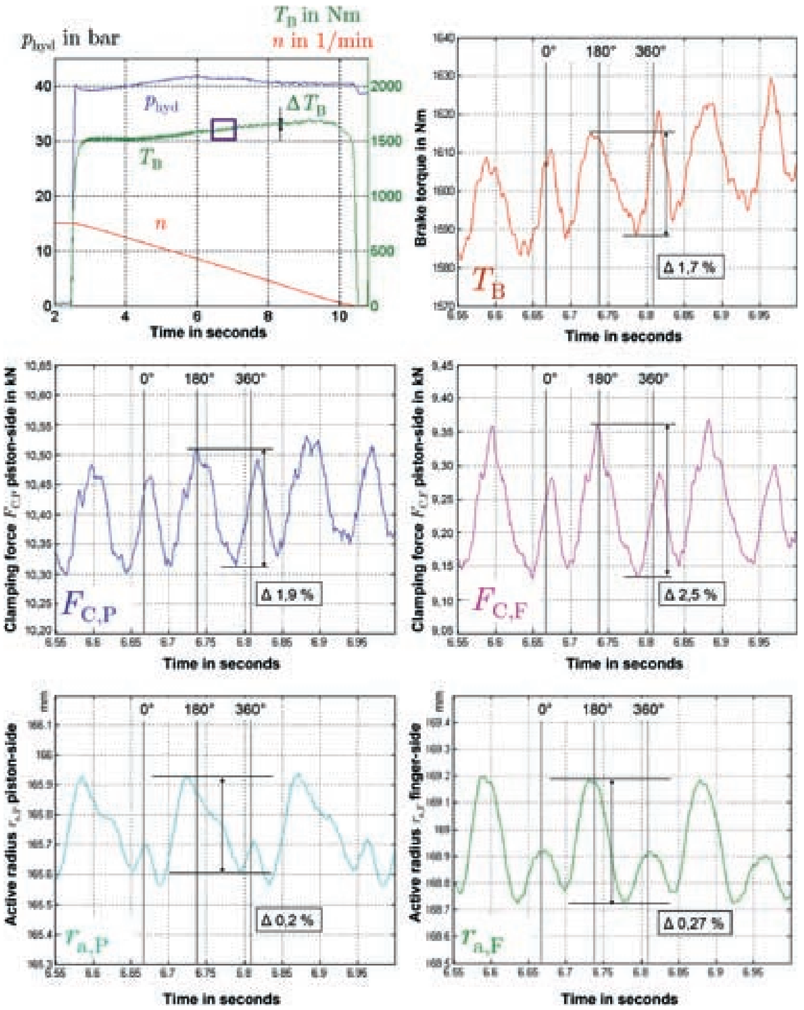

Figure 8: Analysis of a sample braking procedure

tions of this new brake disc are a maximum of 8 µm.

Figure 8 shows the brake torque during a braking process. The brake torque varies by 1.7 % in the area of $\varphi \approx 170°$ to $\varphi \approx 280°$ of the brake disc. In the next two figures, the course of the load magnitude and the point of application of the piston-side and finger-side clamping force are shown to analyse these brake torque variations.

It can be derived that the forces $F_{C,P}$ and $F_{C,F}$ simultaneously rise and fall. This is an indication for disc thickness variants. What is noticeable is that the variants are larger on the finger side than on the piston side and both are larger than the change in the braking torque. The variations in the course of the points of application of the clamping force $r_{a,P}$ and $r_{a,F}$ are less than the variations of the load magnitude. The positions of the maxima and minima are close to the maxima and minima of the load magnitude. The measurement results confirm theories of the braking process, for example Eggleston [5], but for the first time these could be proven both qualitatively and quantitatively. These measurement results show that, during this braking process, the variation in the clamping force is the dominant parameter for the brake torque variations. Further measured data and calculations, such as the curve of the friction value, the curve of the brake pressure and the curve of the point of application during one brake disc rotation, can be seen in [4].

2.5 Conclusions und Outlook

The measuring device presented here enables the amounts and points of application of the clamping forces during a braking process to be measured for the first time. A disc brake without iPads is comparable to a black box. The known input is the hydraulic pressure p_{hyd} and the known output is the brake torque T_B. On the basis of these two parameters, other values were estimated. Using the iPads, it is possible to measure the clamping forces $F_{C,i}$, the points of application and the active radii $r_{C,i}$. Furthermore, it is now possible to calculate the friction value μ_B between the pads and the disc and the degree of efficiency η (shown in [4]).

The integration of the sensor into the brake pad makes it possible to apply this design principle in almost every disc brake. The model concepts according to [1] and the enlarging of the calliper under braking pressure, Figure 2, could be confirmed for this calliper. The benefits include the one-time determination of the change in the point of application of the load for a defined calliper. Subsequently, this information can be used as a correction factor for test bench experiments, and some factors of the real friction coefficient can be determined with more precision. At the same time, the measuring device can be examined for a uniform pressure on the brake pad on the brake disc during a braking process. Piezo quartz sensors are very suitable for high-frequency measurements. Thus, changes in the clamping force can also be recorded in the range of squeal frequencies (up to approximately 20 kHz).

Further benefits can be found for the study of brake disc geometrical failures (for example run-out, disc thickness variation), which are reflected in changes in the point of application of the load depending on the speed. In such studies, a kind of a circular movement of the point of application of the load with a movement diameter of 0.5 mm was determined (shown in [4]). This information could be very helpful for investigations of judder and variations in braking torque.

3 Temperature Measurement

3.1 Objective and State-of-the-Art

The task was to design a measuring system to measure the temperature between the brake pad and the brake disc of a passenger car. The temperature was to be measured within the friction surface. The requirements to be met include a

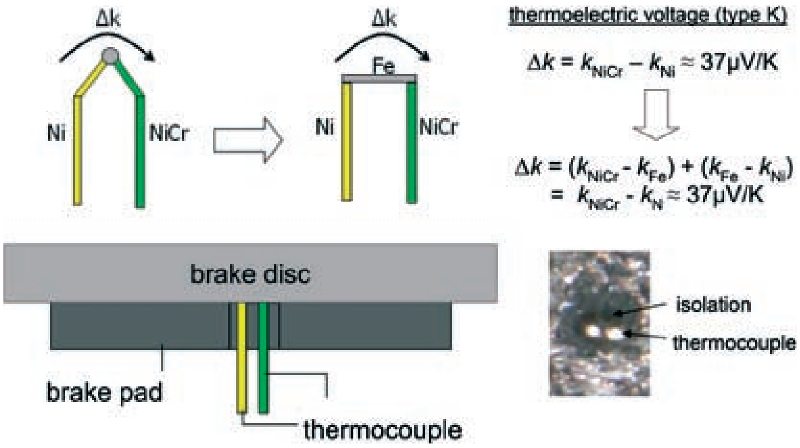

Figure 9: Measuring principle

working temperature range of between -40 °C and 1200 °C, clamping forces up to 40 kN, and the ability to cope with the wear of the brake disc (up to 4 mm) and wear of the brake pad (up to 10 mm). The measuring system has to match the highly dynamic temperature variations found on the brake disc in particular.

Different approaches for this task exist. In mass-produced vehicles, the temperature of the brake disc is estimated only by parameter-based models. In research, two groups of devices are used. Optical measurement systems include pyrometers, thermal cameras and thermal scanners. The use of these systems is limited to those areas in which the line of sight is unobstructed. This prevents them from being used for measuring the outboard temperature of the brake disc in test set-ups including a rim. Thermocouples are deployed both within the brake pad as well as in the brake disc, where collector rings are included in the circuit. Thermocouples are commonly used with a welded tip. The dimensions of this weld, particularly the thermal capacity, determine the response time, which increases with the size of the weld, and the lifetime of the thermocouple, since it is exposed to the wear processes in the friction area. Open-ended thermocouples were found to provide a shorter response time than closed ones, but these have not yet been used for vehicle brake temperature assessment. A similar solution was proposed to determine the surface pressure distribution within the brake pad [1].

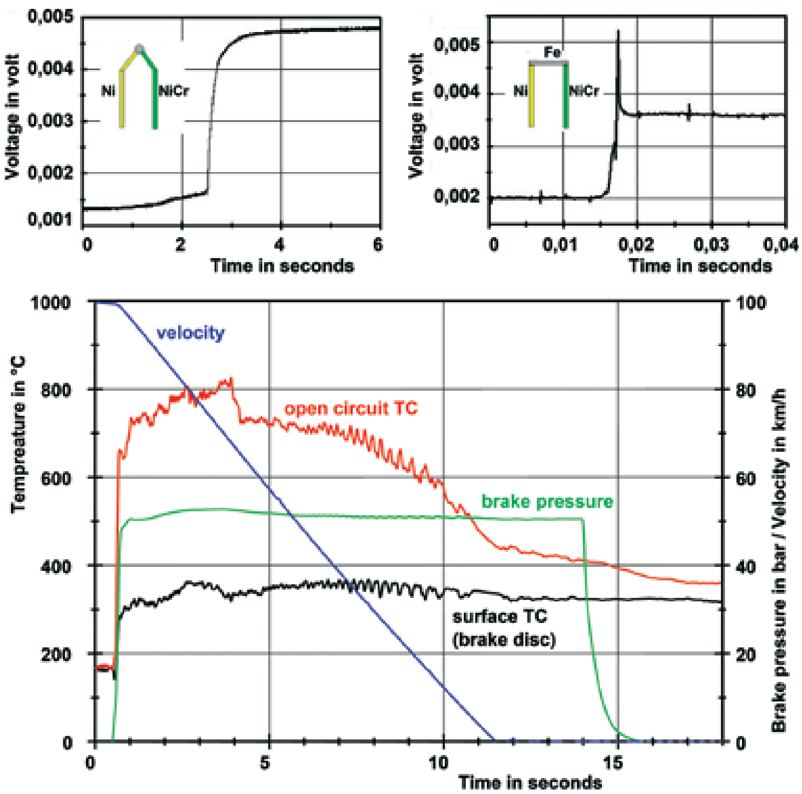

Figure 10: Top: step response of closed and opened thermocouple; bottom: full stop from 100 km/h, constant brake pressure of 50 bar; 5 Hz low-pass filtering of temperature signals

3.2 Idea and Implementation

The idea presented here is to directly embed an open thermocouple in the brake pad in order to measure the temperature in the contact area of the brake pad and disc with a very short response time. The device described here is able to cope with wear in the friction area.

Figure 9 shows a commonly used thermocouple on the left and the new type on the right. They differ in that the thermocouple on the left closes the electric circuit by means of the welded tip, whereas the thermocouple on the right includes the test specimen (that is the brake disc) in the circuit. There is no welded tip and therefore no thermal capacity to heat up or cool down, which means that this set-up promises a very short response time limited to the electrical properties.

For a closed thermocouple, the thermoelectric power per degree Kelvin [μV/K] is given by the difference of the thermoelectric potentials of the two materials (also known as the Seebeck coefficients) of the thermocouple. When the conductors of the thermocouple are connected by the brake disc and both conductors are faced with the same temperature, this equation applies, where obviously the influence of the third material is cancelled out (shown with the equation in Figure 9, proof and details in [6]). Furthermore, the schematic application of an open-circuit thermocouple embedded into a brake pad during a braking process is illustrated. The embedded thermocouple wears simultaneously with the brake pad and the functionality is preserved throughout the life of the brake pad.

There are two methods of closing the circuit of the embedded open-circuit thermocouple in order to assess the temperature in the friction zone between the brake pad and the disc during the braking process. In the case depicted in Figure 9, the circuit of the thermocouple is closed by the electrically conductive surface of the brake pad. The other method is to close the circuit by the brake disk. Two kinds of embedded open-circuit thermocouples that differ in the way that the open circuit is closed were developed. They differ in the use of the insulation of the thermocouple wires.

3.3 Results

Figure 10 depicts the step-input response of a closed, welded-tip thermocouple and the step-input response of an open-circuit thermocouple for the event of a temperature step at the measuring tip. In order to receive a fast response of the thermocouples, the measuring tip of each thermocouple is exposed to an abrupt change in temperature. The measuring tip of the closed-circuit thermocouple makes contact with the measured object. The open-circuit thermocouple is directly faced with an abrupt temperature change of the measured object, which simultaneously incorporates the boundary of the measuring tip of this type of thermocouple. In this case, it takes place during a hundredth of a second, whereas the closed-circuit thermocouple requires a couple of seconds to sense the temperature of the measured object. The faster response of the open-circuit thermocouple compared to the closed-circuit thermocouple is due to the measuring tip, which is simultaneously the measured object, while the measuring tip of the closed-circuit thermocouple has to adopt the temperature of the measured object.

Figure 10 shows the temperatures measured with an open and a closed thermocouple during a braking process with 50 bar brake pressure, starting at a wheel velocity of 100 km/h and coming to a full stop. With the open thermocouple, the steep increase in the friction temperature can be seen. This behaviour could only be recorded by this new measurement method. Subsequently, the temperature decreases even during the braking action. This can be explained by the heat emission due to the friction process into brake disc and pad, which depends on the braking power, and therefore on the velocity.

3.4 Conclusions of the Temperature Measurement

The measuring device described here is capable of dynamically measuring the temperature in the friction area between a brake pad and the brake disc during a braking manoeuvre. It features open-ended thermocouples embedded into the brake pad, providing a response time to a step-input temperature change several times faster than that of a closed-tip thermocouple. The temperature-measuring process by means of the open-ended thermocouples is independent of the velocity and the brake pressure.

As it is embedded into the brake pad, this device, unlike other known measuring methods, which operate outside the brake pad, offers new ways for assessing the processes in the brake disc friction area, for research, development and mass-produced vehicles.

References

[1] Burckhardt, M.; Reimpell, J. (Hrsg.): Fahrwerktechnik: Bremsdynamik und Pkw-Bremsanlagen, Chap. 7, Vogel Fachbuch Kfz-Technik, Vogel Buchverlag, Würzburg 1991

[2] Breuer, B.; Bill, K.: Bremsenhandbuch – Grundlagen, Komponenten, Systeme, Fahrdynamik, 3. Edition, Chap. 3 und 22, ATZ-MTZ-Fachbuch, Vieweg Verlag 2004

[3] Tekscan: Industrial Sensor Catalog, RevDD_072705, Tekscan 2005

[4] Degenstein, T.: Kraftmessung in Scheibenbremsen, VDI Fortschritt-Berichte Reihe 12 Nr. 655, Dissertation am FG Fahrzeugtechnik (FZD) an der TU Darmstadt, VDI-Verlag 2007

[5] Eggleston, D.: Cold Judder. 1999, Technical Bulletin 00029711, Precision Disc Castings, Ltd. Technical Bulletin Series (URL: http://www.eurac-group.com/technote4.htm)

[6] Breuer, B. (Hrsg.): XXVII. International μ-Symposium, VDI-Verlag 2007, pp. 164-188